

VOLTAGE-GATED SODIUM CHANNEL ACTIVITY IN MOUSE SKELETAL
MUSCLE FIBERS: NORMAL GATING AND DEFECTS ASSOCIATED WITH
PERIODIC PARALYSIS MUTANTS

APPROVED BY SUPERVISORY COMMITTEE

Stephen C. Cannon, M.D., Ph.D.

Juan M. Pascual, M.D., Ph.D.

Paul Blount, Ph.D.

Weichun Lin, Ph.D.

DEDICATION

I would like to dedicate this dissertation to my father, Chenggang Fu, my mother, Yingqi Wei, for their support and love with their whole heart.

VOLTAGE-GATED SODIUM CHANNEL ACTIVITY IN MOUSE SKELETAL
MUSCLE FIBERS: NORMAL GATING AND DEFECTS ASSOCIATED WITH
PERIODIC PARALYSIS MUTANTS

by

YU FU

DISSERTATION

Presented to the Faculty of the Graduate School of Biomedical Sciences

The University of Texas Southwestern Medical Center at Dallas

In Partial Fulfillment of the Requirements

For the Degree of

DOCTOR OF PHILOSOPHY

The University of Texas Southwestern Medical Center at Dallas

Dallas, Texas

July, 2010

COPYRIGHT

by

YU FU, 2010

All Rights Reserved

ACKNOWLEDGMENT

First, I would like to thank my mentor, Dr. Stephen C. Cannon, for this four-year study under his great mentorship and support. His knowledge in electrophysiology and enthusiasm on science encouraged me to pursue my scientific career and inspired me all through these years.

I appreciate Dr. Vladislav Markin for his contribution to the computer simulation. Without his work, this part of my project would never be completed.

I would also thank Dr. Fenfen Wu for assistance with the experimental design of molecular biology. Hillery Gray provided technical support for animal care and genotyping. Dr. Fenfen Wu, who is working on analyzing muscle CMAP, Dr. Wentao Mi, who is working on muscle contraction, their works confirm the disease resembling phenotypes of the engineered mice used for my study. Drs David Francis and Volodymyr Rybalchenko, their works on identifying the gating pore currents inspired me for my future research. A special thanks goes to Dr. Arie Struyk, who is already started his new career in industry, for his instruction from the beginning I joined this laboratory. I appreciated every person in Dr. Cannon's laboratory for making this joyful and supportive environment.

In addition, I need to mention my friends, Drs Jun Wu and Tong Zang, who kept encouraging me to finish this dissertation.

Finally, I would like to thank my thesis committee, Dr. Weichun Lin as my committee chair, Dr. Juan M Pascual, Dr. Paul Blount, and Dr. Don C Cooper for their support and insightful suggestions to my research.

This work was supported by NIAMS of the NIH (AR42703) and the Muscular Dystrophy Association.

VOLTAGE-GATED SODIUM CHANNEL ACTIVITY IN MOUSE SKELETAL
MUSCLE FIBERS: NORMAL GATING AND DEFECTS ASSOCIATED WITH
PERIODIC PARALYSIS MUTANTS

YU FU, Ph.D.

The University of Texas Southwestern Medical Center at Dallas, 2010

Stephen C. Cannon, M.D., Ph.D.

Mutations in *SCN4A*, the gene encoding the skeletal muscle Na⁺ channel (Nav1.4) α -subunit, cause several disorders related to skeletal muscle excitability. The functional consequences of these Nav1.4 mutations have been extensively characterized in heterologous expression systems. These studies have significantly advanced our understanding of the pathophysiology of these

disorders. The *in vivo* functional consequences on channel activity, however, have yet to be defined. Animal models are now available in genetically engineered mice, which provide an opportunity to examine channel function in mature skeletal muscle.

We optimized a two-electrode voltage clamp protocol to improve the fidelity of Na⁺ current recording from acutely dissociated intact muscle fibers. Computer simulation, incorporating measured capacitance and ionic current densities, was used to confirm sufficient voltage control and distortion-free Na⁺ currents. The gating properties of endogenous Na⁺ currents were measured and compared between two mouse strains, C57BL/6 and 129-E. The most dramatic finding was a hyperpolarized shift in the voltage dependence of activation (-25 mV) and fast inactivation (-18 mV) as compared to the studies in HEK293 cells expressing Nav1.4 plus the accessory β 1-subunit. A possible contribution from Nav1.5 channels in the mouse muscle preparation was excluded by RT-PCR and TTX-sensitivity. There was no significant difference in voltage dependence of fast gating between C57BL/6 and 129-E. The entry rate into slow inactivation was slower for Na⁺ channel in 129-E fibers; while the recovery from slow inactivation was similar between two mouse strains.

Two Nav1.4 missense mutations associated with divergent clinical phenotypes - Nav1.4-M1592V in hyperkalemic periodic paralysis (HyperPP) and

Nav1.4-R663H (homolog of human R669H) in hypokalemic periodic paralysis (HypoPP) - were characterized with voltage-clamp recordings in fully-differentiated fibers from knock-in mutant mice. The Nav1.4-M1592V mutation produced gain-of-function defects, with the major changes being a slightly increased persistent current and moderately disrupted slow inactivation. In contrast, the HypoPP knock-in mutant R663H resulted in loss-of-function changes, due to an enhancement of inactivation, both fast and slow, and impaired activation. These observations provide important validation of prior findings using heterologous expression systems and yield quantitative information on the severity of the gating defects in mammalian skeletal muscles.

TABLE OF CONTENTS

PRIOR PUBLICATIONS	xiv
LIST OF FIGURES	xv
LIST OF TABLES.....	xviii
LIST OF APPENDICES.....	xix
LIST OF ABBREVIATION	xx
Chapter One : Properties of Voltage-Gated Sodium Channels and Skeletal Muscle Sodium Channelopathies	1
Properties of Voltage-Gated Sodium Channels	1
Structure of Voltage-Gated Sodium Channel	1
Voltage-Gated Sodium Channel Family	4
Gating Behavior of Voltage-Gated Sodium Channels	8
Skeletal Muscle Sodium Channelopathies.....	14
Potassium-Aggravated Myotonia.....	17
Paramyotonia Congenita.....	19
Hyperkalemic Periodic Paralysis	21
PAM-PCM- HyperPP: Gain-of-Function Defects	23
HypoPP: an emerging picture of Na ⁺ channel Loss-of-Function Mutations and gating pore leak currents.....	25

Chapter Two : Gating Behavior of Sodium Currents in Adult Mouse Muscle Recorded with an Improved Two-Electrode Voltage Clamp	30
Introduction.....	30
Materials and Methods.....	35
Results.....	39
Passive Properties of Skeletal Muscle Fibers	39
Constraints on Clamp Speed.....	42
Voltage-Clamp Control is Not Possible in Physiological Na ⁺	44
Computer Simulations Provide Estimates for Conditions Necessary to Maintain Voltage-Clamp Control.....	46
Model Simulations of I _{Na} Provide Quantitative Estimates for the Errors in Determining Na ⁺ Channel Gating Parameters from TEVC Recordings in Foot Pad Muscle Fibers.....	53
Leak Subtraction Strategy.....	61
Discussion	64
Chapter Three : Sodium Currents in Adult Mouse Skeletal Muscle: Hyperpolarized Shift of Gating Relative to Na _v 1.4 in Heterologous Expression Systems	71
Introduction.....	71
Materials and Methods.....	74

Results.....	84
Activation.....	85
Fast Inactivation.....	87
Slow Inactivation	90
Estimated Contribution from $\text{Na}_v1.5$ Expression in Foot Pad Muscle Fibers	96
Voltage Dependence of Fast Gating of $\text{Na}_v1.4$ Sodium Channel in Low $[\text{Na}^+]$	99
Additional Factors That May Cause an Apparent Leftward Shift in Voltage Dependence of Na^+ Channel Gating	100
Discussion.....	105
Chapter Four : Gating Defects for the Hyperkalemic Periodic Paralysis Associated Sodium Channel Mutation M1592V in Fully Differentiated Mouse Skeletal Muscle Fibers	114
Introduction.....	114
Materials and Methods.....	117
Results.....	125
Activation.....	125
Fast inactivation	127
Slow inactivation	130
Persistent Na^+ current.....	135

Expression of mutant channel.....	138
Resurgent current.....	139
Discussion.....	142
Chapter Five : Gating Defects for the Hypokalemic Periodic Paralysis Associated Sodium Channel Mutation R663H in Fully Differentiated Mouse Skeletal Muscle Fibers.....	145
Introduction.....	145
Materials and Methods.....	148
Results.....	153
Activation.....	153
Fast inactivation.....	155
Slow inactivation.....	157
Discussion.....	162
Chapter Six : Summary and Future Directions.....	165
APPENDIX.....	170
BIBLIOGRAPHY.....	173

PRIOR PUBLICATIONS

X.-M. Hao, Y. Fu, H. Jin, and T.-F. Liu. Calcium-Activated Potassium Current in Single Novikoff Cell. *Methods Find Exp Clin Pharmacol* 2001, 23 (2)-55

Abstract report in the ninth conference of Biophysical Society of China. β_1 -adrenergic Stimulation Enhanced Frequency of Calcium Sparks in Rat Cardiac Myocyte through L-type Ca^{2+} Channel. 2002, Hainan, P.R.China.

Fu Yu*, Zhang Guangqin*, Yang Dongmei, Hao Xuemei, Bai Shuhua, Tang Yiqun, Edward G Lakatta, Cheng Heping * equal contributor. Contribution of Spontaneous L-type Ca^{2+} channel activation to the genesis of Ca^{2+} sparks in resting cardiac myocyte. *Sci China C Life Sci.* 2004, 47(1)-31

Fu Y, Zhang GQ, Hao XM, Wu CH, Chai Z, Wang SQ. Temperature dependence and thermodynamic properties of Ca^{2+} sparks in rat cardiomyocytes. *Biophys J.* 2005, 89(4) -41.

Hua Zhang, Anton Maximov, Yu Fu, Fang Xu, Tie-Shan Tang, Tatiana Tkatch, D. James Surmeier, and Ilya Bezprozvanny. Association of $\text{Ca}_v1.3$ L-Type Calcium Channels with Shank. *The Journal of Neuroscience*, 2005, 25(5)-1037

Hua Zhang, Yu Fu, Christophe Altier, Josef Platzer, D. James Surmeier and Ilya Bezprozvanny. $\text{Ca}_v1.2$ and $\text{Ca}_v1.3$ neuronal L-type calcium channels: differential targeting and signaling to pCREB. *European Journal of Neuroscience*, 2006, 23(9)-2297.

Abstract report in the Biophysical Society 52nd Annual Meeting. Characterization of Na^+ currents from Intact Mouse Skeletal Muscle Fibers. 2008, Long beach.

LIST OF FIGURES

Figure 1-1. Structure of voltage-gated sodium channels.	3
Figure 1-2. A phylogenetic tree of rat voltage-gated sodium channel α -subunits. .	5
Figure 1-3. Schematic representation of inactivation structure of sodium channel.	10
Figure 1-4. Locations of $\text{Na}_V1.4$ mutations associated with skeletal muscle disorders.....	15
Figure 1-5. Clinical spectrum of the nondystrophic myotonias and periodic paralyses. and their associated mutations in voltage-gated ion channels.	17
Figure 1-6. The mechanisms underline the symptoms of PAM, PMC and HyperPP, gain-of-function mutations.....	24
Figure 1-7. Gating pore current.	27
Figure 1-8. Resting potential as a function of $[\text{K}^+]_o$ for simulated WT and HypoPP muscle fibers.	28
Figure 2-1. Diagram for current flow in a cylindrical cell such as muscle fiber. .	31
Figure 2-2. Passive properties of mouse skeletal muscle fibers.	41
Figure 2-3. Fiber effects on voltage-clamp speed.	44

Figure 2-4. Two-electrode voltage-clamp was not able to control membrane potential in full $[\text{Na}^+]$.	46
Figure 2-5. Model predictions of voltage control over the length of a fiber.	50
Figure 2-6. Dependency of voltage-clamp error on fiber size, $[\text{Na}^+]$, and voltage.	53
Figure 2-7. Effect of voltage-clamp speed on Na^+ currents in a simulated fiber.	57
Figure 2-8. Effect of fiber length on Na^+ currents in a simulated fiber.	58
Figure 2-9. Errors in activation gating parameters estimated from fits to peak Na^+ currents in simulated fibers of various lengths.	60
Figure 2-10. Leak subtraction protocol to isolate Na^+ currents.	63
Figure 3-1. Voltage dependence of activation.	86
Figure 3-2. Fast inactivation properties.	90
Figure 3-3. Kinetics of slow inactivation.	94
Figure 3-4. Voltage dependence of slow inactivation.	95
Figure 3-5. Contribution of $\text{Na}_v1.5$ channels to the Na^+ current in muscle fibers.	98
Figure 3-6. Voltage dependence of activation in full $[\text{Na}^+]$ and low $[\text{Na}^+]$ solutions.	100

Figure 3-7. Lack of evidence for a systematic shift.....	102
Figure 3-8. Shift after cell impalement.....	104
Figure 4-1. Location of M1592V HyperPP mutation.....	117
Figure 4-2. Representative currents and voltage dependence of activation.....	127
Figure 4-3. Fast inactivation properties.....	128
Figure 4-4. Kinetics of slow inactivation.....	132
Figure 4-5. Voltage dependence of slow inactivation.....	134
Figure 4-6. Persistent currents.....	137
Figure 4-7. Gel photo of the enzymatic treatment.....	139
Figure 4-8. Detection of resurgent current in mouse skeletal muscle fibers.....	141
Figure 5-1. Location of R663H HypoPP mutation.....	147
Figure 5-2. Representative currents and voltage dependence of activation.....	154
Figure 5-3. Fast inactivation properties.....	156
Figure 5-4. Kinetics of slow inactivation.....	160
Figure 5-5. Voltage dependence of slow inactivation.....	162

LIST OF TABLES

Table 1-1 Mammalian sodium channel α -subunits.....	7
Table 3-1 Slow Inactivation Properties.....	94
Table 4-1 Gating parameters for Nav1.4 in mouse skeletal muscle fibers.....	129
Table 4-2 Slow Inactivation Kinetics.....	133
Table 5-1 Gating parameters for Nav1.4 in mouse skeletal muscle fibers.....	157
Table 5-2 Slow Inactivation Kinetics.....	160
Table A.1 Gating Parameter.....	172

LIST OF APPENDICES

APPENDIX A Parameter Estimates for Na ⁺ channel Gating.....	170
--	-----

LIST OF ABBREVIATION

4-AP – 4-aminopyridine

9-AC – anthracene-9-carboxylic acid

bp – base pair

BTS – N-benzyl-p-toluene sulphonamide

CMS – congenital myasthenic syndrome

CNS – central nervous system

COVC – cut-open oocyte voltage clamp

DEPC – diethyl pyrocarbonate

DRG – dorsal root ganglion

EDL – digitorum longus muscle

EMG – electromyography

FDB – flexor digitorum brevis

HEK293 cells – human embryonic kidney 293 cells

HEPES – 4-(2-hydroxyethyl)-1-piperazineethanesulfonic acid

H_{∞} – voltage-dependence of steady-state fast inactivation

HyperPP – hyperkalemic periodic paralysis

HypoPP – hypokalemic periodic paralysis

nAChR – nicotinic acetylcholine receptor

NormoPP – normokalemic periodic paralysis

PAM – potassium-aggravated myotonia

PMC – paramyotonia congenita

PNS – peripheral nervous system

Rs – series resistance

S_{∞} – voltage-dependence of steady-state slow inactivation

TEAOH – tetraethylammonium hydroxide

TEVC – two-electrode voltage clamp

T- tubules – transverse tubules

TTX – tetrodotoxin

V_{command} – command potential

V_{rest} – resting potential

WT – wild type

Chapter One : Properties of Voltage-Gated Sodium Channels and Skeletal Muscle Sodium Channelopathies

Properties of Voltage-Gated Sodium Channels

The primary physiological role of voltage-gated sodium channels in electrically excitable cells such as skeletal muscle, heart, and neurons is to conduct a rapidly-activating inward current to produce the upstroke of the action potential (Hodgkin and Huxley, 1952). The selective permeability for sodium ions and the precisely tuned voltage-dependent gating are critical features that enable the Na⁺ channels to accomplish their physiological role with high fidelity. Even subtle defects in these properties are sufficient to cause paroxysmal disruption of cellular excitability and give rise to epilepsy, migraine headache, arrhythmia, myotonia, or periodic paralysis (Cannon, 2006).

Structure of Voltage-Gated Sodium Channel

The voltage-gated sodium channel is large integral membrane protein complex, composed of an α -subunit (230-270 kDa) and one or several accessory β -subunits (33-36 kDa) (Fozzard and Hanck, 1996; Gellens et al., 1992; George et al., 1992). The α -subunit contains both the pore-forming and the voltage-sensing

domains of the channel complex. Expression of the α -subunit alone in heterologous cells without β -subunits is sufficient to recapitulate the voltage-dependent gating behavior and selectivity of sodium channels. The accessory β -subunits are important for subcellular membrane localization and for regulating the kinetics and voltage dependence of activation and inactivation of the channels. β -subunits are required for regulating the kinetics and voltage dependence of activation and inactivation of the channels. The β -subunits are single-pass type I integral membrane proteins, that contain immunoglobulin-like folds on the extracellular domain and may be linked either covalently (β_2) or non-covalently to the pore-forming α -subunit (Isom et al., 1995).

The principal α -subunit has four repeated homologous domains (DI-DIV). Each domain shares a high degree of sequence similarity and is homologous to the subunit of a tetrameric voltage-gated K^+ channel, K_V , with six transmembrane segments, S1–S6. The re-entrants loops (p regions) between the S5 and S6 from all domains come together to form the ion-selectivity filter (Sato et al., 1998). The fourth transmembrane segment (S4) of each domain contains positively charged amino acids (arginine or lysine) at every third residue. These positive charged residues drive the translocation of the S4 segment in response to changes in transmembrane potential, conferring voltage-sensitivity to channel gating. The intracellular loop between DIII and DIV is necessary for fast inactivation,

putatively acting in a “hinged-lid” mechanism to occlude the cytoplasmic mouth of the pore (Figure 1-1).

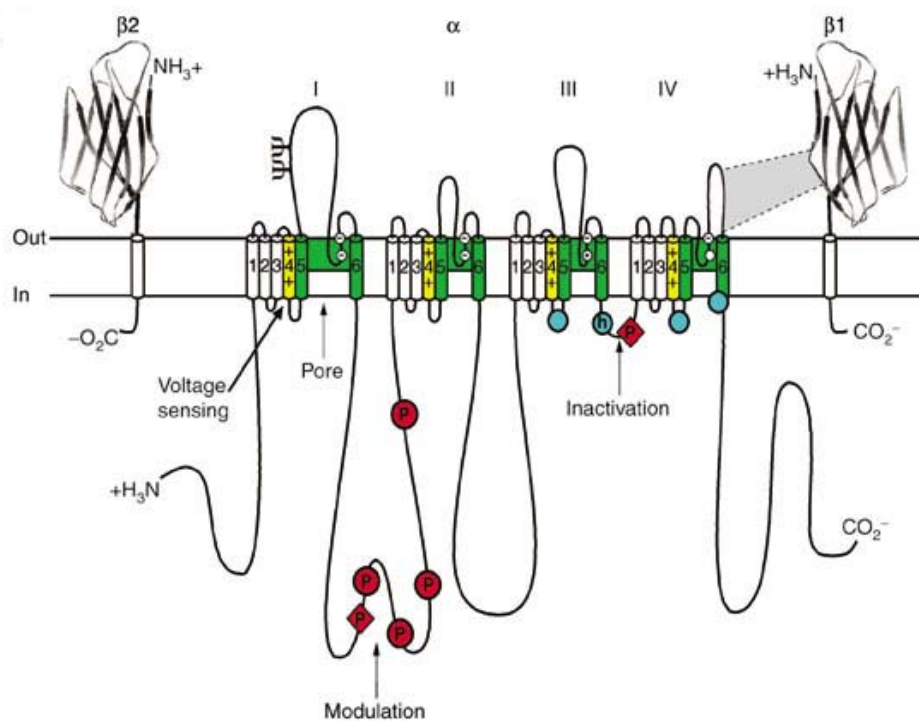


Figure 1-1. Structure of voltage-gated sodium channels. The α -subunit of the $Na_v1.2$ channel is illustrated together with the $\beta 1$ and $\beta 2$ subunits. Four domains are indicated with roman numerals; Blue circle with h inside in the intracellular loop of DIII and DIV indicates the inactivation gate; P label phosphorylation sites (circles, sites for protein kinase A; diamonds, sites for protein kinase C); ψ , indicate N-linked glycosylation site. (Yu and Catterall, 2003)

Sodium channels are widely expressed throughout the animal kingdom, also in prokaryotes. The primordial Na⁺ channel proteins in prokaryotes form a Na⁺ conductance with modest selectivity and voltage-dependent activation, although they contain only a single domain (Ren et al., 2001). To date, it has not been possible to obtain Na⁺ channel crystals suitable for determining the atomic structure of the channel.

Voltage-Gated Sodium Channel Family

Voltage-gated sodium channels have been identified in a variety of mammalian and non-mammalian species (Anderson and Greenberg, 2001; Goldin, 2002; Plummer and Meisler, 1999). Over this wide range of cellular contexts, these channels share remarkably similar functional and molecular characteristics, from humans to invertebrates.

Ten sodium channel α -subunit isoforms (Nav 1.1-Nav1.9 and Nav_x) and four for β -subunits have been cloned from human and rodent tissues (Goldin, 2001; Yu et al., 2003). The α -subunits isoforms are encoded by 10 distinct genes that were divided to four groups on the basis of the evolutionarily conserved features (Figure 1-2).

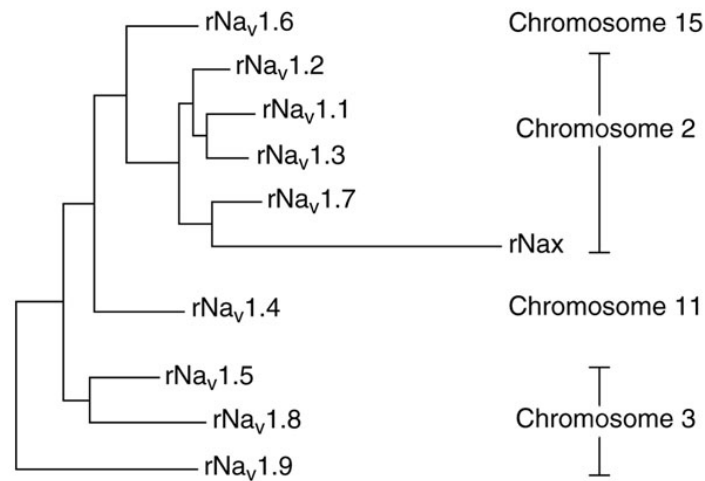


Figure 1-2. A phylogenetic tree of rat voltage-gated sodium channel α -subunits. (Yu and Catterall, 2003)

A cluster of sodium channel genes are located on chromosome 2 and encode the neuronal isoforms Nav_v1.1, Nav_v1.2, Nav_v1.3 and Nav_v1.7. These channels are sensitive to neurotoxin tetrodotoxin (TTX), with nanomolar sensitivity to block (Goldin et al., 2000; Ogata and Ohishi, 2002). A second cluster of sodium channel encoding genes is located on chromosome 3. This group includes cardiac Nav_v1.5, and neuronal Nav_v1.8 and Nav_v1.9 isoforms (Goldin et al., 2000). Nav_v1.5 is expressed both in heart cells and also in embryonic skeletal muscle. Postnatally, the Nav_v1.5 transcript level declines in skeletal muscle and Nav_v1.4 predominates. Upon denervation of skeletal muscle, the Nav_v1.5 transcript is up-regulated. Nav_v1.8 and Nav_v1.9 isoforms are preferentially expressed in peripheral sensory

neurons (Akopian et al., 1999; Dib-Hajj et al., 2002). In terms of amino acid sequence, these genes share approximately 75% similarity with the first group on chromosome 2. But some critical amino acids are not conserved, which makes these sodium channel isoforms resistant to TTX (Ogata and Ohishi, 2002). A single amino acid substitution in the DI pore forming region of these sodium channels causes a > 200 fold decrease in TTX sensitivity compared to the TTX sensitive sodium channel (Satin et al., 1992; Sivilotti et al., 1997). The Nav1.4 isoform is expressed in skeletal muscle and is the predominant isoform in adult innervated muscles. The localization of gene for Nav1.4 is on chromosome 17 or 11 for human or mouse respectively. Another isoform Nav1.6 is abundantly located in the central nervous system (CNS). The localization of the gene encoding Nav1.6 is on chromosome 15 for human (12 for mouse) (Goldin, 2002; Goldin et al., 2000). Nav1.4 and Nav1.6 have more than 85% identity in amino acid sequence, as opposed to the more distantly-localized Nav channels encoded on chromosome 2. In addition these two isoforms are blocked by nanomolar TTX concentrations. Their chromosomal localizations, however, suggest a distant separation from other two groups in evolutionary terms (Yu and Catterall, 2003). The tenth gene encoding Na_X is located on chromosome 2. Functional studies suggest that the function of Na_X may be a sensor of extracellular sodium level, rather than a conventional voltage-activated Na⁺-selective channel (Hiyama et al., 2002). The gene and protein nomenclature as well as tissue distribution and TTX

sensitivity for the voltage gated sodium channel family are summarized in Table 1-1.

Table 1-1 Mammalian sodium channel α-subunits				
Type	Gene Symbol	Chromosomal Location	Primary Tissues	TTX sensitivity
Nav1.1	<i>SCN1A</i>	Mouse 2 Human 2q24	CNS PNS	S
Nav1.2	<i>SCN2A</i>	Mouse 2 Human 2q23-24	CNS	S
Nav1.3	<i>SCN3A</i>	Mouse 2 Human 2q24	CNS (embryonic)	S
Nav1.4	<i>SCN4A</i>	Mouse 11 Human 17q23-25	skeletal muscle	S
Nav1.5	<i>SCN5A</i>	Mouse 9 Human 3p21	Uninnervated skeletal muscle, heart	R
Nav1.6	<i>SCN8A</i>	Mouse 15 Human 12q13	CNS, PNS	S
Nav1.7	<i>SCN9A</i>	Mouse 2 Human 2q24	PNS Schwann cells	S
Nav1.8	<i>SCN10A</i>	Mouse 9 Human 3p22-24	DRG	R
Nav1.9	<i>SCN11A</i>	Mouse 9 Human 3p21-24	PNS	R
Na _x	<i>SCN7A</i>	Mouse 2 Human 2q21-23	heart, uterus, smooth muscle, astrocytes, DRG	R

S: sensitive, R: resistant adapted from (Goldin et al., 2000; Ogata and Ohishi, 2002)

Gating Behavior of Voltage-Gated Sodium Channels

The gating properties of sodium channels are characterized by voltage-dependent transitions between several distinct channel states: closed, activated, fast inactivated and slow inactivated.

Activation

Sodium channel activation refers to the transition from closed to the open conformation of the channel. This transition is steeply voltage-dependent and occurs on a time scale of a millisecond or less. S4, the fourth transmembrane segment is highly conserved among all members of the voltage-gated ion channel super family. This structure plays a pivotal role as the voltage sensor within the voltage-gated sodium channels. S4 voltage sensors contain repetitively spaced positively charged residue separated by two hydrophobic residues, which forms an α helix through the membrane. When the membrane potential is depolarized, the change in the electric field across the cell membrane leads to the outward movement of one or more S4 helices (the number depending on the range of membrane depolarization) (Groome et al., 1999). This translocation induces a conformational change that favors opening of the pore (Catterall, 2000; Tombola et al., 2006). In support of this notion, neutralization of the positive-charged amino acid in S4 reduces the steepness for the voltage dependence of channel

gating (Groome et al., 1999; Ji et al., 1996; Kontis et al., 1997; Stühmer et al., 1989).

Fast inactivation

Inactivated channels are in a non-conducting state that is distinguished by the fact the channels are refractory from opening, even in the setting of on-going depolarization. Sodium channel inactivation has a major effect on regulating the availability of sodium channels, particularly at the termination of an action potential which renders the cell refractory and limits the maximal firing rate. Two forms of inactivation have been delineated: fast inactivation on a time scale of milliseconds and slow inactivation on a scale of hundreds of msec to seconds. Both forms of inactivation occur in all isoforms of voltage-gated sodium channels, and the molecular mechanisms involve distinct domains of the channel.

Fast inactivation occurs within milliseconds after the channel is activated by depolarization, within the time scale of a single action potential. The highly conserved intracellular loop between DIII and DIV is the generally accepted structure for the fast inactivation gate (Figure 1-1). The key motif is the IFM (Ile-Phe-Met), three hydrophobic residues. During channel activation, membrane depolarization induces translocation of S4 voltage sensors. The movement of the S4 voltage sensors, especially in DIII and DIV, exposes the binding sites (in the

S4-S5 linkers of DIII and DIV) (Popa et al., 2004) for the IFM inactivation gate. IFM motif undergoes hydrophobic interactions with the intracellular mouth of the pore to block it. Intracellular application of proteases eliminates fast inactivation (Armstrong, 1981) (Figure 1-3). Site-directed mutations in the IFM motif disrupt fast inactivation, and this defect can be restored by cytoplasmic application peptides containing the IFM residues (Eaholtz et al., 1994). The β -subunit is required for stabilizing normal fast inactivation in sodium channels (Chen and Cannon, 1995; Isom et al., 1992; Yang et al., 1993). The intracellular C terminus of sodium channel α -subunit also is important for stabilizing the inactivated state (Glaaser et al., 2006; Wu et al., 2005).

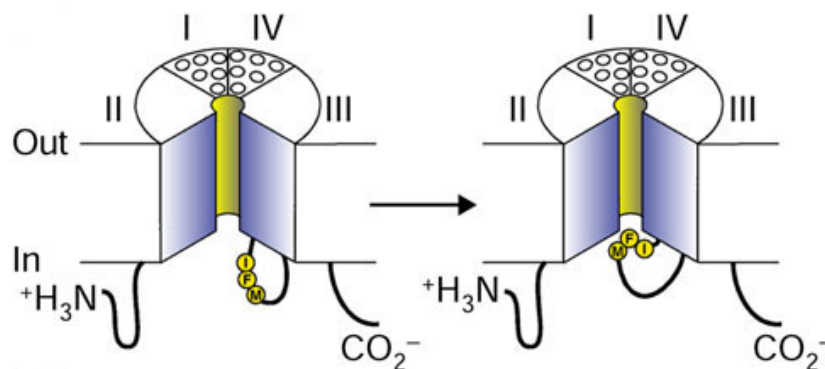


Figure 1-3. Schematic representation of inactivation structure of sodium channel. The intracellular loop between DIII and DIV of the sodium channel forms a hinged lid and occludes the pore during inactivation process. IFM motif labeled as yellow circles.

Fast inactivation has a marked effect on cellular excitability, both in physiological and pathological contexts. Disruption of fast inactivation may induce a sustained depolarization of membrane potential and thereby reduce cellular excitability, as occurs in the heritable muscle disease periodic paralysis (Cannon et al., 1991; Lehmann-Horn and Jurkat-Rott, 1999). Conversely, a subtle disruption of fast inactivation increases the susceptibility to after-discharges, which contributes to the pathogenesis of epilepsy or myotonia.

Slow inactivation

Slow inactivation is a distinct gating process of voltage-gated sodium channels, distinct from fast inactivation. Fast gating of sodium channels takes place over milliseconds. In comparison, slow inactivation occurs in response to prolonged membrane depolarizations lasting from hundreds of milliseconds to tens of seconds. Slow inactivation can also be induced by progressive accumulation during a burst of high-frequency discharges. In this way, slow inactivation may regulate the availability of Na⁺ channels on a longer time scale (seconds to minutes), thus may modulate cell excitability (Almers et al., 1983; Chandler and Meves, 1970; Ruff et al., 1988). Both the duration and the frequency of discharges have a powerful influence on the extent of sodium

channel slow inactivation, thus this inactivation gating maybe a basis for memory of neuronal activity (Toib et al., 1998).

Experimentally, slow and fast inactivation are distinguished on the basis of recovery from inactivation in a two-pulse protocol. Upon repolarization to -100 mV, recovery from fast inactivation occurs within a few msec. In contrast, the time course of recovery from slow inactivation often has a complex, multiple-component time course. A prominent component recovers with a time constant of 300-500 msec and has been termed intermediate inactivation (Kambouris et al., 1998; Veldkamp et al., 2000) “Slow inactivation” in a strict sense, refers to a component that recovers with a times constant of 1-3 sec. In extraordinary circumstances when channels are depolarized for several minutes, and ultra slow component can be detected which requires hundreds of seconds for recovery (Todt et al., 1999).

Fast and slow inactivations have distinct structural underpinnings. For example, obliteration of fast inactivation by adding protease into cytoplasm (Rudy, 1978) or introducing mutations in fast inactivation IFM gate do not impair slow inactivation (Cummins and Sigworth, 1996 ; Featherstone et al., 1996). While there is a weak negative coupling between fast and slow inactivation (e.g. slow inactivation has a faster onset when fast inactivation is impaired), these two forms of inactivation are not mutually exclusive (Featherstone et al., 1996; Richmond et

al., 1998). Moreover, the rapid recovery of the fast inactivation gate is not impeded in channels that are also slow inactivated (Vedantham and Cannon, 1998).

The precise molecular basis for slow inactivation is still unclear. Several lines of evidence indicate a conformational change of pore region (p region) is involved in slow inactivation. Chimeric studies with different Nav isoforms have provided some of the best evidence. Slow inactivation for the skeletal muscle Nav1.4 isoform is much more pronounced than for the cardiac Nav1.5 channel (as might be expected with the long duration of a cardiac action potential) (Featherstone et al., 1996; O'Reilly et al., 1999; Richmond et al., 1998). This distinct property between the two isoforms provided an opportunity to study the structure basis of slow inactivation gating. Replacing p regions of Nav1.4 by the corresponding structure of Nav1.5 makes a channel recapitulate the slow inactivation properties of Nav1.5 (Vilin et al., 1999). Even single amino acid within the DIIS5-S6 linker is critical for slow inactivation (Vilin et al., 2001). Disease-related mutations at the intracellular mouth of the pore in S6 segments disrupt slow inactivation (Bendahhou et al., 2000; Cummins and Sigworth, 1996; Hayward et al., 1997; Hayward et al., 1999; Struyk et al., 2000; Takahashi and Cannon, 1999; Veldkamp et al., 2000; Wang and Wang, 1997). Furthermore, slow inactivation is regulated by the ionic environment. Low external $[Na^+]$, which affects the surrounding area of the pore, enhances slow inactivation of sodium

channels (Townsend and Horn, 1997). Take together, the p region is a critical structure for slow inactivation gating in sodium channels.

A pivotal role for slow inactivation was first discovered in $Na_v1.4$ mutations associated with periodic paralysis. For the subset of $Na_v1.4$ mutations that disrupt slow inactivation, the predominant clinical phenotype is always periodic paralysis (Hayward et al., 1999). Dysfunction of slow inactivation was subsequently detected in sodium channelopathies in other diseases, such as idiopathic ventricular fibrillation and long-QT syndrome (Vilin and Ruben, 2001).

Skeletal Muscle Sodium Channelopathies

The membrane excitability of skeletal muscle fibers is critical for propagation of action potentials from the endplate to depolarize the transverse tubule (T-tubule) system and trigger excitation-contraction coupling. The first clear evidence of a sodium channel associated human muscle disease was obtained by Lehmann-Horn and colleagues who observed an aberrant sustained sodium current in muscle biopsies from patients with paramyotonia and hyperkalemic periodic paralysis (Lehmann-Horn et al., 1987; Lehmann-Horn et al., 1983). Subsequently, $Na_v1.4$ mutations associated with myotonia and periodic paralysis were identified (McClatchey et al., 1992; Ptacek et al., 1991; Rojas et al., 1991; Wagner et al., 1997). To date, five skeletal muscle sodium channelopathies

CMS is a group of rare inherited disorders with defective neuromuscular transmission and usually caused by mutations in both pre- and postsynaptic components of the neuromuscular junction, such as the nicotinic acetylcholine receptor (nAChR) (Engel et al., 2003). One $\text{Na}_v1.4$ missense (V1442E) is responsible for CMS (Tsujino et al., 2003). This mutation is localized near the S4 voltage sensor in DIV (Figure 1-4) and significantly enhances fast inactivation (33 mV hyperpolarized shift) for mutant channel. This severe loss-of-function for the mutant allele effectively causes a state of haploinsufficiency which impairs the fidelity of neuromuscular transmission by intermittent failure of a normal endplate potential to trigger a muscle action potential.

Four clinically distinct disorders of skeletal muscle excitability, with varying types of myotonia and/or periodic paralysis have been clearly linked to sodium channel defects (Cannon, 2002; Jurkat-Rott et al., 2010; Jurkat-Rott and Lehmann-Horn, 2005). All of these disorders are autosomal dominant. They are distinguished from each other mainly based on distinct clinical features. Figure 1-5 presents the clinical spectrum ranging from enhanced excitability in myotonia to the intermittent loss of excitability characterizing periodic paralyses. This group of disorders includes mutations in other voltage-gated ion channels (Cl^- , Ca^{2+} and K^+ channels) (Cannon, 2006). Interestingly patients in the center of this spectrum, which are all due to Na^+ channel mutations, may have both symptoms of myotonia and muscle weakness.

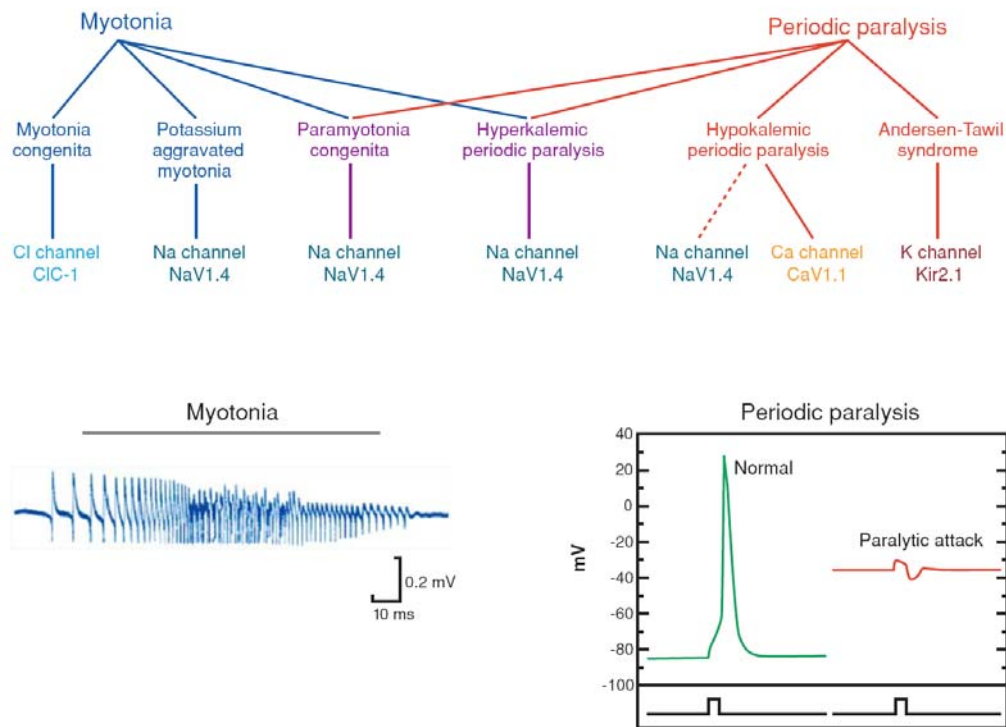


Figure 1-5. Clinical spectrum of the nondystrophic myotonias and periodic paralyses and their associated mutations in voltage-gated ion channels. The bottom part show an electromyographic recordings for a myotonic burst (left) and during an attack of periodic paralysis. (Cannon, 2006)

Potassium-Aggravated Myotonia

PAM is a purely myotonic disorder. Compared with PMC, HyperPP and HypoPP, by definition there is no weakness in PAM (Kubota et al., 2009;

Petitprez et al., 2008; Stunnenberg et al., 2010). The prevalence of PAM is estimated around 1:400,000 (Lehmann-Horn et al., 2004).

The attacks of PAM usually occur after strenuous work with a 10 to 30 min delay. The myotonic stiffness may last for several hours. This symptom may be improved by further contractions (warm-up phenomenon) and can be aggravated by taking potassium and other depolarization causing agents. That is the reason this disease is called potassium-aggravated myotonia (Heine et al., 1993; Mitrovic et al., 1995). Sometimes cold can may the symptoms worse.

Figure 1-4 gives an overview of the Na_v1.4 mutations associated with skeletal muscle diseases. Nine PAM associated mutations are described to date. Among them, G1306A/V/E mutations are localized in the inactivation gate near the IFM motif, suggesting an altered fast inactivation. These three mutations substitute one critical amino acid glycine which acts as the “hinge” for the “hinge-lid” inactivation model. Although these three mutations replace the same residue, their clinical symptoms are not identical. The severity of disorder is dependent on the divergence between the substituting amino acid and the original glycine. The symptoms are progressively more severe from alanine (A) to valine (V), and to glutamic acid (E) (Lerche et al., 1993; Mitrovic et al., 1994).

Studies using heterologous expression in human Embryonic Kidney 293 (HEK293) cells showed G1306A/V/E mutations decrease the rate of fast

inactivation and accelerate recovery from inactivation, whereas properties of slow inactivation are unaffected. In addition to disrupted channel inactivation, activation also altered by these mutations (Lerche et al., 1993; Mitrovic et al., 1994). To explain the symptoms of PAM, briefly, the impaired fast inactivation yield a larger inward sodium current, which increases the membrane excitability and triggers repetitive firing of action potential, finally causes the myotonia (Adrian and Marshall, 1976). Increasing potassium concentration can depolarize the sarcolemma and T-tubular membrane system, further facilitate muscle excitability, and thereby aggravate the symptoms.

Paramyotonia Congenita

The distinguishing feature of PMC is paramyotonia, which is myotonia that paradoxically worsens with repeated muscular contraction. A commonly associated finding is cold-induced muscle stiffness. The symptoms of PMC usually last an hour, which is much shorter in comparison with PAM (several hours). Patients may show mask-like face in low temperature, and cannot open eyes for several seconds even to minutes. With a further decreased temperature, instead of stiffness, muscles may become inexcitable to produce periodic paralysis. Attacks of PMC can be triggered by rest after exercise or taking potassium and also can occur spontaneously. Warm conditions remit the

symptoms. The prevalence of PMC is estimated about 1:200,000 (Lehmann-Horn et al., 2004).

There are sixteen PMC associated $\text{Na}_v1.4$ mutations are identified (Figure 1-4). Electrophysiology studies revealed slower onset of fast inactivation and faster recovery rate (Chahine et al., 1994; Goldman, 1999). Similar to the mechanism for PAM, mutant channels have an increased sodium current, and thus the muscles become hyperexcitable. A recent study suggested resurgent Na^+ currents may also contribute to the pathogenesis of PMC (Jarecki et al., 2010). Resurgent Na^+ currents refer to re-opening for a small fraction of Na^+ channels upon repolarization at the end of an action potential. This phenomenon was first detected in cerebellar Purkinje cells, and in fact has never been documented for Na^+ channels in skeletal muscle. Resurgent currents are produced by rapid open-channel block by an endogenous particle (perhaps the $\beta 4$ subunit) that competes for binding with the fast inactivation gate. The slower rate of fast inactivation for PMC mutant channels could, in principle, increase the likelihood of endogenous open-channel block, thereby increasing the resurgent current.

As mentioned above, attacks of PMC may be precipitated by cold conditions. Therefore, the temperature sensitivity of gating was investigated for PMC mutant channels. Nearly all studies indicate there is no significant altered sensitivity to temperature for PMC associated channel mutations (Dice et al., 2004;

Fleischhauer et al., 1998; Lerche et al., 1996). One possibility is that cold sensitivity arises from a threshold effect. The rate of fast inactivation is slowed by cooling for both wild type (WT) and mutant channels. Because PMC mutant channels start at a slower rate of inactivation, however, cooling will cause these channels to cross a critical point (before WT) where the decreased rate of inactivation triggers myotonia. In addition, a recent study suggests the slow inactivation is temperature dependent, which may contribute to the temperature sensitivity of this disease (Webb and Cannon, 2008).

In addition to the predominant symptom of myotonia, PMC patients also may suffer from episodic weakness as described below for PAM-PMC-HyperPP.

Hyperkalemic Periodic Paralysis

In the late nineteenth century, periodic paralyses were firstly described as a skeletal muscle disorder. Subsequently, physicians observed deviations in serum potassium levels occurred during attacks of weakness (Biernacki and Daniels, 1934; Gamstorp, 1956). Moreover, administration of potassium salts could hasten recovery from attacks in some families while in others this same intervention triggered attacks. These clinical observations led to the delineation of separate forms of periodic paralysis classified into HyperPP, HypoPP, and normokalemic periodic paralysis (NormoPP).

A main feature of HyperPP is episodic attacks of muscle weakness combined with an elevated serum potassium levels. However, this increase in serum potassium is not constantly observed in HyperPP patients. In one comprehensive study, only half of the HyperPP patients showed hyperkalemia (Fontaine, 2008). The provocation of weakness by potassium ingestion is another feature used to diagnose HyperPP. In addition to oral potassium loading, HyperPP also can be triggered by rest after exercise, fasting and cold exposure. HyperPP tends to have a milder phenotype in women compared to men. Attacks usually start during the first decade of life, and last from minutes to several hours. A chronic progressive myopathy, which can result in a permanent muscle weakness, may develop at late stage (fourth or fifth decade of life). The prevalence of familiar HyperPP is still unclear but is estimated to be around at 1:100,000. Although it is a periodic paralysis disease, more than half of HyperPP patients also show mild myotonia, which can be diagnosed by clinical exam or as latent myotonia by electromyography (EMG) (Plassart et al., 1994).

An anomalous TTX-sensitive current was observed in muscle fibers dissociated from HyperPP patients (Lehmann-Horn et al., 1987). The first gating defect identified in periodic paralysis was an increase in the persistent Na^+ current for cultured myotubes derived from HyperPP patients and manifest as bursts of mutant channel re-openings during a sustained voltage-clamp depolarization (Cannon et al. 1991). T704M and M1592V (Figure 1-4) are the two most

common Nav1.4 mutations associated with HyperPP. Studies of T704M in heterologous systems indicate a hyperpolarized shift in the voltage dependence of activation (Cummins et al., 1993; Yang et al., 1994) and a depolarized shift in the steady state fast inactivation (Yang et al., 1994). Subsequently, a defect of slow inactivation was detected for HyperPP mutations (Cummins and Sigworth, 1996; Hayward et al., 1997; Hayward et al., 1999). Sustained sodium current also was reported for HyperPP mutants expressed in heterologous systems (Cannon and Strittmatter, 1993; Cummins et al., 1993; Rojas et al., 1999; Yang et al., 1994).

PAM-PCM- HyperPP: Gain-of-Function Defects

All mutations associated with the PAM–PMC–HyperPP complex share a common feature, gain-of-function defects (Cannon, 1997). Missense mutations in the same ion channel protein (Nav1.4) cause a spectrum clinical of phenotypes, from pure myotonia (PAM) to mixed myotonia/paralysis (PMC and HyperPP). The mechanisms that underline these various phenotypes are illustrated in Figure 1-6.

The functional consequences of the gain-of-function defects (due to impaired inactivation and for some cases due to an enhancement of activation) on muscle excitability are bimodal. Mutations with a more subtle gain-of-function defect increase excitability because more Na⁺ channels remain available at the end of an

action potential. This effect promotes the repetitive discharges that underlie myotonia. Other mutations with more pronounced gain-of-function defects may cause susceptibility to sustained depolarized shifts in resting potential (V_{rest}), especially in the setting of elevated extracellular potassium. During these episodes, the vast majority of Na^+ channels are inactivated which results in a loss of excitability and paralysis.

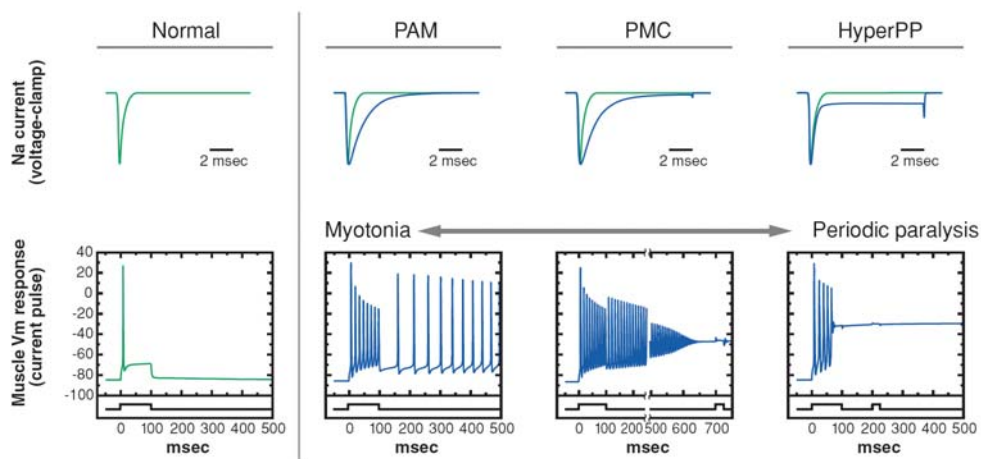


Figure 1-6. The mechanisms underlie the symptoms of PAM, PMC and HyperPP, gain-of-function mutations (Cannon, 2006)

In addition to altered fast gating, HyperPP and PMC mutations often impair slow inactivation (Hayward et al., 1999). In contrast, all PAM (pure myotonia)

associated mutations have normal slow inactivation. The persistent current arising from a disruption of fast inactivation will normally be attenuated within a few seconds by slow inactivation. When slow inactivation is also disrupted, however, then the propensity of depolarization induced attacks of weakness is greatly enhanced (Hayward et al., 1997).

HypoPP: an emerging picture of Na⁺ channel Loss-of-Function Mutations and gating pore leak currents.

The cardinal features of HypoPP are recurrent attacks of flaccid muscle weakness associated with a decreased serum potassium level and the absence of myotonia. The onset age is the second decade. In comparison with HyperPP, HypoPP attacks last longer and more severe (Elbaz et al., 1995). Attacks usually occur after exercise or are triggered by taking carbohydrates. The penetrance of HypoPP is incomplete, especially for women. The prevalence of this disease is estimated at 1:100,000, similar to HyperPP (Buruma and Schipperheyn, 1979).

HypoPP are linked to mutations in two voltage-gated ion channels, Cav1.1 and Nav1.4 (Bulman et al., 1999; Fontaine et al., 1994; Jurkat-Rott et al., 1994; Jurkat-Rott et al., 2000). Mutations in Nav1.4 account for ~10% of HypoPP patients, whereas the more commonly occurring missense mutations in Cav1.1 are found in ~70% of HypoPP families (Sternberg et al., 2001).

Up until 1999, the general consensus was that mutations of $\text{Na}_V1.4$ were associated with disorders in the Myotonia-HyperPP spectrum, whereas HypoPP was caused by missense mutations of $\text{Ca}_V1.1$. The report by Bulman and colleagues (Bulman et al., 1999) of $\text{Na}_V1.4\text{-R669H}$ in HypoPP was followed by the discovery of 7 additional missense mutations of $\text{Na}_V1.4$ in HypoPP families. Amazingly, all 8 mutations are missense substitutions of arginines in S4 voltage-sensing segments (Figure 1-4). Electro-physiological studies of HypoPP associated $\text{Na}_V1.4$ mutations revealed an enhanced fast or slow inactivation (Jurkat-Rott et al., 2000; Struyk et al., 2000), which cause loss of channel function. These gating defects are predicted to reduce the availability of sodium channels thereby lead to decreased membrane excitability and muscle paralysis. They do not, however, account for the aberrant depolarization during attacks of weakness or the sensitivity to hypokalemia.

To date, 8 HypoPP associated $\text{Na}_V1.4$ mutations have been identified, with all being missense mutations at arginines in S4 voltage sensors. Recently, a novel current was detected for these HypoPP mutations (Sokolov et al., 2007; Struyk and Cannon, 2007). This small amplitude current flows through an alternative pathway (S4 gating pore) rather than the traditional ion conducting pore, and so is called gating pore current (Figure 1-7). Similar gating currents (ω -currents) have been observed in Shaker K^+ -channels with substitution mutations at arginines in S4 voltage sensor (Starace and Bezanilla, 2001; Tombola et al., 2005).

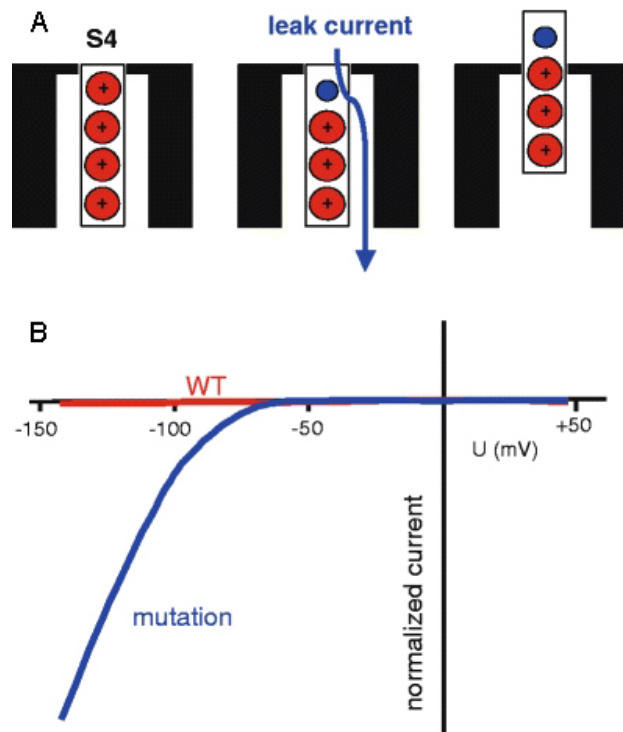


Figure 1-7. Gating pore current. A. substitution of a outermost arginine (red) by a smaller amino acid (blue) produces a conductive pathway activated at hyperpolarized potentials. B. Hyperpolarization-activated gating pore current associated with S4 arginine mutation. (Jurkat-Rott et al., 2010)

All six HypoPP mutations in DIIS4 and DIII S4 (R669H, R672H/G/C/S, and R1132Q) have been studied in *Xenopus laevis* oocytes with the cut-open oocyte voltage clamp (COVC) technique. All of them produce hyperpolarization-activated gating pore currents (Francis et al., 2010; Sokolov et al., 2007; Struyk and Cannon, 2007; Struyk et al., 2008). These gating pore currents are active at

the resting potential and oppose the “outward limb” of the inward rectifier potassium current ($I_{K_{ir}}$) that maintains V_{rest} just slightly depolarized from E_K .

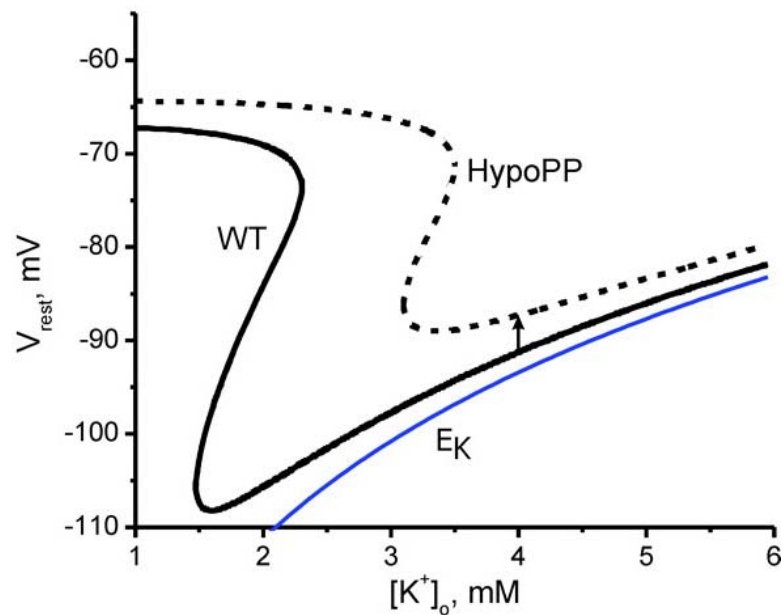


Figure 1-8. Resting potential as a function of $[K^+]_o$ for simulated WT and HypoPP muscle fibers. (Cannon, 2010)

As extracellular K^+ is lowered, the contribution of the inward rectifier current is diminished. For drastic reductions in K^+ , about 1.5 mM, the inward rectifier current is insufficient and V_{rest} is decoupled from E_K . Instead, the balance on inward and outward currents does not occur until the membrane is depolarized enough to activate the delayed rectifier K^+ channels (about -50 mV).

Consequently, skeletal muscle is susceptible to a paradoxical depolarization of V_{rest} at very low external K^+ . The anomalous gating pore current in HypoPP mutants causes this transition to occur at higher concentrations of external K^+ , about 2.5 to 3 mM (Struyk et al., 2008). Consequently, the relation between external $[K^+]$ and V_{rest} is highly non-Nernstian, with the catastrophic break point for paradoxical depolarization being shifted to higher $[K^+]$ in the presence of a gating pore current (Figure 1-8, (Cannon, 2010))

Chapter Two : Gating Behavior of Sodium Currents in Adult Mouse Muscle Recorded with an Improved Two-Electrode Voltage Clamp

Introduction

The voltage gated sodium channel is responsible for the initial rapidly depolarizing phase and propagation of the action potential in electrically excitable cells, including skeletal muscle, heart cells, neurons and secretory tissue. In adult skeletal muscle, the major type of voltage-gated Na⁺ channel is Na_v1.4. Until now, over 50 mutations in *SCN4A*, the gene encoding the pore-forming α subunit of Na_v1.4 channel, have been found and linked with several neuromuscular disorders (Cannon, 2006). Although enormous studies using heterologous expression systems, such as human HEK293 and *Xenopus laevis* oocytes (Hayward et al., 1999; Rojas et al., 1999; Struyk et al., 2000) have clarified the Na_v1.4 channel gating behavior and the dysfunction of these disease associated Na_v1.4 channel mutations, it is still unclear how mutant Na_v1.4 channels behave in their native milieu, skeletal muscle fibers.

The obstacle for analyzing Na_v1.4 function in situ is the inherent difficulty obtaining reliable voltage control over the long, cylindrical muscle fibers. Spherical cells are commonly used for electrophysiology study because the membrane potential is uniform at all points of the cell surface (space-clamped). In

contrast, long thin cylindrical cells act as a linear cable, which has a more complex response. Because of the effect of the series resistance along the cylindrical membrane (Figure 2-1), the voltage drops along the membrane length and it is very difficult to control the membrane potential over the entire cylindrical cell. Another difficulty for characterizing Na^+ current behavior in skeletal muscle fibers is the requirement of high-speed voltage clamp over large cylindrical cells ($> 300 \text{ pF}$). The kinetics of Na^+ channel fast gating occurs in milliseconds. Compared with HEK293 cells, rapid voltage control of skeletal muscle fibers would require large current injection in short time over long cylindrical cells.

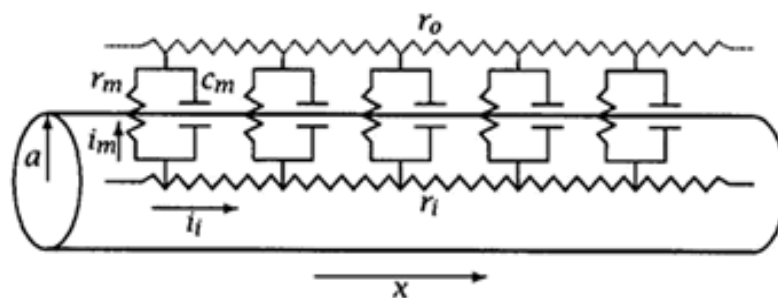


Figure 2-1. Diagram for current flow in a cylindrical cell such as muscle fiber. r_m , membrane resistance per unit length; c_m , membrane capacitance per unit length; r_o , external resistance per unit length; i_m , membrane current per unit length; i_i , internal current per unit length; r_i , internal resistance per unit length; x , the length of the cylinder cell; a , the radius of the cylinder cell. Taken from Foundation of cellular neurophysiology, the MIT Press.

Although cable properties impede the study of Na^+ channel behavior in muscle fibers, several groups have made great effort to characterize Na^+ currents in situ. In 1977, Adrian et al. described a method which allows the approximate computation of Na^+ current from measurements with three electrodes in the mid-region of a muscle fiber (Adrian and Marshall, 1977). This method calculated the membrane current according to the change of membrane voltage at two widely separated recording electrodes. This method is useful for obtaining quantitative coarse description of ionic currents in muscle fibers. Even with the computational correction for (linear) cable properties, the fundamental problem remains that the voltage-clamp control is poor over the length of the fiber. Moreover, the series resistance introduced by transverse tubules (T-tubule) impedes adequate voltage control. Another technique was used in 1980 by Pappone (Pappone, 1980). These studies in rat skeletal muscle were based on the Vaseline-gap technique developed by Hille and Campbell (Hille and Campbell, 1976). The Vaseline seals enable the isolation of membrane current flowing through a short length of the fiber. This method permits better voltage control than the three-electrode method, although the T-tubule problem remains. This method requires cutting the fiber ends, however, to allow the solution in the end pools to diffuse into the fiber. Consequently, the intracellular milieu was altered, potentially disrupting the effect of cytoplasmic modulators of channel gating. A third method for studying intact skeletal muscle fibers used a loose-patch voltage-clamp technique (Roberts and

Almers, 1984; Ruff, 1999). When pushed the recording pipette is pushed against the cell surface, the pipette will electrically isolate a membrane patch. To decrease the contamination by uncontrolled current across the sarcolemma membrane beneath the pipette wall, the modified method used concentric pipette and collected data only from the central region of a large cell patch. Because this method uses a large pipette to make a loose patch to record the current, it inevitably suffers from a large leak currents. Additionally, because the loose patch method works as a cell attached patch, the measured membrane potential is estimated by subtracting the intrinsic sarcolemmal resting potential (V_{rest}) from the command potential ($V_{command}$). The exact value of the intrinsic sarcolemmal V_{rest} in an individual fiber is difficult to control during loose patch recordings and spontaneous shifts in V_{rest} will reduce the accuracy of measuring the voltage dependence of gating within a margin of error of only a few mV, as is necessary to characterize disease mutants. Another method of recording Na^+ currents from muscle is to use myoball/myotubes derived from cultured myoblast cells (Probstle et al., 1988). A major disadvantage of using this approach is that although the myoball/myotubes can mimic many aspects of the fully differentiated myocytes, it is still an immature system. Moreover, channel behavior is dependent on culture conditions. Yet another problem is the high expression level of Nav1.5 channels (cardiac and denervated muscle isoform). Whole cell (Wang et al., 2005) and cell attached (Morel et al., 2010; Rannou et al., 2009) patch-clamp techniques also

have been used to study Na^+ current in skeletal muscle fibers. For whole-cell patch clamp studies, short muscle fibers and low resistance pipettes were used to allow a better control of the space clamp. But it is still questionable whether the clamp speed is fast enough for characterizing fast gating behavior of sodium channel, and the T-tubule problem remains. For cell attached patch clamp, it is difficult to compensate for shifts in the resting potential. Using high external K^+ solutions to null V_{rest} is not a solution, because the gating behavior of $\text{Na}_v1.4$ is modified by shifts in V_{rest} (Filatov et al., 2005). In addition, both techniques require making gigaseal, which is difficult because of the extracellular matrix in differentiated skeletal muscle fibers.

Because muscle fibers are huge cells compared to HEK293 cells, they can endure the insertion of two microelectrodes without causing severe damage. Two-electrode voltage clamp (TEVC) with sharp electrodes does not require gigaseal, and keeps the internal cytoplasm intact. The purpose of this project is to optimize the TEVC sharp microelectrode technique to characterize the Na^+ current in intact adult mouse skeletal muscle fibers while alleviating many of the problems described above. Computer simulation confirmed the recording conditions were favorable for accurately characterizing Na^+ current in skeletal muscle fibers. Using this method we obtained a more accurate description of Na^+ channel behavior in situ and assessed the functional impact of disease-associated missense mutations on gating properties of mutant $\text{Na}_v1.4$ channels.

Materials and Methods

Muscle Fiber Preparation

Individual muscle fibers were isolated by enzymatic digestion and mechanical disruption from mixed muscles of the hind foot of adult C57/Bl6 mice (age 2 – 6 months). Animals were sacrificed by isoflurane inhalation and cervical dislocation, in accordance with guidelines by our Institutional Animal Care and Use Committee. The muscle was rapidly dissected free and placed in DMEM plus 1 mg/ml collagenase (Gibco, Grand Island, NY). The muscle was incubated at 37 °C for 90 minutes. Fibers were dissociated by trituration in a wide-bore pipette, pelleted by centrifugation, and resuspended in DMEM plus 10% fetal bovine serum, 1% glutamine, 100U/ml Penicillin/streptomycin and 10mM HEPES. Approximately 100 fibers were plated in 35 mm culture dishes coated with rat tail collagen and matrigel (BD Biosciences, San Jose, CA). Cultures were maintained for 1 to 3 days in 5% CO₂ at 37 °C.

Voltage Clamp Recording

Currents were recorded with the two-electrode voltage clamp (TEVC) technique, using an AxoClamp2B amplifier (Molecular Devices, Sunnyvale, CA) with the HS-2A headstage. Fibers were visualized on an inverted microscope (IMT-2 Olympus, Center Valley, PA) with Hoffman optics. Disruption of the T-

tubule system from the sarcolemma was achieved by hyperosmolar shock in Ringer's solution plus 400 mM glycerol for 1 hr, and the fibers were then returned to isomolar Ringer's solution for 30min before recording (Dulhunty and Gage, 1973). Isolated fibers adherent to the collagen/matrigel coated dish and < 600 μm in length were selected for recording by impalement near their midpoint with both stimulating and recording sharp microelectrodes. The standard bath was a Cl-free low- Na^+ solution containing NaOH 10 mM, tetraethylammonium hydroxide (TEAOH) 130 mM, $\text{Mg}(\text{OH})_2$ 1 mM, $\text{Ca}(\text{OH})_2$ 1 mM, 4-(2-hydroxyethyl)-1-piperazineethanesulfonic acid (HEPES) 10 mM, glucose 10 mM, 4-aminopyridine (4-AP) 5 mM, anthracene-9-carboxylic acid (9-AC) 100 μM , nifedipine 5 μM , pH adjusted to 7.4 by methanesulfonic acid. Dantrolene 3 $\mu\text{g}/\text{ml}$ and the skeletal muscle myosin II inhibitor N-benzyl-p-toluene sulphonamide (BTS) 20 μM (Cheung et al., 2002) were added to suppress depolarization-induced contraction in studies on fibers with intact T-tubules. The extracellular Na^+ concentration was lowered to 10mM to reduce the current amplitude and thus to improve the voltage control. The current injection pipette was filled with 2 M Cs-Aspartate (resistance of 3-5 $\text{M}\Omega$) and the voltage sensing electrode contained 3 M CsCl (resistance 7-10 $\text{M}\Omega$). All measurements were performed at room temperature.

Voltage-clamp control, current recording, and analysis of traces were performed using pClamp9.2 (Axon Instruments, Foster City, CA). Sodium

currents were elicited by step depolarizations from holding potential of -100 mV. Leak compensation was performed by using a conditioning pulse to inactivate Na^+ channels and thereby characterize the (nonlinear) background currents, see RESULTS for details. Measured values are presented as the mean \pm standard error of the mean unless otherwise noted.

Model Simulation

A finite-length cable model was used to simulate the spatial-temporal voltage response, $V(x,t)$ of a short muscle fiber of length l , voltage clamped at the midpoint ($x = 0$). The model does not include a radial component because fibers in this study were detubulated. The passive linear cable model was modified to replace the Ohmic term that represents the transmembrane current per unit length, $V(x,t)/r_m$, by the sum of the ionic currents, I_{ionic_j} , contributed by the sarcolemmal conductances.

$$c_m \frac{\partial V(x,t)}{\partial t} + \sum_j I_{ionic_j} = \frac{1}{r_i} \frac{\partial^2 V(x,t)}{\partial^2 x} \quad \text{Eq. 1}$$

where c_m is the capacitance ($\mu\text{F}/\text{cm}$) and r_i is the internal resistance (Ω/cm) per length. The fiber dimensions were modeled as $l = 450 \mu\text{m}$ and radius of $a = 28 \mu\text{m}$, which represent the mean values for the population for fibers selected for study. With this fiber radius, and a specific capacitance of $1.0 \mu\text{F}/\text{cm}^2$ and specific internal resistance of $150 \Omega\text{-cm}$, the parameters for the cylindrical representation per unit length in Eq. 1 are $c_m = 18 \text{ nF}/\text{cm}$ and $r_i = 6.1 \text{ M}\Omega/\text{cm}$. Under the recording conditions used herein to block K^+ , Ca^{2+} , and Cl^- currents, the ionic conductances were modeled as the sum of an Ohmic leak conductance plus a voltage-gated Na^+ conductance simulated with the Hodgkin-Huxley model.

$$\sum_j I_{ionic_j} = G_{leak}(V - E_{leak}) + m^3 h G_{Na}(V - E_{Na}) \quad \text{Eq. 2}$$

The equations to simulate m and h kinetics, and the parameter estimates based on recordings from mouse foot pad muscle are presented in Appendix A. The muscle fiber was considered to be sealed at the ends, which sets the boundary condition $\partial V(\pm l/2, t)/\partial x = 0$. The voltage clamp condition was applied at the center of the fiber, $x = 0$, and step voltage commands, $V(0, t)$, were simulated by one- or two-component exponentials. Numerical integration was performed over half the fiber length, $0 < x < l/2$, since the fiber was symmetrical about the point at which the

command voltage was applied ($x = 0$). The axial current at $x = 0$ that is flowing toward $x > 0$ represents half of the total current passed by the current-electrode (ionic and capacitive currents in the membrane, I_{mem}) was computed as:

$$I_{mem}(t) = -\frac{1}{r_i} \frac{\partial V(0,t)}{\partial x} . \quad \text{Eq. 3}$$

The total Na^+ current conducted over the entire length of the fiber, $I_{Na}(t)$, was computed as:

$$I_{Na}(t) = 2 \int_0^{l/2} m(x,t)^3 h(x,t) [V(x,t) - E_{Na}] dx . \quad \text{Eq. 4}$$

Solutions to the nonlinear finite-cable equation were computed with Mathematica 7.0 (Wolfram Research, Champaign, IL).

Results

Passive Properties of Skeletal Muscle Fibers

Muscle fibers varied in length from 350 to more than 600 μm . We selected fibers $< 600 \mu\text{m}$, as measured optically with a reticle, and the group in this study

had a mean length of $455 \pm 9 \mu\text{m}$ and a diameter of $56 \pm 1 \mu\text{m}$ (Figure 2-2A). Osmotic shock with 400 mM glycerol was effective in detubulating fibers, as demonstrated by an acceleration of the capacitance transient elicited by a 10 mV depolarization from a holding potential of -100 mV (Figure 2-2B). The apparent specific capacitance, defined as $C_{\text{app}} = (Q/\Delta V) / (2\pi al)$ decreased from $4.3 \pm 0.2 \mu\text{F}/\text{cm}^2$ in control fibers to $2.1 \pm 0.1 \mu\text{F}/\text{cm}^2$ after detubulation. With our recording conditions to isolate Na^+ currents (TEA, 4-AP to block K^+ currents, 9-AC, nifedipine to block L-type Ca^{2+} current), the steady-state I-V relation measured by TEVC applied at the center of the fiber was linear with a slope conductance of $350 \pm 5 \text{ nS/nF}$ ($0.74 \text{ mS}/\text{cm}^2$), and decreased to $46 \pm 0.9 \text{ nS/nF}$ ($0.097 \text{ mS}/\text{cm}^2$) with removal of Cl^- to reduce Cl^- current (Figure 2-2C). Alternatively stated, the average input resistance, R_{in} , was $11 \text{ M}\Omega$ for the detubulated Cl^- -free condition, which was used for following experiments.

By applying the linear finite-length cable model¹, and assuming a myoplasmic resistance of $R_i = 150 \Omega\text{-cm}$ with a fiber length of $450 \mu\text{m}$ and radius of $28 \mu\text{m}$, the computed length constant based on the measured R_{in} is $\lambda = 0.28 \text{ cm}$. The corresponding specific conductance is $G_{\text{leak}} = 120 \pm 8 \mu\text{S}/\text{cm}^2$. Thus, in Cl^- -free conditions with K^+ and Ca^{2+} channels blocked, food pad muscle

¹ For a finite cable of length, l , with current injected at the center, $R_{in} = \frac{1}{2} r_i \lambda \coth((l/2)/\lambda)$.

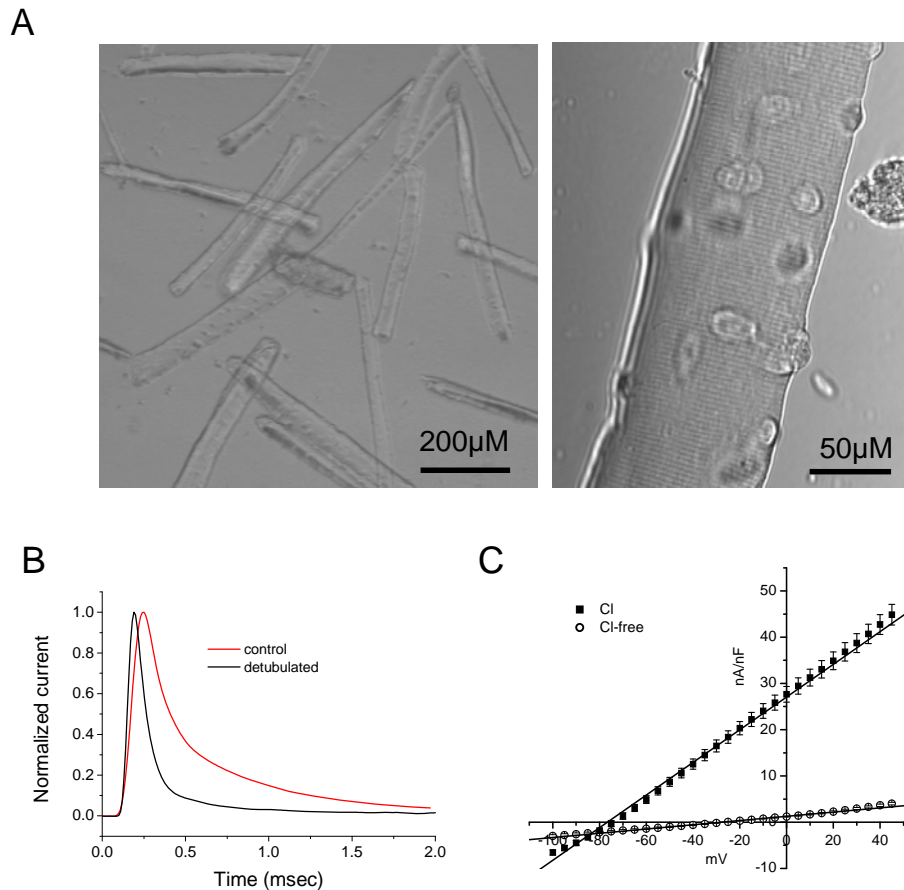


Figure 2-2. Passive properties of mouse skeletal muscle fibers. (A) Photomicrograph of dissociated fibers viewed at low magnification with phase contrast to show fiber length / width ratio (left) and at higher magnification with DIC optics (right) to show fiber integrity and schematically indicate the orientation of microelectrodes. (B) Membrane currents elicited by a depolarization of 10 mV from -100 mV are normalized to peak amplitude and superimposed to illustrate the reduction in apparent capacitance by detubulation. Peak currents were 83 nA and 81 nA for control and detubulated fibers with associated capacitances of 3.5 nF and 1.6 nF. (C) Average steady-state current-voltage relation for detubulated fibers, normalized by fiber capacitance, was linear with a slope conductance of 350 ± 5 nS/nF $n = 23$ that decreased to 46 ± 0.9 nS/nF $n = 30$ in Cl-free bath.

fibers are on the order of 0.16λ in length. When a Cl-containing bath solution was used, $R_{in} \sim 1.7 \text{ M}\Omega$ which equates to $\lambda = 0.11 \text{ cm}$ or a fiber length of 0.4λ and a specific conductance of $790 \pm 51 \mu\text{S}/\text{cm}^2$. This relatively small change in λ implies the chloride conductance is not predicted to degrade the spatial control of the clamp potential in short muscle fibers. For example, even in a Cl-bath, the steady-state voltage change at the end of a $450 \mu\text{m}$ fiber will reach 96.8% of the value imposed at the midpoint.

Constraints on Clamp Speed

Rapid depolarization of the membrane in a near step-like fashion is essential to accurately characterize the gating properties of voltage-gated Na^+ channels. Channel activation occurs on a time scale of $50 \mu\text{sec}$, and voltage-clamps that settle experimentally with a time constant of $> 100 \mu\text{sec}$ produce distortion because activation will be prolonged and overlap with the onset of inactivation. The voltage response at $x = 0$, measured for a typical foot pad muscle fiber under TEVC recording, is shown in Figure 2-3A. A bi-exponential fit had time constants of $18 \mu\text{sec}$ (76%) and $190 \mu\text{sec}$ (24%). The computed delay and attenuation of the voltage transients at $l/4$ and $l/2$ (end) in response to a voltage

clamp applied at $x = 0$ for a 450 μm fiber in a Cl-free bath are shown in Figure 2-3B, which demonstrates that very little distortion of the clamp potential is predicted over these fibers. As a worst case scenario, the computed response is also shown for a fiber of length 600 μm , the upper limit of our exclusion criteria (Fig 2-3B, dashed lines). Another method to characterize the clamp speed of a muscle fiber is to consider the hypothetical scenario of a very fast clamp at $x = 0$, and then determine the effective clamp time constant by fitting the simulated voltage transient at different locations along the fiber. In simulations with a rapid single-exponential clamp (10 μsec) applied at $x = 0$, the voltage transients at $l/4$ and $l/2$ were fit well by a single exponential. Because the fiber length was relatively short ($< 0.5 \lambda$), the time constants for the membrane voltage transients were nearly equal at $l/4$ and $l/2$ ($\sim 4\%$ difference). For a simulated fiber of 450 μm , the time constant was 25 μsec . When the fiber length was increased to the maximum allowable size of 600 μm , the time constant increased to 40 μsec . The implication of this simulation is that no matter how well a fiber is clamped for a step input command at $x = 0$, the passive cable properties impose a low-pass filter that results in voltage transients having time constants with a minimum of 25 – 40 μsec for fibers of 450 – 600 μm in length. One caveat is that this analysis does not take into account the dramatic reduction of R_{in} (shorter λ) that occurs when Na^+ channels are activated by larger depolarizations (see below).

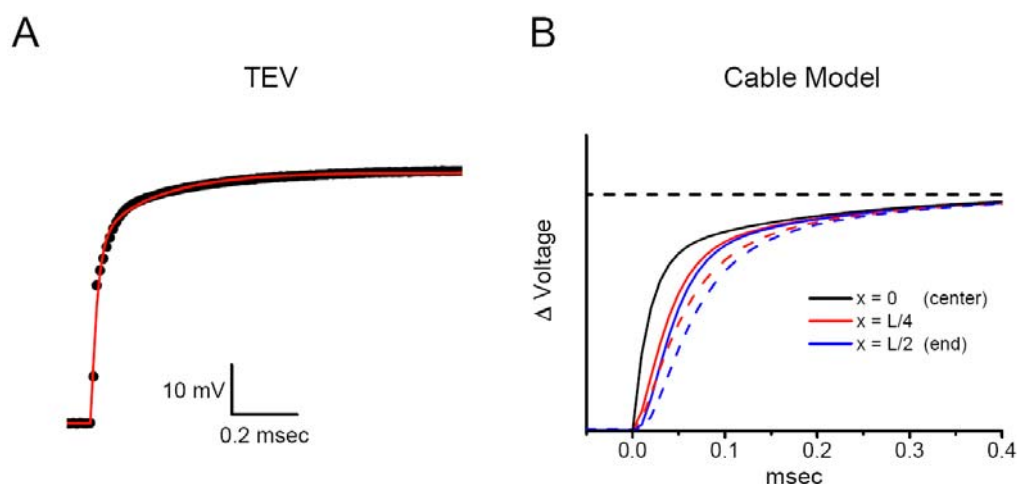


Figure 2-3. Fiber effects on voltage-clamp speed. Attenuation and delay of voltage clamp due to the leak conductance is shown for a typical mouse foot pad fiber in Cl-free bath ($G_{leak} = 120 \mu\text{S}/\text{cm}^2$; $G_{Na} = 0$). (A) Voltage transient recorded at $x = 0$ for a 50 mV step voltage command. Red line shows a double exponential fit with $\tau_{fast} = 0.018$ msec (76%) and $\tau_{slow} = 0.19$ msec (24%). (B) Computed voltage clamp transient (Eq. 1) midway out to the end of the fiber (red line, $x = l/4$) and at the end of the fiber (blue line, $x = l/2$) using the double-exponential fit for voltage clamp at $x = 0$ as the input for a 450 μm fiber. Dashed lines show the respective transients computed for a 600 μm fiber.

Voltage-Clamp Control is Not Possible in Physiological Na^+

While the cable model predicts accurate voltage-clamping of footpad skeletal muscle fibers is possible for the background leakage conductance, TEVC recordings showed pronounced series resistance (R_s) errors when large Na^+ currents were elicited by depolarization in physiological saline (145 mM Na^+). Figure 2-4A shows the characteristic features of an R_s error with a delayed

acceleration of high-amplitude Na^+ currents for moderate depolarization (-70 to -10 mV) plus the obvious loss of clamp control revealed by the voltage-sensing electrode. Our strategy to minimize the R_s error was to reduce the Na^+ current density by lowering the external $[\text{Na}^+]$. The voltage-clamp quality for TEVC recordings in 10 mM Na^+ appeared to be greatly improved (Figure 2-4B) in a series of responses measured for depolarizations from a holding potential of -100 mV to test potentials of -80 to +40 mV. Based on the voltage responses measured at a variety of Na^+ concentrations, we conclude that Na^+ current transients up to 150 nA in peak amplitude can be recorded without appreciable distortion of the clamp potential at $x = 0$.

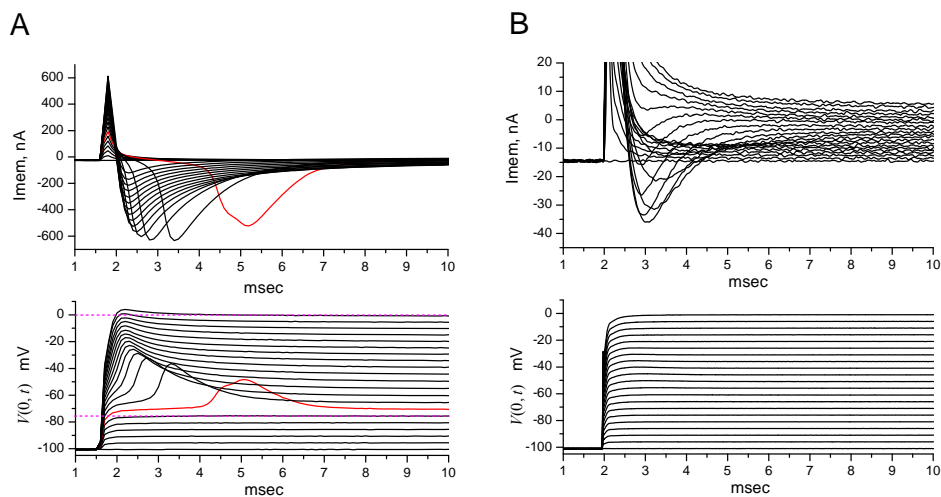


Figure 2-4. Two-electrode voltage-clamp was not able to control membrane potential in full $[\text{Na}^+]$. Na^+ currents were recorded in detubulated muscle fibers, clamped by TEV at the midpoint. K^+ , Cl^- , and Ca^{2+} currents were blocked or suppressed, as described in the Methods. No leak subtraction has been performed. (A) In 145 mM $[\text{Na}^+]$, loss of voltage-clamp control is obvious from the lag and marked peak of the current (*top*) and voltage overshoot (*bottom*) elicited by a depolarization to -70 mV (red trace). The voltage-clamp had a brief lag of 0.4 msec to reach steady-state for small depolarizations that did not open Na^+ channels (dashed line, -75 mV), and had an overshoot for $V \geq -70$ mV that persisted even at a test potential of 0 mV where the driving force for Na^+ was greatly reduced (dashed line). (B) Reducing the $[\text{Na}^+]$ to 10 mM improved the quality of the voltage-clamp.

Computer Simulations Provide Estimates for Conditions Necessary to Maintain Voltage-Clamp Control

Parameter sensitivity studies were performed with the nonlinear cable model to ascertain the quality of voltage-clamp control and to determine the range of experimental conditions (current density, fiber size, clamp speed) for which the TEVC recordings provide an accurate measure of Na^+ channel gating behavior in mouse foot pad skeletal muscle fibers. The Rs error produced by large-amplitude ionic currents is readily apparent from the records in Figure 2-4A, but there could be additional mechanisms that impede the ability to characterize Na^+ currents by voltage-clamp measurements from a point at the center of the muscle fibers. For example, the membrane conductance increases 50 to 100-fold with maximal activation of Na^+ channels, which would transiently decrease the length constant by an order of magnitude. Simulations are needed to determine whether more

pronounced cable effects are occurring at the ends of the fiber, even if the peak Na^+ current is less than 150 nA and the clamp control appears to be adequate based on the measured voltage at $x = 0$. It is important to recognize that in the computer simulations the membrane voltage at $x = 0$ is constrained to equal the predetermined value; $V(0,t)$ is a boundary condition for the solution to Eq. 1. Unless otherwise specified, all simulations were performed with $V(0,t)$ computed by the two-exponential fit to the measured TEVC response shown in Figure 2-3A.

The closed-form solution for the finite-length cable equation applies only to the case of constant (voltage-independent) conductances. Therefore, we used numerical integration to solve the generalized finite-length cable equation with an m^3h – type Na^+ conductance. The computed spatial-temporal profile of the voltage-clamp is shown in Figure 2-5A (*left* panel) for a small 20 mV depolarization from -100 mV, which does not activate the Na^+ conductance. The surface plots in Figure 2-5 show the voltage profile over half the fiber length, from the midpoint ($x = 0$) out to one end ($x = l/2$). The quality of the clamp was excellent, in terms of speed and spatial uniformity, for this simulated 450 μm fiber in Cl-free bath. The plot in the *right* panel shows the deviation or voltage error, computed as the difference between the voltage at any position, x , relative to the clamp voltage at $x = 0$. The sharp transient error at the beginning of the applied voltage step is produced by the brief delay from the passive RC cable properties of fiber. Depolarization to -40 mV in 145 mM Na^+ , however, caused a

loss of voltage-clamp due to the depolarizing effect of the large-amplitude inward Na^+ current (Figure 2-5B). In experimental practice, the large ionic current in 145 mM $[\text{Na}^+]$, (typically 600 nA, see Figure 2-4A) would produce a loss of voltage control at $x = 0$ as well. This simulation illustrates the voltage error (*right panel*) that would occur even if a sufficiently high-compliance amplifier, with low R_s in the current path could be used to maintain clamp control at $x = 0$. We simulated the effect of reducing extracellular $[\text{Na}^+]$ to 10 mM, which qualitatively improved the clamp quality (Figure 2-4B), by reducing the peak Na^+ conductance, G_{Na} , by a factor of (10/145) and by shifting the equilibrium potential, E_{Na} , to 0.4 mV. Both changes reduced the inward Na^+ current, and resulted in a dramatic improvement of voltage-clamp quality (Figure 2-5C). These model results imply that voltage control over the entire length of the fiber is very good for the experimental conditions shown in the measurements of Figure 2-4B.

We developed a quantitative measure for the fidelity of the voltage-clamp along the fiber, as a tool to perform sensitivity studies on the effects of fiber length and Na^+ current density in simulated fibers. Our measure is based on the deviation of the membrane potential from the clamped value at $x = 0$, $[V(x,t) - V(0,t)]$, as illustrated by the *right panels* in Figure 2-5. The square of this difference is summed over the length of the fiber and over the duration of the test pulse, T . Finally, this integral is normalized by the fiber length, l , and the square of voltage step, ΔV , to yield the dimensionless error measure, V_{err} .

$$V_{err} = \frac{2}{l(\Delta V)^2} \int_0^T \int_0^{l/2} [V(x,t) - V(0,t)]^2 dx dt \quad \text{Eq. 5}$$

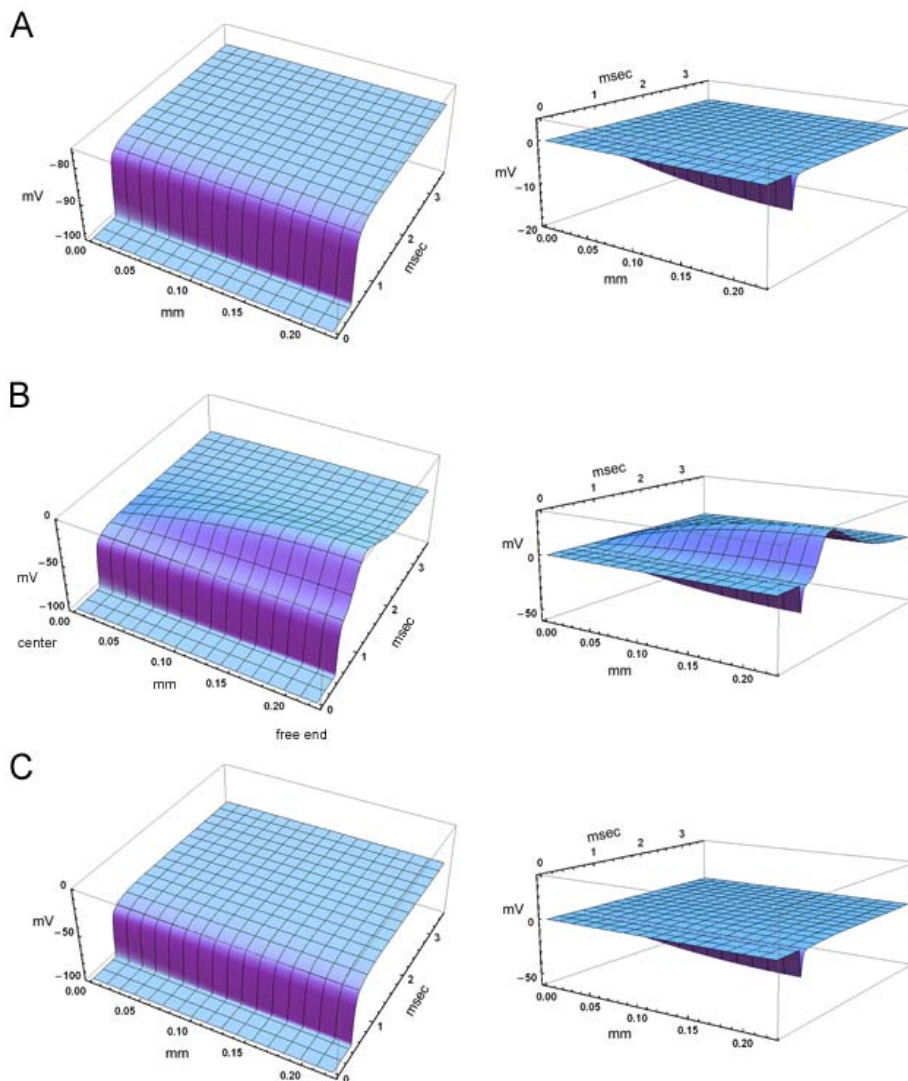


Figure 2-5. Model predictions of voltage control over the length of a fiber. Membrane voltage was clamped at $x = 0$ (center of fiber) with a rapid depolarization applied at 0.5 msec. *Left* panels show the voltage response over a half-fiber length (0.225 μm), from the center to one end, and is symmetrical for the other half. *Right* panels show the voltage error relative to the clamp potential, $V(x,t) - V(0,t)$. Voltage scale (vertical) has been held constant between the *left* and *right* panels to aid in visual comparison. (A) Response to a +20 mV depolarization from -100 mV was below the threshold activation for Na^+ channels and therefore voltage-clamp along the fiber was well controlled. (B) Depolarization from -100 mV to -40 mV in 145 mM $[\text{Na}^+]$ elicited a large Na^+ current that created a loss of voltage control at positions away from the midpoint ($x = 0$). (C) A simulated reduction of $[\text{Na}^+]$ to 10 mM decreased the peak Na^+ current to -28 nA (not shown) with a concomitant improvement in voltage clamp over the length of the fiber.

The voltage deviations that contribute to V_{err} may arise either from a delay and attenuation caused by the cable properties (Figure 2-3B) or from the overshoot caused by large inward Na^+ currents in combination with the axial series resistance (Figures 2-4A and 2-5B). An intuitive interpretation for V_{err} is provided by computing values for the model responses in Figures 2-3B and 2-5. For our average foot pad muscle fiber of length 450 μm in a Cl-free bath, $V_{err} = 0.0063$ for a small depolarization of 20 mV that did not activate Na^+ channels (Figure 2-3B, *solid lines*). Increasing the fiber length to 600 μm increased the lag and attenuation (Figure 2-3B, *dashed lines*), with a concomitant increase of V_{err} to 0.014. The large overshoot of $V(x,t)$ produced by activation of a high-density Na^+ current (Figure 2-5B) has a V_{err} of 0.30. To provide a more global image of how fiber length and Na^+ current density affect the clamp quality, we computed V_{err}

for a range of lengths and $[\text{Na}^+]$ that were encountered in our experiments with foot pat muscle fibers. The contour plot in Figure 2-6A shows V_{err} for a step depolarization from -100 mV to -40 mV. For very short fibers ($< 250 \mu\text{m}$), V_{err} is small and independent of $[\text{Na}^+]$ from 0 to 20% of the normal physiological concentration (145 mM), as depicted by the flat horizontal orientation of the contour lines. As fiber length increases (movement upward along the vertical direction in Figure 2-6A), the quality of the clamp deteriorates at all levels of $[\text{Na}^+]$, as indicated by contour line crossings. This length-dependence of V_{err} is exacerbated by higher Na^+ current densities, as indicated by the closer spacing of the contour lines on the right edge of Figure 2-6A. For any selection of an acceptable clamp quality, for example $V_{err} < 0.025$, the contour plot in Figure 2-6A shows the permissible values of fiber length and $[\text{Na}^+]$ that could be used experimentally achieve this level of clamp control.

The deviation in voltage-clamp control is voltage-dependent, due to the voltage-dependence of Na^+ channel activation. Figure 2-6B shows how V_{err} varies with test potential, for a series of simulated fibers with different lengths. The peak Na^+ conductance was scaled by 0.15, corresponding to an external $[\text{Na}^+]$ of 22 mM, to simulate the borderline case with the highest permissible Na^+ current (-100 nA) in a 450 μm fiber without distortion of the clamp voltage at $x = 0$ (as judged experimentally from the voltage sensing electrode response). The voltage-clamp error increases for $V > -60$ mV, as Na^+ channels are activated, and

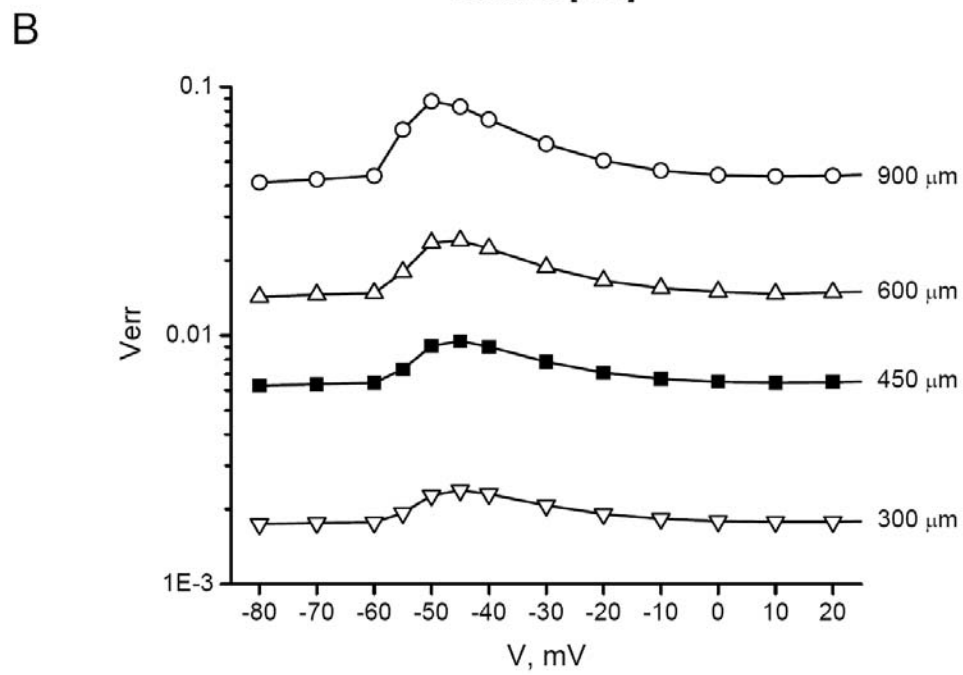
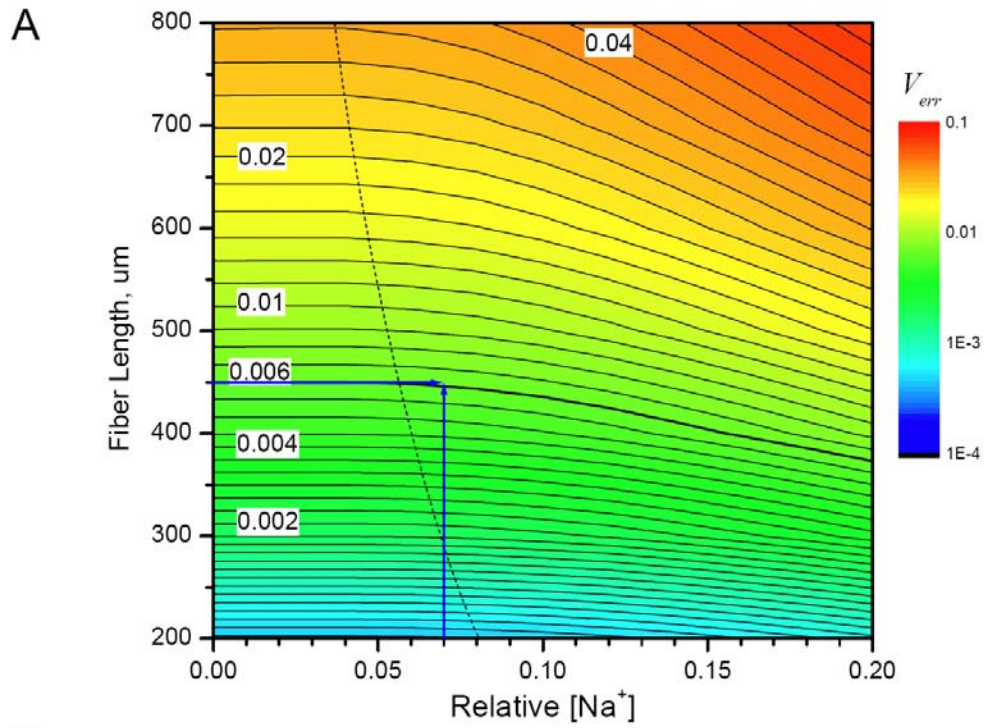


Figure 2-6. Dependency of voltage-clamp error on fiber size, $[\text{Na}^+]$, and voltage. A single metric, V_{err} as defined in Eq. 5, was used to quantify the accuracy of the clamp potential across the entire length of a simulated fiber. (A) Contour plot shows V_{err} on a logarithmic scale for a range of fiber lengths and $[\text{Na}^+]$ used in these studies. The clamp potential was a rapid depolarization from -100 mV to -40 mV. The arrows (blue) indicate the average fiber length and $[\text{Na}^+]$ in our experiments to characterize Na^+ channel gating. Numbers indicate the value of V_{err} for several contour lines. (B) Voltage dependence of V_{err} for several different fiber lengths. The $[\text{Na}^+]$ was held at 22.8 mM (G_{Na} equal to 15% of value in physiologic Na^+) and a series of test depolarizations was applied from a holding potential of -100 mV.

this occurs at all fiber lengths. With further depolarization, V_{err} decreases because the Na^+ currents become smaller as the membrane potential approaches E_{Na} (+20.8 mV in this simulation). The contour plot of V_{err} in Figure 2-6A was constructed with a test potential of -40 mV, which is the voltage at which the peak I-V relation has the largest inward Na^+ current. Figure 2-6B shows that the relative voltage error is larger at potentials more negative than -40 mV, in the voltage range for the steep activation of the Na^+ conductance.

Model Simulations of I_{Na} Provide Quantitative Estimates for the Errors in Determining Na^+ Channel Gating Parameters from TEVC Recordings in Foot Pad Muscle Fibers

Sodium current responses were computed for voltage-clamp studies of a simulated foot pad muscle fiber to quantitatively characterize how well parameter

fits of the simulated currents gave accurate estimates for the gating parameters of the Na^+ conductance. The idealized control response was defined by the parameter estimates obtained from voltage-clamp simulations of a perfectly space-clamped spherical cell with no series resistance error. The standard simulated fiber was 450 μm in length with an external $[\text{Na}^+]$ of 22 mM, corresponding to a G_{Na} of 9 mS/cm^2 or 15% that in normal physiological sodium and an E_{Na} of 22.8 mV. These model parameters were selected to produce a maximal peak inward Na^+ current of about -100 nA, which is comparable to the maximal Na^+ current that could be recorded experimentally in the TEVC clamp without obvious loss of voltage control detectable with the voltage-sensing electrode. This configuration is a worst-case scenario, in the sense that the conditions ultimately used to experimentally characterize Na^+ currents in foot pad muscle fibers were more conservative ($[\text{Na}^+] = 10 \text{ mM}$).

Clamp Speed

The speed of the voltage-clamp at the fiber midpoint ($x = 0$) had a pronounced effect on the time to peak Na^+ current and the peak amplitude, as is well-known to also occur with a space-clamped spherical cell. Figure 2-7 shows the range of simulated clamp speeds (panel A) and the effect on the Na^+ current transient elicited by a depolarization to -30 mV (panel B). Simulated clamp

speeds with a single exponential time constant of 200 μsec or longer produced a noticeable lag to peak and a decrease in amplitude. Simulations with faster clamp speeds (20 – 100 μsec) were clustered, in part because these transients were faster than the saturating rate of activation for simulated channels ($\bar{a}_m = 6 \text{ msec}^{-1}$, equivalent to $\tau_m = 170 \mu\text{sec}$) and also because the cable properties of the fiber act as a low-pass filter. Simulation with a two-exponential voltage trajectory to model our experimentally measured clamp speed at $x = 0$ (Figure 2-3A, 18 μsec 76% and 190 μsec 24%) yielded results similar to the fast clamp (100 μsec or less). The peak Na^+ current amplitude is reduced with slower clamp speeds because inactivation commences before activation is complete (Figure 2-7B). In addition, the shape of the peak I-V relation is also distorted by slow clamp speeds that produce an apparent depolarized shift of the reversal potential (Figure 2-7C). This phenomenon occurs because channel activation is substantial before the voltage trajectory has reached its maximal depolarized value. As a result, Na^+ current flows when the driving force ($V(t) - E_{\text{Na}}$) is larger than that will occur as V reaches its steady-state value. Consequently, the I-V relation is distorted toward more negative (inward) currents at depolarized potentials $> -10 \text{ mV}$ (Figure 2-7C). Despite these obvious distortions of the simulated Na^+ current transients for slow clamp speeds, the amplitude-normalized peak I-V curves are nearly identical for all but the slowest simulated clamp (Figure 2-7D, 500 μsec).

We conclude that clamp speed is important to accurately determine the latency and amplitude of the peak Na^+ current, but the normalized I-V characteristics (and hence the determination of midpoint and slope of a Boltzmann fit) are less sensitive. Unacceptably slow clamp speeds will be reflected by an apparent depolarized shift of the reversal potential compared to the predicted E_{Na} , and the resulting distortions will produce an apparent depolarized shift of $V_{1/2}$ and larger slope factor k from a Boltzmann fit to estimate the voltage dependence of activation.

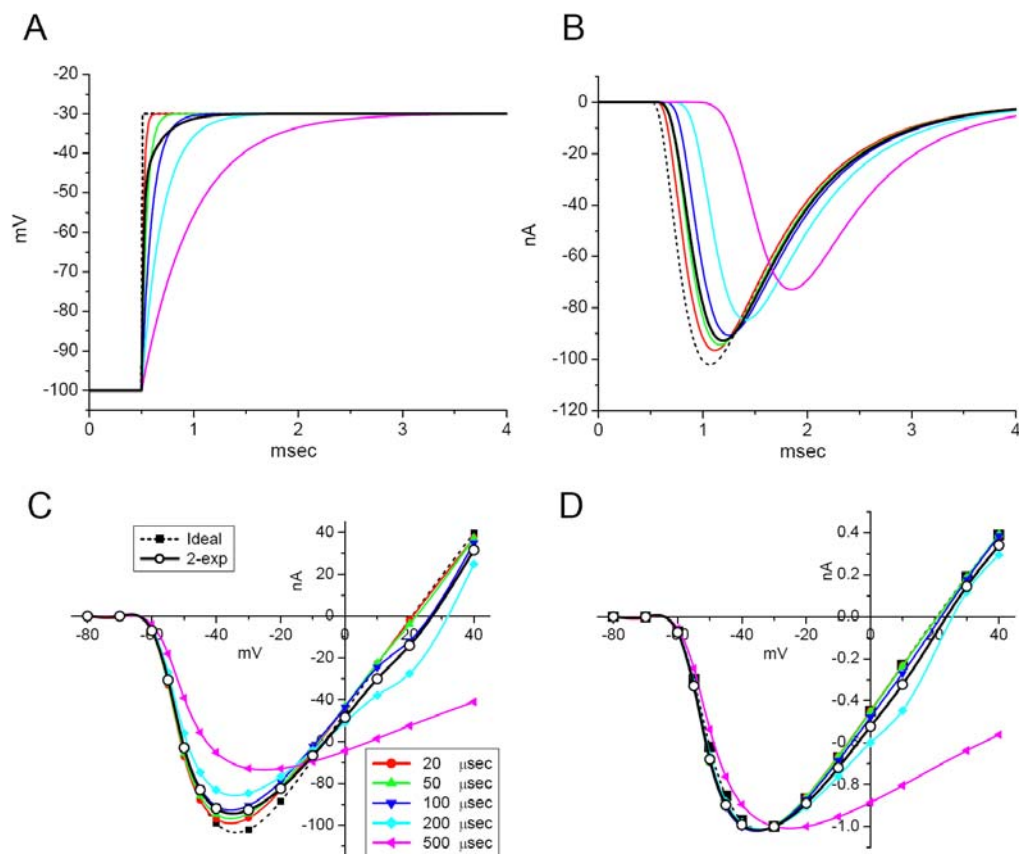


Figure 2-7. Effect of voltage-clamp speed on Na^+ currents in a simulated fiber. (A) Voltage transients applied at the simulated fiber midpoint, $x = 0$. Voltage-clamp kinetics were modeled as a single exponential rise (time constant 20 to 500 μsec) or a double-exponential to recapitulate the experimentally measured voltage transient (fast = 0.018 sec (76%) and slow = 0.19 sec (24%), or an idealized instantaneous jump. (B) Simulated Na^+ currents elicited by depolarization from -100 to -30 mV. Model fiber had a length of 450 μm and was in 22 mM $[\text{Na}^+]$. (C) Peak $I_{\text{Na}} - V$ relation reveals distortion produced by voltage clamp commands with a time constant of 200 μsec or larger. (D) Amplitude normalized I-V relation shows the apparent voltage dependence of activation is not affected until the clamp has a time constant of 500 μsec .

Fiber Length

The influence of fiber length was investigated over a range from 300 to 1200 μm , as compared to a mean length of 450 μm (range 300 – 600 μm) for the fibers selected for experimental studies. The center of the simulated fiber was clamped with the two-exponential model of the measured voltage trajectory (Figure 2-3A). Figure 2-8A shows model Na^+ current responses for a simulated depolarization from -100 to -30 mV. Current amplitudes have been scaled by a factor of ($Length / 450 \mu\text{m}$) to facilitate a visual comparison of the non-linear effects from variation in fiber length. With increasing fiber length, the scaled Na^+ current that would be measured at the midpoint is attenuated and delayed for two reasons. First, the rise time for the voltage clamp is slower at the ends of an elongated fiber, which results in significant channel inactivation during the trajectory toward peak activation. Second, because the time to peak Na^+ current is delayed at the ends of the fiber, temporal dispersion attenuates the summated current response recorded

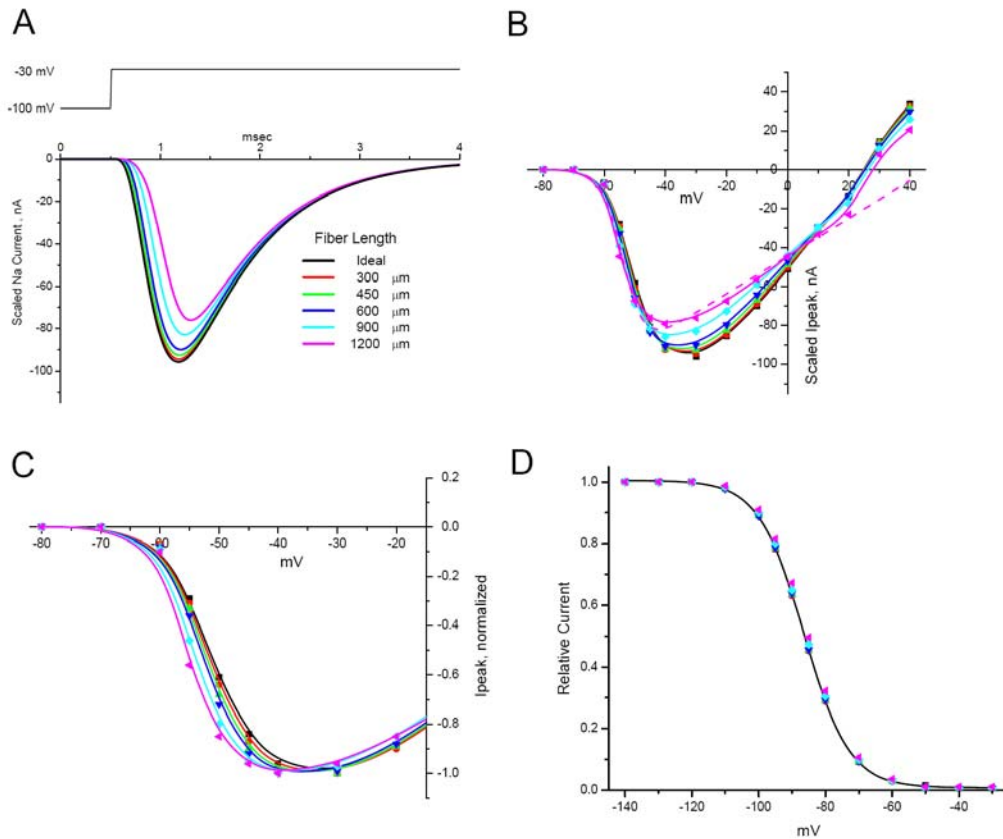


Figure 2-8. Effect of fiber length on Na^+ currents in a simulated fiber. (A) Na^+ currents elicited by depolarization from -100 mV to -30 mV. The simulated fiber was in 22 mM $[\text{Na}^+]$ and clamped at the midpoint with double exponential command potential as in Fig 2. Current amplitudes have been linearly scaled by fiber length, relative to a 450 μm fiber. (B) Peak I-V relation shows attenuation of maximal inward current and distortion near E_{rev} for longer simulated fibers. Curves show spline interpolation for visual comparison and do not represent Boltzmann fits. Dashed line shows the error in estimating E_{rev} from extrapolation of a Boltzmann fit to the data from -80 to 10 mV for a 1200 μm fiber. (C) When amplitude normalized for maximal inward current, the peak I-V relation shows the hyperpolarized (leftward) shift in the apparent voltage dependence of activation for longer simulated fibers. (D) The voltage dependence of steady-state fast inactivation, measured as the relative peak current for a test depolarization to -30 mV from various holding potentials, is not distorted in simulated fibers up to 1200 μm in length.

at the fiber midpoint. The net effect on simulated peak I-V relation is an attenuation at voltages near the maximal inward current (-40 to -10 mV, Fig. 2-8B) and a distortion of the normally linear portion of the response near the reversal potential. This latter effect is produced by the slower rise time of membrane depolarization (see above for clamp speed effects). If the peak I-V relation is normalized to the maximal inward current, then it becomes clear by visual inspection that for longer fibers the apparent midpoint of activation will be shifted toward more negative potentials (Fig. 2-8C). It is important to recognize that this apparent left shift in the voltage-dependence of activation with longer fibers can occur without an obvious loss of voltage control from R_s effects (Figs. 2-4, 5, 6). The demands on the fidelity of the voltage clamp are less stringent when characterizing the voltage dependence of fast inactivation at steady-state, using a 100 msec conditioning pulse. The simulated responses to such an “ h -infinity” pulse protocol show no perceptible distortions, even for fibers up to 1200 μm in length (Fig 2-8D).

The overall effect of fiber length on the determination of Na^+ channel gating parameters, based on fits to peak currents measured in standard pulse protocols, is summarized in Figure 2-9. The idealized parameter fits for a perfectly space-clamped cell are represented by the values plotted for a “0 μm ” length fiber. Our simulations show that as fiber length increases the activation parameters G_{max} and k will be underestimated while the apparent midpoint of activation, $V_{1/2}$, will be

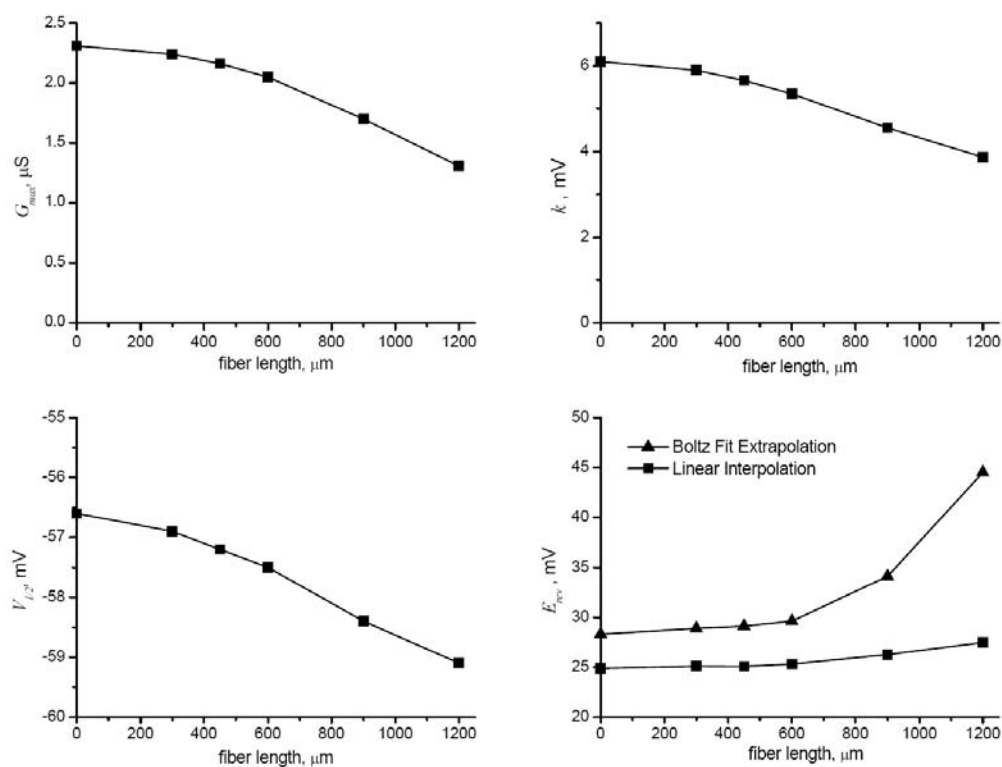


Figure 2-9. Errors in activation gating parameters estimated from fits to peak Na^+ currents in simulated fibers of various lengths. Parameters shown for fiber length of 0 μm were determined from simulations with a perfectly space-clamped spherical cell. The estimate for E_{rev} (bottom right panel) was determined by two methods: linear interpolation (squares) or extrapolation of a Boltzmann fit from -80 to -10 mV (triangles).

shifted toward more negative voltages. The error in parameter estimation is predicted to be very modest for fibers of 600 μm or shorter. The reversal potential estimated by linear interpolation of the peak I-V as the current shifts from inward to outward is accurate (Fig 2-9, bottom right). Large errors in estimating E_{rev} may occur, however, if the parameter is determined by

extrapolation from a more limited data set wherein only inward Na^+ currents are recorded as often occurs experimentally to avoid fiber damage from large positive test depolarizations. For example, a standard Ohmic – Boltzmann fit to the peak I-V data for voltages from -80 to 10 mV for a 1200 μm fiber (Fig 2-8B, dashed line) erroneously estimates a positive-shifted E_{rev} (Fig 2-9, bottom right). These simulations illustrate the importance of experimentally measuring a reversal in current direction to determine E_{rev} .

Leak Subtraction Strategy

Isolation of Na^+ currents from other ionic currents and capacitance transients is challenging for TEVC recordings from mature differentiated skeletal muscle fibers. The standard “P/N” method of subtracting linearly scaled background currents measured over a narrow range of test potentials for which Na^+ channels are not active has limitations from several sources. First, the use of sharp microelectrodes precludes the ability to dialyze the ionic composition of the myoplasm and therefore it is not possible to adequately suppress contributions from nonlinear ionic currents conducted by other channels. Second, under conditions of reduced $[\text{Na}^+]$ to minimize R_s errors, the nonlinear charge displacement currents from Na_v and Ca_v channels may be of comparable amplitude to the ionic Na^+ current. Application of tetrodotoxin (TTX) to block

Na_V channels presents one possible method to measure the total background currents for leak subtraction. This approach will work, but is cumbersome and becomes impractical for prolonged pulse protocols (e.g. to measure slow inactivation over minutes) during which the nonspecific leak may have changed between control and TTX conditions.

We developed an alternative leak subtraction strategy, based on Na_V channel inactivation, to isolate Na^+ currents in TEVC recordings from foot pad skeletal muscle fibers. This approach proved to be especially helpful for use with large voltage jumps ($> +80$ mV) in the channel activation pulse protocol. The rationale is to measure the background leak currents after a conditioning pulse (30 msec) that would inactivate the majority of Na^+ channels. The pulse sequence and current responses are shown in Figure 2-10A. First, total currents (Na^+ and otherwise) are measured by an initial application of the test pulse (P1). Next, the conditioning pulse of 30 msec at -20 mV is applied to inactivate Na_V channels. A brief gap repolarization (8 msec at -100 mV) is used to reset the voltage sensors and then the test pulse paradigm is reapplied (P2) to measure the background currents while the majority of Na_V channels remain inactivated. Subtraction of the current elicited by P2 from the response to P1 yields the isolated Na^+ current (Fig. 2-10B). This technique has several advantages. First, the leak and total current responses are measured over a very short time span of 50 msec. This approach, like the conventional P/N, enables leak compensation to be continually updated for uncontrolled drift of background currents. Second, the technique will compensate for nonlinearities in the background currents over the entire range of test potentials, as does the TTX method.

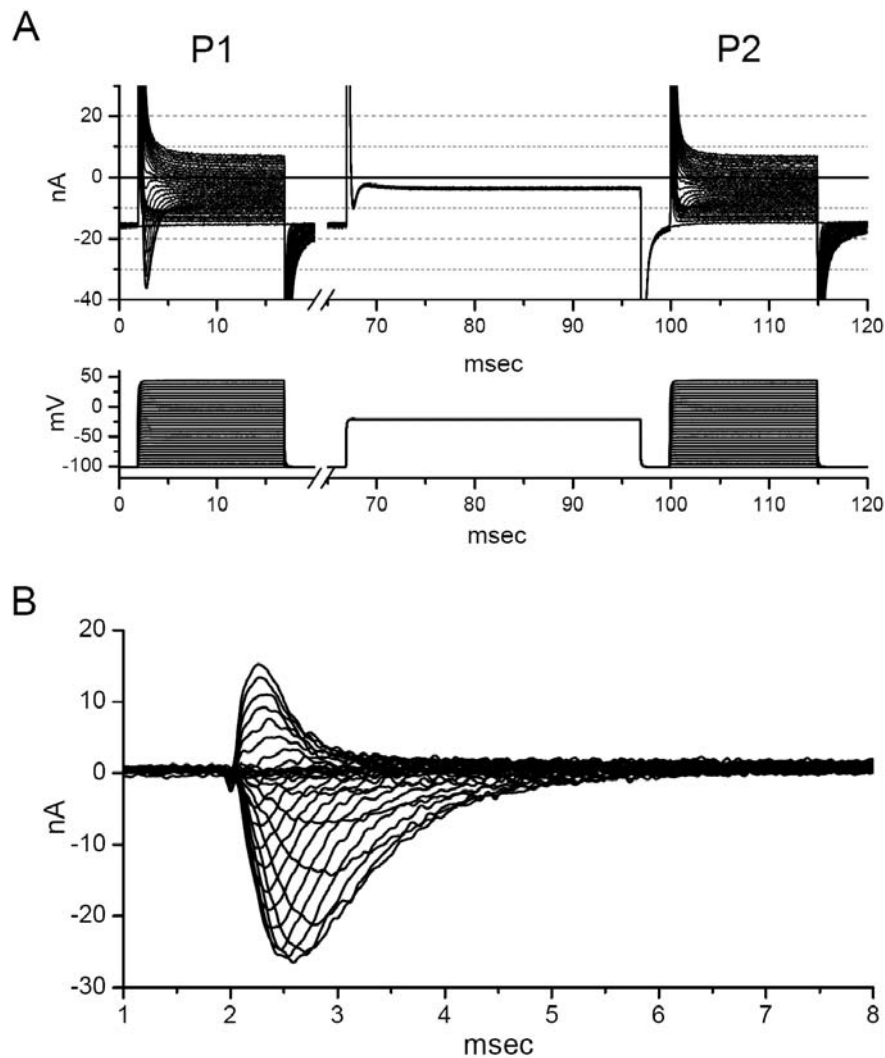


Figure 2-10. Leak subtraction protocol to isolate Na⁺ currents. (A) The pulse protocol is applied twice. Once to measure total currents (P1), and then a second time (P2) after Na⁺ channels have been inactivated by a 30 msec conditioning pulse. A repolarization gap of 3 msec to -100 mV was applied after the conditioning pulse to reset the voltage sensors. Most Na⁺ channels do not recover within 3 msec, as shown by the attenuation of the early transient inward current during P2. The entire pulse sequence, P1 – conditioning – P2 was programmed into a single epoch. (B) Subtraction of residual currents in P2 from P1 yields the Na⁺ current. Fiber 06922001, total capacitance after detubulation was 1.4 nF.

The major limitations to this inactivation strategy are: (1) partial recovery from inactivation occurs during the brief repolarizing gap at -100 mV (~40% of channels) and so some Na⁺ current remains in the “leak” response; (2) the Na⁺ current is a relatively small component, computed from the difference of large-amplitude currents P1 - P2; (3) pulse protocols that would enable recovery from inactivation before the test pulse cannot be used. Limitation (1) implies the Na⁺ current density is higher than indicated from the subtracted raw currents, but this difference current is indeed very specific for I_{Na}. If greater accuracy is needed to determine Na⁺ current density, then TTX subtraction can be used. For determination of Na_v (fast) gating behavior, however, the inactivation method is preferred.

Discussion

This study provides a methodological guide for optimization of a two-electrode voltage clamp to record Na⁺ currents from isolated mouse skeletal muscle fibers. The model simulations define the range of experimental conditions (clamp speed, fiber length, and current amplitude) for which voltage-clamp control is achieved and also provide quantitative estimates for the magnitude of potential artifacts and the influence these have of the determination of voltage-dependant gating parameters. If these conditions are met, then accurate

measurement of Ca^{2+} , K^+ or Cl^- currents is also assured, since the technical challenges of current density and gating kinetics are less demanding for these other voltage-gated conductances.

Short muscle fibers isolated from enzymatic dissociation of the mouse foot pad muscles ($< 600 \mu\text{m}$, equivalent to an apparent capacitance for detubulated fibers of $< 3 \text{ nF}$) and detubulated with hyperosmolar shock are well suited for TEVC studies. Despite the length / diameter ratio of ~ 10 , space clamp is quite good because the relatively large diameter compared to an axon, results in an effective electrical length for the entire fiber of $0.2\lambda - 0.3\lambda$ under resting conditions. During the large conductance increase that occurs with Na^+ channel activation, space-clamp of the membrane potential remains good, provided the peak ionic current is $< 150 \text{ nA}$. In practice, the two experimentally controllable parameters that are most critical to obtain accurate TEVC recordings from detubulated short muscle fibers are the clamp quality at the site of electrode impalement and limiting the amplitude of the peak ionic current. The settling time of the voltage clamp at $x = 0$ should be $< 100 \mu\text{sec}$ (Figure 2-7), which requires a high-compliance amplifier and minimization of the resistance for the current injection pathway. Faster clamp speeds will not improve performance because the intrinsic low-pass properties of the fiber have an effective time constant of $25 - 50 \mu\text{sec}$. If the clamp time constant is $> 100 \mu\text{sec}$, then the

greatest errors are an underestimate of peak current amplitude and prolonged latency to peak (Figure 2-7B and (Ruben et al., 1997)). Additional caution is warranted for determination of the reversal potential by linear extrapolation (Figure 2-7C), which has an apparent rightward (depolarized) shift. Surprisingly, the parameter estimates for the midpoint and slope of voltage-dependent activation are relatively unaffected even for clamp time constants up to 200 μ sec. Peak ionic current, studied herein by changing the concentration of the permeant ion, must be constrained to < 150 nA (equivalent to $[\text{Na}^+] < \sim 25$ mM) or the axial resistance of the fiber will lead to “escape” from the voltage clamp at the distal ends (Figure 2-5B). With regard to fiber length, voltage control is well maintained up to fiber lengths of about 600 μ m (again, provided the peak ionic current < 150 nA). Simulations show that estimates for the midpoint of activation from the peak I-V relation are within 1 mV of the true value (Figure 2-9, lower left). When the fiber length exceeds 600 μ m, there is an apparent hyperpolarized (left) shift for the voltage dependence of activation, which also becomes steeper (smaller, k) and has a lower apparent peak conductance.

The TEVC method with short detubulated fibers has many advantages over other voltage-clamp techniques applied to skeletal muscle. The sucrose or vaseline gap techniques require a more difficult dissection and mounting of single fibers of several mm in length, and the cut ends of the fiber disrupt the internal

milieu. Moreover, because the current and voltage are measured at opposite ends of the cut fiber (including the sucrose or vaseline segments) the voltage drop between these two points may distort the current measurement (Moore et al., 1975). The three-electrode voltage-clamp applied to long fibers (Adrian et al., 1970) preserves the integrity of the myoplasm, but the voltage control is poor. Voltage control in the transverse tubules is a well recognized complication for voltage-clamp studies of skeletal muscle (Adrian et al., 1970; Hille and Campbell, 1976). Supercharging protocols have been developed (Kim and Vergara, 1998) and are very useful when the objective is to induce a step change in T-tubule potential, as in studies of excitation-contraction coupling. Only recently, it has become recognized that the electrical coupling between the sarcolemmal and T-tubule is much stronger for mouse muscle fibers (Woods et al., 2005) than prevailing views from traditional studies in frog (Adrian and Peachey, 1973). Nevertheless, even in mouse fibers, there can be considerable dissociation between the sarcolemmal membrane potential recorded with a microelectrode and the T-tubule potential measured with potentiometric dyes (DiFranco et al., 2005). In the setting of large Na^+ current transients exceeding several μA in mouse skeletal muscle fibers, a modest deviation of voltage control at the sarcolemma (~ 9 mV) was associated with ~ 80 mV deviation in T-tubule potential. Detubulation with osmotic shock yields an excellent preparation for voltage-clamp studies of ion channels in the sarcolemma without the “escape” from voltage control due to

active currents in the T-tubule. Moreover, detubulation reduces the fiber capacitance which improves the clamp speed.

Several variations of the patch-clamp technique have been developed to overcome the space-clamp and series resistance problems for recording ionic currents from skeletal muscle. The loose-patch technique measures macroscopic currents in a cell-attached mode with a wide-tip pipette 10 - 15 μm in diameter (Almers et al., 1984; Stuhmer and Almers, 1982). This is the preferred approach for measuring the spatial variation of channel density between junctional and extra-junctional fiber segments. Limitations of the loose patch technique include: the need to measure the resting potential (often an assumed value or measured only at the end of an experiment), poor clamp of the T-tubular membrane and large leakage currents from the seal. One strategy to overcome these difficulties is to use a depolarizing extracellular solution to eliminate the offset produced by the resting potential. Caution is warranted, however, as it has recently become recognized that changes in holding potential can have a profound effect within minutes on the voltage-dependence of Na^+ channels in mammalian skeletal muscle (Filatov et al., 2005). Tight-seal cell-attached patch recordings resolve the issue of large leakage current. The challenge remains, however, for resting potential offset. Other considerations include the need for extensive enzyme treatment to promote tight seal formation and mechanical deformation of the local membrane environment which may alter channel function. Whole-cell patch

recording has been applied to the enzymatically dissociated flexor digitorum brevis (FDB) fiber preparation (Beam and Knudson, 1988). One advantage of the whole-cell approach is the ability to introduce impermeant molecules to the myoplasm. Careful consideration of cell capacitance and series resistance of the patch pipette is required, however, as these factors make recording fast Na^+ currents impractical for adult fibers. Lueck and colleagues (Lueck et al., 2007) selected the shortest fibers from the dissociated FDB of young mice (10-20 d), which were smaller (~ 0.6 nF) and formed gigaseals more readily. Even with these precautions, a typical pipette series resistance of $0.5 \text{ M}\Omega$ will result in a clamp time constant of $300 \mu\text{sec}$, which was plenty fast for their studies on CIC-1 but inadequate for Na^+ channels. In studies on adult mice 7 months old, dissociated FDB fibers were larger with an average cell capacitance of 1.7 nF and a clamp time constant of 1 msec (Wang et al., 1999). Voltage errors from the pipette R_s are a greater concern. Even with efforts to reduce the Na^+ current amplitude by 90% to ~ 100 nA the transient voltage error for a $0.5 \text{ M}\Omega$ patch electrode is 50 mV. Another problem is the relatively low resting membrane resistance for muscle fibers, which in combination of the pipette R_s will produce a steady-state voltage error, $R_s/(R_m + R_s)$. For example in a bath with chloride, the effective whole-cell membrane resistance of a dissociated fiber is about $2 \text{ M}\Omega$ so that a pipette R_s of $0.5 \text{ M}\Omega$ will result in a 20% steady-state voltage error. Even in a chloride free bath, the membrane resistance increases to only $\sim 10 \text{ M}\Omega$ so the

steady-state voltage error is still 5%. For these reasons, we recommend the TEVC clamp over whole-cell recording.

**Chapter Three : Sodium Currents in Adult Mouse Skeletal Muscle:
Hyperpolarized Shift of Gating Relative to Nav1.4 in Heterologous
Expression Systems**

Introduction

Over the past two decades, the characterization of voltage-gated conductances in excitable membranes has shifted from classical microelectrode studies in acutely dissociated preparations to expression systems wherein a relatively pure population of channels can be studied with excellent voltage-clamp control. A resurgence of the classical approach has emerged with the recognition of the importance of cellular context for the regulation and modulation of channel activity and to study the functional impact of disease-associated mutations in ion channel genes in a more biologically relevant environment. The present study to characterize Na⁺ currents in fully differentiated intact fibers of mouse skeletal muscle was motivated by the availability of knock-in mutant mouse models for periodic paralysis based on missense mutations in Nav1.4 (Hayward et al., 2008).

A variety of preparations have been developed to study Na⁺ currents in mammalian skeletal muscle, with the challenge being a high current density and cylindrical geometry that render the measurements susceptible to series resistance

and space-clamp errors. Adrian developed a three-electrode preparation to record from fibers longer than the space constant (Adrian et al., 1970), whereas Duval and Loety (Duval and Loety, 1978) and then Pappone (Pappone, 1980) developed gap preparations in cut fibers. The next major development was the application of patch recording, either in cell-attached mode (Chua and Betz, 1991) or from membrane blebs in mechanically disrupted fibers (Stein and Palade, 1989). We sought a method to preserve the integrity of a fully differentiated mouse skeletal muscle fiber and also achieve accurate voltage control. A combination of short fibers ($< 600 \mu\text{m}$), low external $[\text{Na}^+]$ to reduce current density, and detubulation by glycerol shock was found to work well with a conventional two-electrode voltage-clamp using sharp microelectrodes to preserve the myoplasmic contents. Using the improved two-electrode voltage clamp we can generate more accurate descriptions of Na^+ channel behavior in situ. The accuracy of Na^+ current recording with this modified technique has been proved by computer simulation (chapter two).

This study is focused on the characterization of gating behavior of Na^+ channel in fully differentiated skeletal muscle fibers dissociated from wild-type mouse. There are some long-standing controversies in the literature about the Na^+ channel gating behavior study. For instance, one contentious issue is the behavior of the so-called “slow” inactivation process of Na^+ channels, which takes place in response to membrane depolarization of tens of seconds’ duration. In

heterologous expression systems, the voltage-dependence of steady-state slow inactivation (S_{∞}) is similar to that of fast inactivation (H_{∞}) (Hayward et al., 1997; Hayward et al., 1999). In contrast, in a loose patch study of intact muscle fibers, Ruff found a marked hyperpolarized shift of S_{∞} compared to H_{∞} (Ruff, 1999). Does this difference reflect the true behavior of Na^+ channel in skeletal muscle fibers or is it just due to the inaccuracy of loose patch recording method? The voltage-dependence of slow inactivation is a critical parameter determining the phenotype of some skeletal muscle diseases, such as periodic paralysis (Struyk et al., 2000). Thus, an unambiguous description of voltage-dependence of inactivation in situ is an important component of understanding the mechanism of these skeletal muscle disorders. This study can help provide novel insight into these literature controversies.

Nowadays the mouse has become the preferred animal in genetic manipulations and biomedical research. Engineered mouse models were used in various scientific fields and brought considerable progresses for the understanding of mechanism of diseases and for the innovation of therapeutic strategies. There are several hundreds of mouse strains with diverse genetic backgrounds available for the biomedical research. Different mouse strains may result in significant variation in scientific study. Comparison between wild-type and engineered mutant mice in different mouse strains may lead to faulty interpretation of data. Consequently, characterization of strain-dependent properties is important for

experimental design and unambiguously interpretation of data from scientific research.

Electrophysiology parameters of Na⁺ channel have been compared in various mouse strains using primary cultured skeletal myocytes (Mille et al., 2009). But the comparison of Na⁺ channel behavior in fully differentiated skeletal muscle fibers is still lacking. In our laboratory, we have several engineered mice mainly in two genetic backgrounds, C57/B16 and 129-E, which are most commonly used in transgenic studies. In this study, gating behavior of sodium channel was characterized using these two mouse strains.

The voltage dependence of activation and fast inactivation were hyperpolarized by more than 20 mV in comparison to expression studies of Nav1.4 in HEK293 cells. This behavior is similar to that observed from early studies with cut fiber preparations and emphasizes the importance of the muscle environment in the regulation of channel activity. We also extended the classical studies by measuring slow inactivation properties which revealed a 20 mV depolarized shift of slow compared to fast inactivation that was not previously appreciated in HEK293 cell studies.

Materials and Methods

Muscle Fiber Preparation

Individual muscle fibers were isolated by enzymatic digestion and mechanical disruption from mixed muscles of the hind foot of adult C57/Bl6 and 129-E mice (age 2 – 6 months). Animals were sacrificed by isoflurane inhalation and cervical dislocation, in accordance with guidelines by our Institutional Animal Care and Use Committee. The muscle was rapidly dissected free and placed in DMEM plus 1 mg/ml collagenase (Gibco, Grand Island, NY). The muscle was incubated at 37 °C for 90 minutes. Fibers were dissociated by trituration in a wide-bore pipette, pelleted by centrifugation, and resuspended in DMEM plus 10% fetal bovine serum, 1% glutamine, 100U/ml Penicillin/streptomycin and 10mM HEPES. Approximately 100 fibers were plated in 35 mm culture dishes coated with rat tail collagen and matrigel (BD Biosciences, San Jose, CA). Cultures were maintained for 1 to 3 days in 5% CO₂ at 37 °C.

Two-Electrode Voltage Clamp Recording

Currents were recorded with the two-electrode voltage clamp (TEVC) technique, using an AxoClamp2B amplifier (Molecular Devices, Sunnyvale, CA) with the HS-2A headstage. Fibers were visualized on an inverted microscope (IMT-2 Olympus, Center Valley, PA) with Hoffman optics. Disruption of the T-tubule system from the sarcolemma was achieved by hyperosmolar shock in

Ringer's solution plus 400 mM glycerol for 1 hr, and the fibers were then returned to isomolar Ringer's solution for 30min before recording (Dulhunty and Gage, 1973). Isolated fibers adherent to the collagen/matrigel coated dish and < 600 μm in length were selected for recording by impalement near their midpoint with both stimulating and recording sharp microelectrodes. The standard bath was a Cl-free low- Na^+ solution containing NaOH 10 mM, tetraethylammonium hydroxide (TEAOH) 130 mM, $\text{Mg}(\text{OH})_2$ 1 mM, $\text{Ca}(\text{OH})_2$ 1 mM, 4-(2-hydroxyethyl)-1-piperazineethanesulfonic acid (HEPES) 10 mM, glucose 10 mM, 4-aminopyridine (4-AP) 5 mM, anthracene-9-carboxylic acid (9-AC) 100 μM , nifedipine 5 μM , pH adjusted to 7.4 by methanesulfonic acid. Dantrolene 3 $\mu\text{g}/\text{ml}$ and the skeletal muscle myosin II inhibitor N-benzyl-p-toluene sulphonamide (BTS) 20 μM (Cheung et al., 2002) were added to suppress depolarization-induced contraction in studies on fibers with intact T-tubules. The extracellular Na^+ concentration was lowered to 10mM to reduce the current amplitude and thus to improve the voltage control. The current injection pipette was filled with 2 M Cs-Aspartate (resistance of 3-5 $\text{M}\Omega$) and the voltage sensing electrode contained 3 M CsCl (resistance 7-10 $\text{M}\Omega$). All measurements were performed at room temperature.

Whole Cell Recording with HEK293 Cells

HEK293 cells were transiently transfected using the calcium phosphate method as described previously (Hayward et al., 1996). In brief, supercoiled plasmid DNA encoding wild-type Na⁺ channel α subunits (1 μ g per 35-mm dish) was cotransfected with a human β 1 subunit plasmid (McClatchey et al., 1993) at fourfold molar excess, and a CD8 marker (0.1 μ g per 35-mm dish). Two to three days after transfection, the HEK293 cells were briefly trypsinized and passaged to 12 mm round glass cover slips for electrophysiological recording. Individual transfection-positive cells were identified by labeling with anti-CD8 antibodies cross-linked to microbeads (Dynal, Great Neck, NY) (Jurman et al., 1994).

Na⁺ currents were measured using conventional whole-cell recording techniques as described previously (Hayward et al., 1996). Recordings were made with an Axopatch 200B amplifier (Axon Instruments, Foster City, CA). Patch electrodes were fabricated from borosilicate capillary tubes with a multistage puller (Sutter, Novato, CA). The shank of the pipette was coated with Sylgard (Dow Corning, Midland, MI), and the tip was heat-polished to a final tip resistance in the bath solution of 0.5-2.0 M Ω . More than 80% of the series resistance was compensated by the analog circuitry of the amplifier. Leakage conductance was corrected using standard P/N protocols. Cells with peak currents of <1 nA upon step depolarization from -120 to -40 mV were excluded. In addition, cells with peak currents >20 nA were excluded to reduce series resistance errors. After establishing whole-cell access, cells were allowed to

equilibrate for 10 min before acquiring data to achieve standardized responses across cells.

The internal pipette solution contained (in mM): 130 CsF, 10 NaCl, 10 EGTA, and 10 HEPES, pH 7.4 by CsOH. Fluoride was used in the pipette solution to prolong seal stability. The bath contained (in mM): 140 NaCl (or 130 TEACl + 10 NaCl), 4 KCl, 2 CaCl₂, 1 MgCl₂, 5 glucose, and 10 HEPES, pH 7.4 by NaOH. All recordings were made at room temperature.

Data Analysis

Voltage-clamp control, current recording, and analysis of traces were performed using pClamp9.2 (Axon Instruments, Foster City, CA). The data were analyzed by the using of computer programs: Excel (Microsoft Corporation) and Origin 6.0 (MicroCal, Northampton, MA).

Conductance was calculated as:

$$G(V) = I_{\text{peak}}(V)/(V-E_{\text{rev}})$$

where the reversal potential (E_{rev}) was measured experimentally for each cell. The voltage dependence of activation was quantified by fitting the current measure to a Boltzmann function:

$$I_{\text{peak}}(V)/(V-E_{\text{rev}}) = G_{\text{max}}/[1 + \exp(-(V - V_{1/2})/\kappa)]$$

The steady-state voltage dependence was measured for fast and for slow inactivation by using wither brief (300 msec) or long (30 sec) conditioning pulse respectively. The relative current availability (I_{test}/I_{max}) was fitted to a Boltzmann function with a non-zero pedestal (I_0), calculated as:

$$I_{test}/I_{max} = (1 - I_0)/[1 + \exp((V-V_{1/2})/\kappa)] + I_0$$

where $V_{1/2}$ is the half-maximum voltage and κ is the slope factor.

The kinetics of fast inactivation was quantified from single-exponential fits to the macroscopic current decay . The time constant of the decay (τ), was estimated by fitting macroscopic Na^+ currents (I) to a single exponential plus a constant term(I_0) as:

$$I=(I_{max}-I_0)*\exp^{-t/\tau}+I_0$$

where I_{max} is the maximal amplitude. A similar function was used to estimate the time constant for the entry to fast inactivation revealed by two-pulse protocols at conditioning voltage -90mV ~ -60mV.

$$I_{test}/I_{ref}=(1-I_0)*\exp^{-t/\tau}+I_0$$

In this case I_{test} is the peak current elicited by a test pulse to -40 mV after a conditioning inactivation pulse of varying duration (t). I_{test} was normalized to the peak amplitude of a reference current (I_{ref}), elicited by a -40mV pulse before

application of the conditioning pulse. The same equation was used for the analysis of the kinetics of entry to slow inactivation.

To measure the time course of recovery from fast inactivation, a 30 msec conditioning pulse to -20 mV was applied to fast inactivate the channels fully, followed by a return to the recovery potential (between -120 and -90 mV) for a variable interval (t). The fraction of available (recovered) channels was assayed with a test pulse to -40 mV. The relative peak current (I_{test}/I_{ref}) was fit to the equation:

$$I_{test}/I_{ref} = A_1 * (1 - \exp(-t/\tau_1)) + A_2 * (1 - \exp(-t/\tau_2)) + I_0$$

A_1 and A_2 are the amplitudes of the two components, τ_1 and τ_2 are the time constants, t is the recovery time. The faster time constant was used to characterize the kinetics of recovery from fast inactivation.

The recovery of Na^+ channel availability after prolonged depolarization is characterized by multiple exponential components (Cummins and Sigworth, 1996), including "intermediate" component (I_M , recovers within 100-300 msec), slow-inactivated component (I_S , recovers within 1-3 sec), and ultraslow-inactivated channels (I_U , recover over minutes). Recovery from intermediate (I_M)- and slow (I_S)-inactivated states was measured by the use of a sequential recovery protocol in which a single conditioning pulse (up to 120 sec) was followed by a series of brief test pulses (7.5 msec) during the recovery interval. Peak current from each

test pulse was normalized to a reference current (I_{ref}), measured as the mean peak value from five separate step depolarizations to -40 mV before the conditioning pulse. $I_{\text{test}}/I_{\text{ref}}$ values were then fit with the same two-exponential equation as used for recovery from fast inactivation.

Measured values are presented as the mean \pm standard error of the mean unless otherwise noted. Statistical significance was determined by student t test. P values were noted in the text. Values of $P < 0.05$ were considered significant.

Sodium Channel Expression

A competitive RT-PCR assay was used to estimate the relative expression level of $\text{Na}_v1.4$ and $\text{Na}_v1.5$ in dissociated foot muscle fibers. To test the expression level of $\text{Na}_v1.5$ Na^+ channel in muscle fibers during the time course of cell culture, single cell RT-PCR was processed. First, single cell RT-PCR can help us to understand heterogeneity of gene expression between individual skeletal muscle fibers. Another advantage of this approach is it allows results to be combined with electrophysiology studies (Phillips and Lipski, 2000). Unfortunately, after optimizing the RT-PCR conditions including 3 times PCR to amplify the signal, the final product from single fiber is still undetectable. That is possibly because the difficulty to get RNA samples from the highly structured

“cytosol” of skeletal muscle fiber. In the following experiments, around 50 fibers were pooled together per group to collect enough RNA for RT-PCR analysis.

Approximately 3×50 fibers were collected at three time points: acutely, 24hr, and 48hr after dissociation. After washing by PBS, cells were lysed in 0.25ml TRIZOL reagent (Sigma, St. Louis, MO) by trituration with needle. Total RNA was precipitated with chloroform/ isopropanol/ETOH. Extracted RNA samples were treated with 4U RNase-free Deoxyribonuclease I (DNaseI, 2μl, 2000U/ml, BioLabs, Ipswich, MA) to remove genomic DNA.

Total RNA from each sample was reverse transcribed in a 20μl reaction with Superscript III first strand kit (Invitrogen, Carlsbad, CA). 20μl per sample RT reaction containing 1×RT buffer (2μl 10× buffer), 10mM DTT (2μl, 0.1M), 1mM dNTPs (2μl, 10mM), 5mM MgCl₂ (25mM 4μl), 40U RNAase inhibitor (1μl, 40u/μl), 100ng random hexamer (2μl 50ng/μl), 50U Superscript III (0.25μl, 200U/μl) and 10μl RNA sample, add diethyl pyrocarbonate (DEPC) treated water to make the final volume 20μl; keep mix on ice at all times. Reverse transcription was performed following the supplier recommended protocol. An "enzyme minus" negative control was set up side by side to test the contamination of genomic DNA.

To compare the transcriptional levels of the Na_v1.4 and Na_v1.5 Na⁺ channels, competitive RT-PCR was used to simultaneously amplify two Na⁺ channel

fragments in a single reaction. The primers, which allow the amplification of two Na⁺ channels at same time, were designed by Haufe and colleagues in their work to study the transcription of various Na⁺ channel cDNA species in developing mouse heart (Haufe et al., 2005). In this study, they tested and illustrated Nav1.4 and Nav1.5 Na⁺ channel fragments were amplified with equivalent efficiencies by their primers, suggesting a competitive condition in the reaction system.

To perform the competitive RT-PCR, 2µl cDNA product from each sample was used for a conventional PCR reaction with Tag DNA polymerase (for each sample, 20µl PCR reaction containing 10µl choice tag mastermix (Denville scientific Inc., Metuchen, NJ), and 10 µmol forward and reverse primers). The cycling parameters were denaturation at 94°C for 30 sec, annealing at 52°C for 30 sec, and extension at 72°C for 45 sec, total 30 cycles. A constitutively expressed gene β-actin was used to rule out the failed RT-PCR. Only samples containing mRNA for β-actin were used for subsequent analysis. The primer pairs used for PCR were:

Nav1.4/1.5 forward 5'-GCCTTCGAGGACATCTAC-3',

reverse 5'-AAGAAGGAGCCGAAGATG-3';

β-actin forward 5'-GCGATGGAGATCATGGAAGCCTACT-3',

reverse 5'- TGGTACTCAGCTTGCTCACAGACA-3'.

Original PCR products for Nav1.4 and Nav1.5 Na⁺ channel both are 710 base pair (bp). To distinguish the different channel isoforms, the PCR products were processed by specific restriction endonuclease treatment. A Nav1.5-specific restriction digest (*KpnI*) yields 561 bp and 149 bp fragments from the original amplicon, whereas the Nav1.4 fragment remained undigested. Enzyme treated products were analyzed by 2% agarose gel electrophoresis. Quantification was done by measuring the fluorescence intensities of bands of appropriate size with molecular image FX (Bio Rad, Hercules, CA) and software Quantity One (Bio Rad). To obtain the molar ratio, the respective intensity values were corrected according to the product length.

Results

The gating behavior for wild-type (WT) Na⁺ channels was determined for two mouse strains commonly used in transgenic studies, C57BL/6 and 129-E. All recordings were in enzymatically dissociated fibers from the foot pad muscle of the hind limb. Data were pooled for male and female mice. Recordings were made between 4 and 72 hours after dissociation, with fibers maintained in culture as described in the Methods.

Activation

The voltage dependence of activation was determined from the peak Na⁺ current elicited by a brief test depolarization from a holding potential of -100 mV. Maximal peak Na⁺ current density was greater for fibers from 129-E mice than C57BL/6 (-19.1 ± 2.3 nA/nF versus -14.9 ± 0.88 nA/nF, $p = 0.010$) and occurred at a test potential of -45 mV (Figure 3-1A). The voltage threshold for activation and steepness were comparable for C57BL/6 and 129-E mice. Boltzmann fits to the peak I-V data yielded activation midpoints of -53.3 ± 0.45 mV (C57BL/6) and -53.9 ± 0.73 mV (129-E) and steepness factors of 4.2 ± 0.17 mV (C57BL/6) and 4.4 ± 0.38 mV (129-E). The voltage dependence of Na⁺ channel activation in these acutely dissociated foot pad muscle fibers was markedly shifted by -26 mV toward hyperpolarized potentials in comparison to results from heterologous expression studies of Na_v1.4 + β1 subunits in HEK293 cells. This difference is illustrated by the conductance-voltage curves in Figure 3-1B for which the data from muscle fibers are compared to typical behavior reported for Na_v1.4 expressed in HEK293 cells from many laboratories (Bouhours et al., 2004; Hayward et al., 1996; Yang et al., 1994). We have carefully tested for and excluded two factors that have previously been associated with a leftward shift of activation. First, we can exclude a loss of voltage-clamp control. The measured control of membrane potential at the fiber midpoint was excellent (see Fig 2-10 A in chapter two), and the extensive set of model simulations presented in the

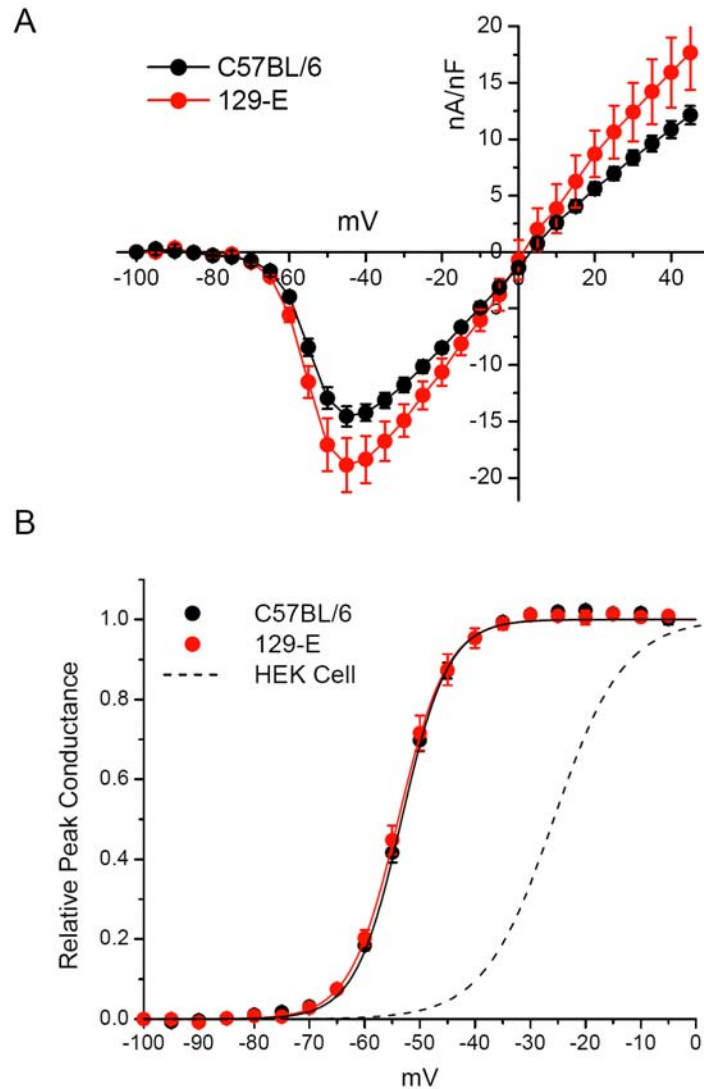


Figure 3-1. Voltage dependence of activation. (A) Peak Na⁺ current was normalized to fiber capacitance and plotted as the average for fibers from C57BL/6 mice ($n = 41$) or 129-E mice ($n = 6$). Error bars show SEM and the smooth curve is a cubic spline interpolation. (B) The data from (A) are replotted as relative peak conductance. Boltzmann fits were indistinguishable for C57BL/6 and 129-E fibers, both of which were shifted to hyperpolarized potentials in comparison to the response reported for Na_v1.4 expressed in HEK293 cells (midpoint of -26 mV, dashed line).

chapter two demonstrate that for the fiber lengths and current amplitudes in our measurements it is very unlikely that poor voltage control occurred distally. Moreover, the steepness for the voltage-dependence of activation we observed is not unusually high (small k) as would be expected for a series resistance artifact with loss of voltage control. Second, the Na^+ current in our fiber may have a substantial contribution from $\text{Na}_v1.5$, the cardiac / fetal skeletal muscle isoform which does activate at more negative voltages than $\text{Na}_v1.4$ (Chahine et al., 1996). We have used TTX sensitivity and RT-PCR to exclude this possibility, as detailed below.

Fast Inactivation

The steady-state voltage dependence of fast inactivation was measured as the relative Na^+ current elicited by a test depolarization to -40 mV, following a 300 msec conditioning pulse (Figure 3-2). In this protocol a standard P/8 leak subtraction method could be used because for a test potential of -40 mV the residual nonlinear capacitance transient did not obscure the peak ionic current (Figure 3-2A, inset). The steady-state voltage dependence was not different between fibers from C57BL/6 and 129-E mice, with fits to a Boltzmann function being -87.7 ± 0.59 mV (C57BL/6, $n = 36$) and -88.7 ± 1.0 mV (129-E, $n = 13$) for

the half-inactivation midpoint and a steepness factor of 6.8 ± 0.13 mV (C57BL/6) and 6.3 ± 0.12 (129-E).

Recovery from inactivation measured after a 30 msec conditioning pulse to -20 mV, from which recovery was more than 80% complete within 10 msec (Figure 3-2B, C57BL/6) confirming that channels were predominantly in the fast inactivated state. The data for recovery at potentials of -120 mV to -90 mV were fit by a double exponential (solid lines, Figure 3-2B), with the faster component used to characterize the kinetics of recovery from fast inactivation. The kinetics for entry to fast inactivation from the open state was determined by a single exponential fit to the Na^+ current decay measured for test depolarizations of -55 to -20 mV. Finally, the rate of closed-state entry to fast inactivation (-90 to -60 mV range) was determined with a two-pulse protocol in which the conditioning pulse duration was progressively increased and the decay of peak Na^+ current at -40 mV was fit by a single exponential. A summary for all three measures of fast inactivation kinetics is shown in Figure 3-2C. The responses for C57BL/6 and 129-E fibers were comparable, and both were left shifted by ~ 25 mV in comparison to the voltage-dependence of fast inactivation kinetics for $\text{Na}_v1.4$ expressed in HEK293 cells. Because fast inactivation is strongly coupled to activation (Aldrich et al., 1983; Kuo and Bean, 1994), the comparison of inactivation kinetics is more informative when the HEK293 cell kinetic data are shifted leftward by the -26 mV difference observed for the peak conductance-

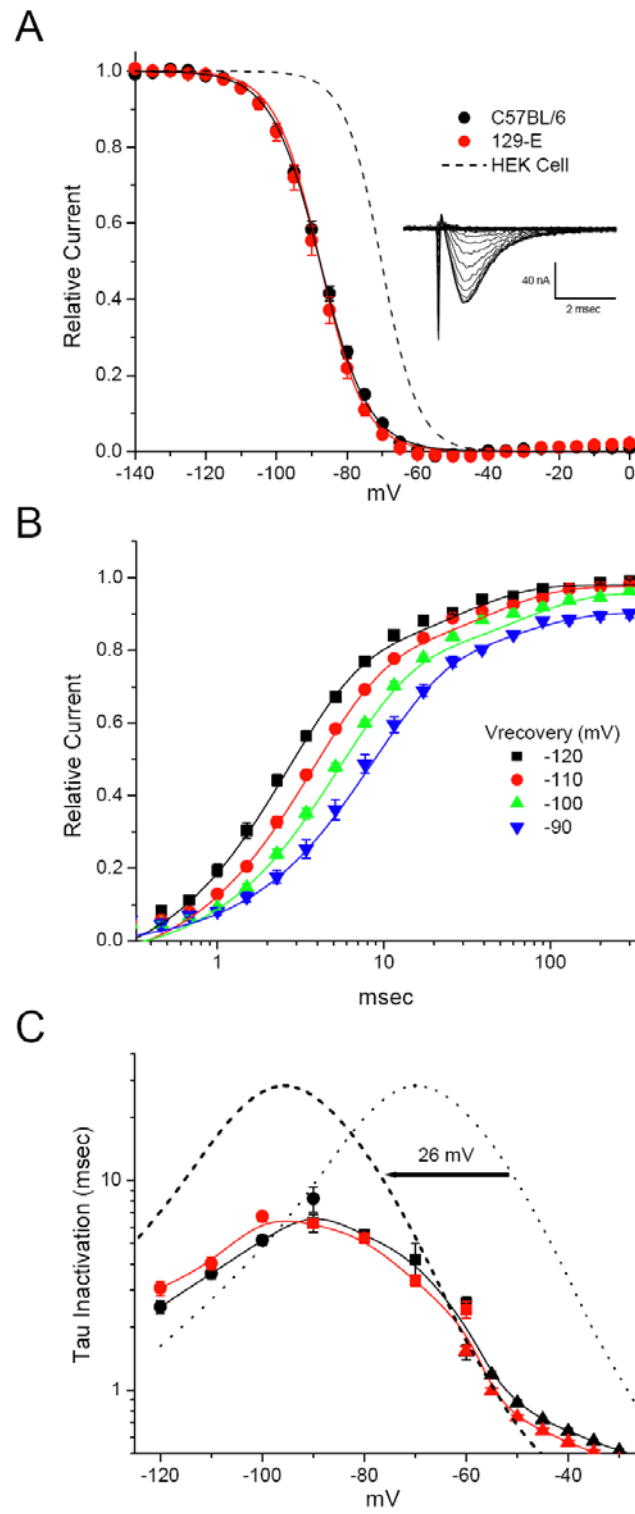


Figure 3-2. Fast inactivation properties. (A) Voltage dependence of activation was indistinguishable for muscle fibers from WT and M1592V Het mice. Voltage-dependence of fast inactivation was measured as the relative current after a 300 msec conditioning pulse. Inset shows an example of currents recorded from a C57BL/6 fiber. Boltzmann fits were indistinguishable for C57BL/6 and 129-E (solid lines), but were left shifted by 18 mV in comparison to the midpoint of fast inactivation (-70 mV) for $\text{Na}_v1.4$ channels expressed in HEK293 cells. (B) Recovery from inactivation induced by a 30 msec conditioning pulse to -20 mV. Curves show two exponential fits. (C) Kinetics of fast inactivation are displayed as the time constant for recovery (circles) or entry from closed states (square) or the open state (triangles). Kinetic properties were comparable for C57BL/6 and 129-E fibers, both of which were left shifted compared to reported values for $\text{Na}_v1.4$ expressed in HEK293 cells (dashed line).

voltage relationship in Fig. 3-1B. With this compensation, the dashed line in Fig 3-2C shows the major difference for the kinetics of fast inactivation is a four-fold faster rate of recovery (smaller time constant) for $\text{Na}_v1.4$ channels expressed in skeletal muscle fibers compared to HEK293 cells.

Slow Inactivation

Extracellular cations have effects on slow inactivation of sodium channels (Townsend and Horn, 1997), and the low external $[\text{Na}^+]$ used to minimize the series resistance error will produce a hyperpolarized shift in the voltage dependence of slow inactivation on the order of 20 mV (Webb et al., 2009). Consequently, we characterized slow inactivation in 140 mM $[\text{Na}^+]$. Series resistance errors were avoided by using a test potential of 20 mV which was close

to the reversal potential of +68 mV and therefore elicited only small Na⁺ currents on the order of -300 nA.

Two-pulse protocols used to measure slow inactivation rely upon recovery from fast, but not slow inactivation during an intervening gap at hyperpolarized potentials as a means to distinguish between these two non-conducting states. The first step therefore was to determine the optimal recovery gap duration by measuring the full time course of recovery from inactivation. The control response was measured as the peak Na⁺ current for a depolarization to 20 mV from a holding potential of -100 mV. A 30 sec conditioning pulse to 0 mV was then applied to inactivate channels and recovery at -100 mV was monitored as the peak Na⁺ current elicited by brief (7.5 msec) test depolarizations to 20 mV applied at a series of progressively longer intervals (see inset, Figure 3-3A). Recovery is plotted in Figure 3-3A as the relative amplitude of the Na⁺ current elicited by the test pulse / control pulse. Approximately 10% of the available current recovers within the first 20 msec and little additional recovery occurs by 50 msec. We interpret this initial response as an indication that 90% of the channels were slow inactivated at the end of the 30 sec conditioning pulse. There was no discernable difference for the maximal extent slow inactivation or time course of recovery for Na⁺ channels from C57BL/6 or 129-E fibers. Recovery followed a monotonic trajectory that was best fit by a two-exponential curve (solid lines, Fig. 3-3A). The two components had time constants of about 0.8 sec

and 6 sec, and had comparable magnitudes of 0.45 (Table 3-1). This recovery from slow inactivation in foot pad muscle fibers was about two-fold slower than is typically observed for $\text{Nav}1.4$ expressed in HEK293 cells (dashed line, Fig. 3-3A), where the two constants are 0.4 and 3 sec (Hayward et al., 1997).

Based on the kinetics of recovery at -100 mV following a brief conditioning pulse to 0 mV for 30 msec (Fig. 3-2B, green triangles) compared to that after a long 30 sec conditioning pulse (Fig. 3-3A), we chose a gap duration of 100 msec at -100 mV as the optimal recovery interval to distinguish fast from slow inactivation. With this recovery interval, 90% of channels would have recovered from fast inactivation, whereas only 5% of channels would have recovered from slow inactivation.

The time course for entry to slow inactivation was measured by depolarizing the membrane potential to 0 mV, and then interjecting a series of 100 msec recovery intervals at -100 mV immediately followed by a test depolarization at 20 mV (Figure 3-3B, inset). The peak current at these test depolarizations, normalized to the control response elicited at 20 mV from a holding potential of -100 mV, provided a measure for the onset of slow inactivation at 0 mV. The onset of slow inactivation occurred over a course of seconds and was more sluggish for Na^+ channels in 129-E fibers than for C57BL/6 (Fig. 3-3B). The time course for entry to slow inactivation was fit well by a single exponential with time

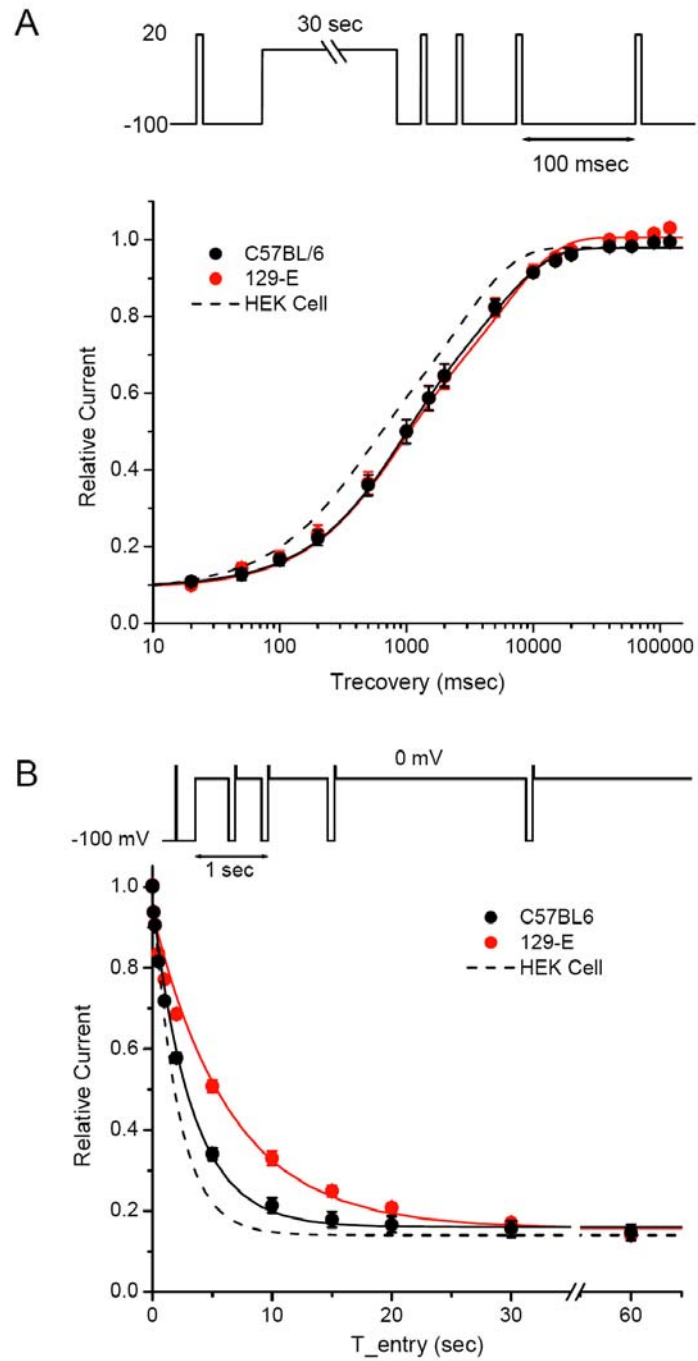


Figure 3-3. Kinetics of slow inactivation. (A) Recovery from slow inactivation at -100 mV was measured as the relative Na⁺ current elicited by 7.5 msec test pulses at varying times after a 30 sec conditioning pulse to 0 mV. Solid lines show double exponential fits to the recovery time course, which yield comparable values for C57BL/6 and 129-E fibers as listed in Table 3-1. Dashed lines show recovery from inactivation at -100 mV observed for Na_v1.4 expressed in HEK293 cells (Hayward et al., 1997) (B) Entry to slow inactivation at 0 mV was monitored as the relative Na⁺ current measured for a series of test pulses that were preceded by a 100 msec recovery gap to -100 mV. Single exponential fits demonstrated a two-fold larger time constant for 129-E fibers (6.50 sec) than C57BL/6 (3.28 sec).

Table 3-1 Slow Inactivation Properties

	C57BL/6	129-E
Steady-state		
$V_{0.5}$ (mV)	-69.9 ± 1.9	-67.6 ± 1.5
K (mV)	10.7 ± 0.5	10.8 ± 0.4
I_0	0.16 ± 0.02	0.17 ± 0.02
	(7)	(10)
Entry Kinetics		
Amp	0.80 ± 0.02	0.78 ± 0.01
Tau (sec)	3.28 ± 0.21	$6.50 \pm 0.40^{**}$
	(9)	(8)
Recovery Kinetics		
Amp_0	0.10 ± 0.01	0.12 ± 0.02
Amp_1	0.43 ± 0.04	0.48 ± 0.03
Tau_1 (sec)	0.73 ± 0.09	0.87 ± 0.12
Amp_2	0.45 ± 0.04	0.42 ± 0.02
Tau_2 (sec)	5.0 ± 0.5	7.1 ± 1.0
	(9)	(11)

** p<0.01

constants of 3.28 ± 0.21 sec for C57BL/6 ($n = 9$) and 6.50 ± 0.40 sec for 129-E ($n = 8$), which were different ($p < 0.001$). Prior studies of $\text{Na}_v1.4$ expressed in HEK293 cells have reported a faster entry to slow inactivation (Webb et al., 2009; Wu et al., 2005), with a time constant of about 2 sec (dashed line, Fig 3-3B).

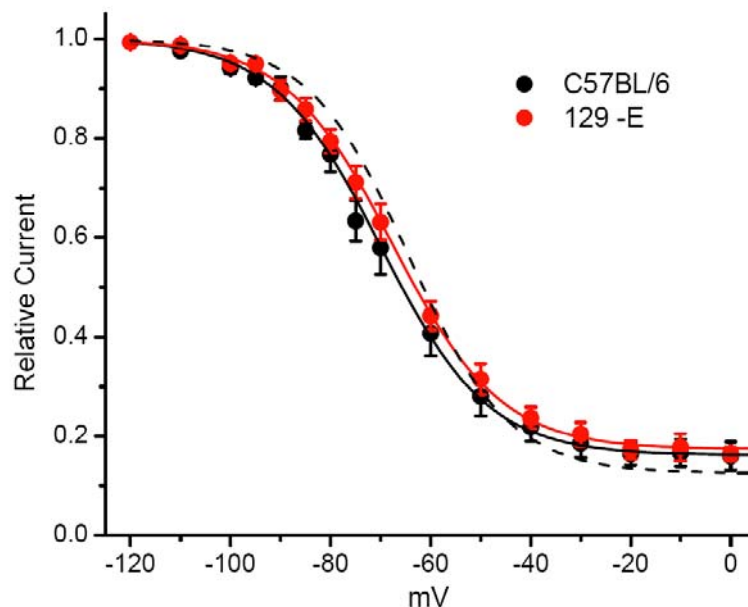


Figure 3-4. Voltage dependence of slow inactivation. Slow inactivation was measured as the relative Na^+ current that recovered within 100 msec at -100 mV, after 30 sec conditioning pulses at varying potentials. Responses from C57BL/6 and 129-E fibers were identical. Solid lines show Boltzmann fits with the parameters listed in Table 3-1. Dashed line shows slow inactivation behavior typical for $\text{Na}_v1.4$ expressed in HEK293 cells ($V_{0.5} = -64$ mV, $k = 10$ mV, $I_o = 0.13$).

The steady-state voltage-dependence of slow inactivation was measured as the relative Na^+ current that recovered within 100 msec at -100 mV, following a series of 30 sec conditioning pulses to varying potentials (Figure 3-4). The maximal extent of slow inactivation reached a plateau of 80% (0.20 relative current) at depolarized potentials, and the midpoint for the voltage dependence was about -70 mV for Na^+ channels in both C57BL/6 and 129-E fibers (see Table 3-1). Unlike the voltage dependence for fast inactivation which was left-shifted compared to $\text{Na}_v1.4$ expressed in HEK293 cells (Figure3-2A), the voltage dependence for slow inactivation was comparable for currents recorded herein for muscle foot pad muscle fibers and $\text{Na}_v1.4$ expressed in HEK293 cells.

Estimated Contribution from $\text{Na}_v1.5$ Expression in Foot Pad Muscle Fibers

The voltage dependence of activation and of fast inactivation in skeletal muscle fibers were shifted leftward (hyperpolarized), as compared to gating behavior of $\text{Na}_v1.4$ expressed in HEK293 cells (Figs. 3-1B and 3-2B). One possible explanation for this difference would be a contribution from $\text{Na}_v1.5$, which activates at more hyperpolarized potentials than $\text{Na}_v1.4$ (~20 mV shift (Chahine et al., 1996)). Moreover, $\text{Na}_v1.5$ expression is up-regulated in denervated skeletal muscle (Yang et al., 1991), and our recordings were from fibers maintained in aneural cultures for up to 48 hours. Two independent

methods were used to assess the relative expression of Nav1.4 and Nav1.5 in dissociated muscle fibers.

Nav1.5 channels are relatively resistant to tetrodotoxin (TTX) blockade, with an IC_{50} of 0.4-6 μ M compared to 5-50 nM for Nav1.4 channels (Haufe et al., 2005). Figure 3-5A shows Na^+ currents recorded from a muscle fiber were almost completely blocked by application of 200 nM TTX, which implies the majority of the current was conducted by Nav1.4 channels. The average TTX sensitivity for muscle fibers maintained in culture for three days is shown by 200 nM block in Figure 3-5B. Assuming an IC_{50} of 30 nM for Nav1.4 and 3 μ M for Nav1.5, these data show that 98% of the Na^+ current was conducted by Nav1.4 channels.

The relative abundance of Nav isoforms was also estimated from mRNA levels. A competitive RT-PCR assay was performed on acutely dissociated fibers and for those in culture for 24 or 48 hours. Nav1.4 and Nav1.5 transcripts were both amplified by a single PCR reaction with a common set of primers, and the relative abundance of amplicons was determined by optical densitometry after Nav1.5-specific digestion with *KpnI* (Fig. 3-5C). The Nav1.5 transcript was initially 15% of the total and remained under 20% even after three days in culture.

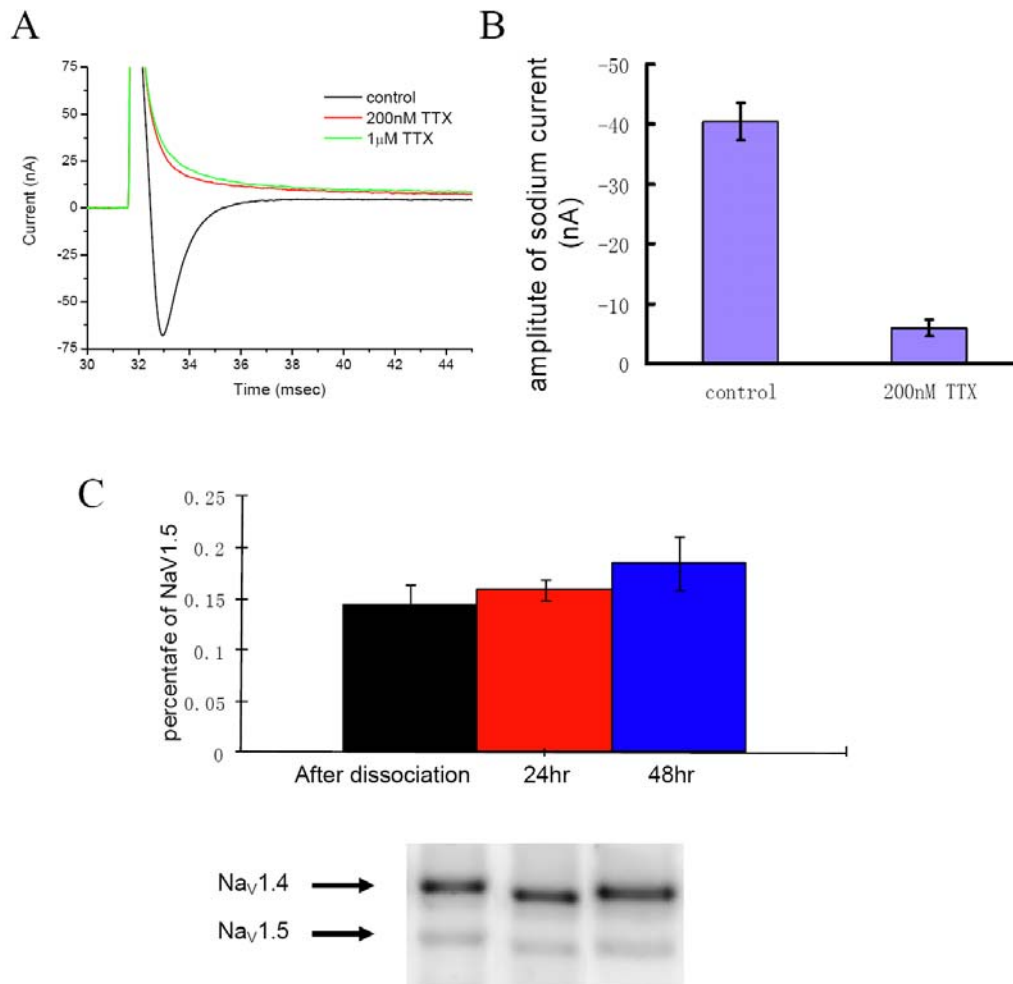


Figure 3-5. Contribution of Na_v1.5 channels to the Na⁺ current in muscle fibers. (A) Na⁺ currents recorded from muscle fibers are sensitive to TTX block. (B) Reduced Na⁺ current density for a population of muscle fibers exposed to 200 nM TTX. The 87% reduction in current density is consistent with 98% TTX-sensitive Na_v1.4 channels (IC₅₀ 30 nM) and 2% TTX-resistant Na_v1.5 channels (IC₅₀ 3 µM). (C) RT-PCR amplification of Na_v1.4 and Na_v1.5 transcripts, followed by Na_v1.5-specific digestion with *Kpn*I reveals a predominance of the Na_v1.4 transcript that remains stable for two days in culture. Left column is *Kpn*I digestion result for muscle fibers immediately collected after dissociation, middle is after 24hours, and right is after 48hours.

Both the TTX block and RT-PCR data show $\text{Na}_v1.5$ was a minor contributor to the Na^+ channel population in our muscle fibers. Therefore, we conclude the leftward shift of activation and fast inactivation observed for Na^+ currents in muscle fibers compared to $\text{Na}_v1.4$ gating in HEK293 cells is not caused by the up-regulation of $\text{Na}_v1.5$ expression.

Voltage Dependence of Fast Gating of $\text{Na}_v1.4$ Sodium Channel in Low $[\text{Na}^+]$

Extracellular cations have effects on slow inactivation of sodium channels (Townsend and Horn, 1997). It is still unclear how does low $[\text{Na}^+]$ change the fast gating behavior of sodium channel. Does the usage of low Na^+ (10mM) bath solution contribute to the hyperpolarized shift of the voltage dependence of activation in skeletal muscle fibers compared to the gating behavior of $\text{Na}_v1.4$ expressed in HEK293 cells? To answer this question, HEK293 cells transfected with $\text{Na}_v1.4$ were used to analyze the activation of sodium channel in full $[\text{Na}^+]$ (140mM) and low $[\text{Na}^+]$ (10mM) bath solutions (Figure 3-6). The G-V curves were fitted with a Boltzmann equation. The estimated parameter values were comparable for recording in full $[\text{Na}^+]$ and low $[\text{Na}^+]$. The activation midpoints are -29.8 mV and -26.3 mV for full $[\text{Na}^+]$ and low $[\text{Na}^+]$ respectively. The steepness factors are 6.8 mV (full $[\text{Na}^+]$) and 7.1 mV (low $[\text{Na}^+]$).

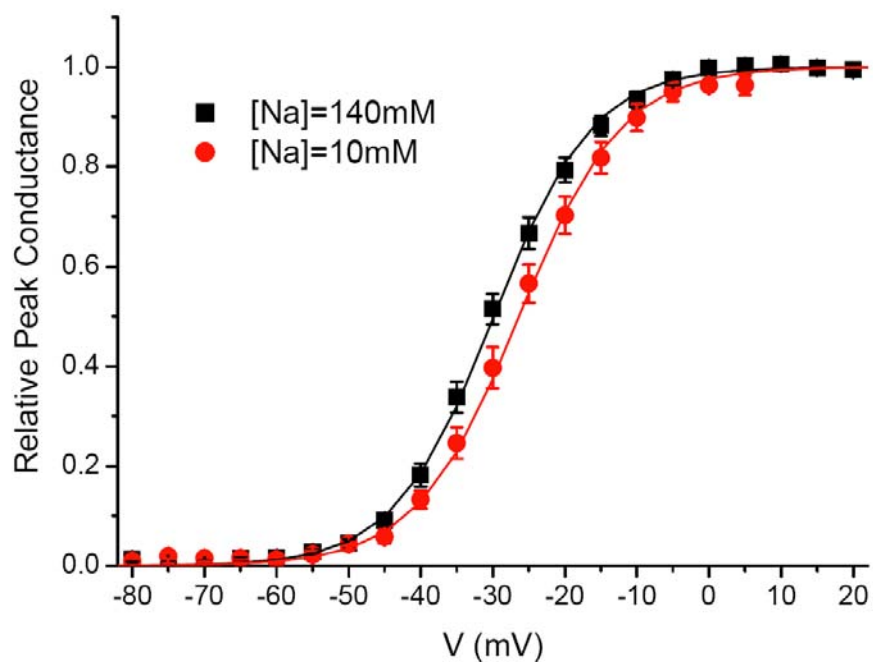


Figure 3-6. Voltage dependence of activation in full $[\text{Na}^+]$ and low $[\text{Na}^+]$ solutions. Na^+ currents were analyzed in HEK293 cells expressing $\text{Na}_v1.4$ channel. The current was recorded in bath solutions containing full $[\text{Na}^+]$ (140mM, N=12) or low $[\text{Na}^+]$ (10mM, N=12). The G-V relation was not leftward shifted in low $[\text{Na}^+]$.

Additional Factors That May Cause an Apparent Leftward Shift in Voltage

Dependence of Na^+ Channel Gating

Junction Potential Offset

An uncompensated junction potential is a possible source of error for voltage-clamp. The junction potential developed from the contact of microelectrode and bath solution can be eliminated by the offset function of the amplifier. A remaining concern, however, is that when the muscle fiber was impaled, the recording electrode was contacted with the cytoplasm. Electrode tip is then in an environment with a different ion composition compared to the bath solution. To address this possibility, 140mM K^+ bath solution was used in a set of pilot experiments to cancel the resting potential and thereby allow a direct measurement of the shift in junction potential as a consequence of fiber impalement. The shift in junction potential was around +8mV. This shift implies that the correction for the shift in junction potential would require subtracting 8mV from the experimental measured value, i.e. a greater leftward shift. Not only is the junction potential shift in the wrong direction to account for the apparent left shift of $Na_v1.4$ gating, the shift in voltage-dependence of gating was different for activation (-25 mV), fast inactivation (-18 mV) and slow inactivation (~ 0 mV). These observations rule out the possibility that the leftward shift in voltage dependence of Na^+ channel in skeletal muscle fibers is due to incorrectly compensated junction potential.

Systematic Shift

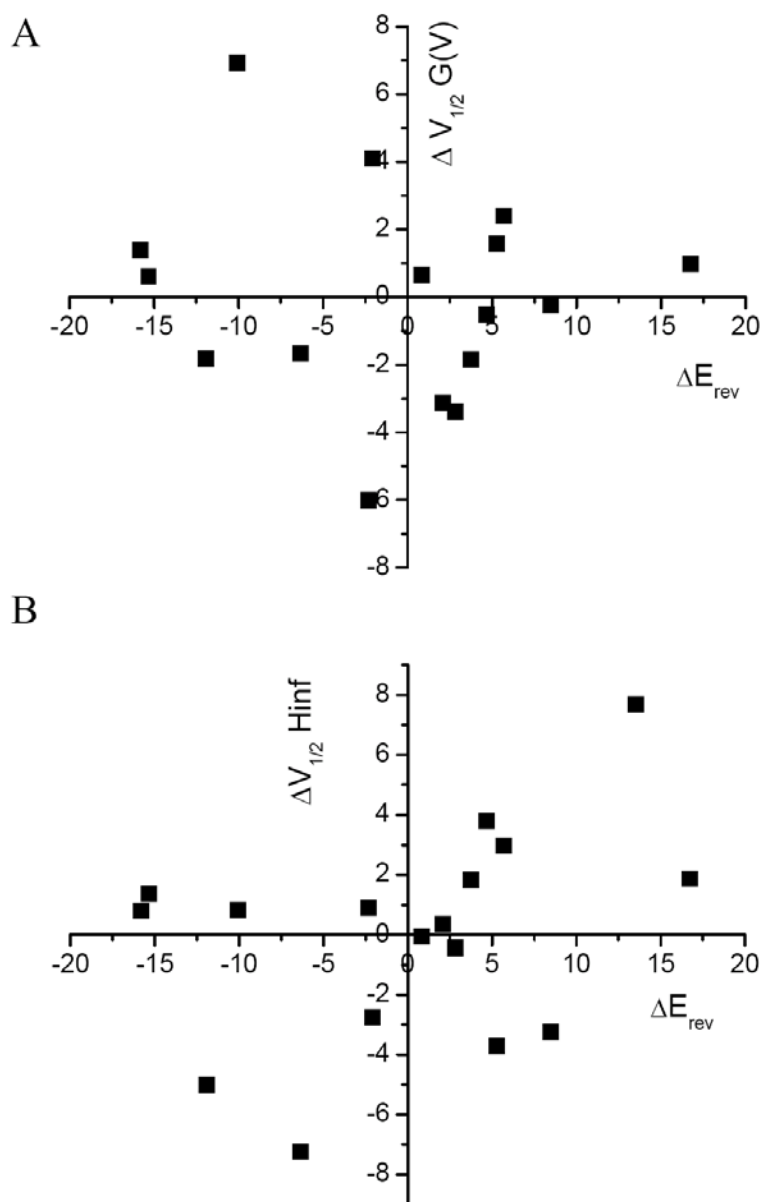


Figure 3-7. Lack of evidence for a systematic shift. The distribution of $\Delta V_{1/2}$ for the G-V curve (A) and $\Delta V_{1/2}$ of H_{∞} (B) curve were plotted as a function of the ΔE_{rev} . Each dot presents a single muscle fiber. The Δ indicates the difference of the parameters from single fiber to the average value computed from all the cells. The shift of $V_{1/2}$ of G-V relation and H_{∞} does not correlate with ΔE_{rev} .

The distribution of voltage dependencies of activation and fast inactivation of individual fibers was calculated as the differences of $V_{1/2}$ for G-V relation and H_{∞} of each fiber from the average value. The values of $\Delta V_{1/2}$ were plotted with the distribution of E_{rev} (ΔE_{rev}) (Figure 3-7). The shift of $V_{1/2}$ of G-V relation and H_{∞} does not correlate with the change of E_{rev} , which indicates there is no systematic shift under the experimental condition.

Shift Due to the Cell Damage

Whole cell patch recording is known to cause a slow leftward shift in voltage-dependence of Na^+ channel gating that may be > 10 mV over several minutes. Na^+ currents were measured in same muscle fiber every 4min up to 20min. E_{rev} , $V_{1/2}$ of G-V relation and $V_{1/2}$ of H_{∞} were plotted to the time duration after cell impalement (Figure 3-8). The E_{rev} had a depolarized shift of up to 10mV after the muscle fiber was impaled. The $V_{1/2}$ for G-V relation is stable and the $V_{1/2}$ for H_{∞} is slightly leftward shift (around 5mV) during 20min recording. Figure 3-8 indicates the leftward shift of voltage dependence of Na^+ channel gating observed in intact muscle fibers compared to $\text{Na}_V1.4$ expressed in HEK293 cells is not due to a non-specific progressive leftward shift of gating as occurs in whole-cell patch experiments.

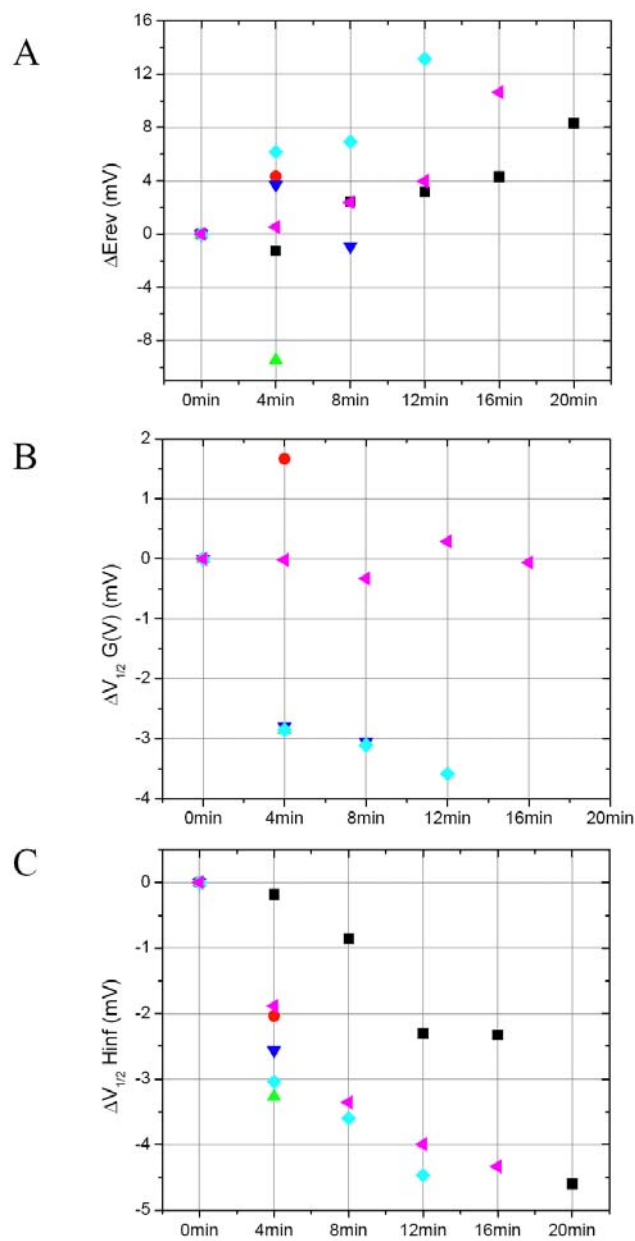


Figure 3-8. Shift after cell impalement. Na^+ currents were measured in same muscle fiber every 4min. The E_{rev} (A), $V_{1/2}$ of G-V curve (B) and $V_{1/2}$ of H_{∞} curve (C) were plotted to the time duration after cell impalement. Total recording time was up to 20min.

Discussion

The goal of this study was to characterize the gating behavior of voltage-activated sodium channels expressed in fully differentiated skeletal muscle of the mouse. Sodium currents have been measured previously in many mammalian skeletal muscle preparations (Adrian and Marshall, 1977; Almers et al., 1984; Duval and Leoty, 1978; Pappone, 1980). The motivation herein was to obtain data specifically for the mouse, as this is the preferred mammalian system for exploring genetically engineered animals. Indeed, knock-in mutants of $\text{Na}_V1.4$ have been constructed in the mouse to study myotonia and periodic paralysis (Hayward et al., 2008). Moreover, the recording technique was optimized to maintain the endogenous regulation of Na^+ channels (fully-differentiated intact fibers and sharp microelectrodes to preserve the myoplasmic contents) and to achieve a more accurate two-electrode voltage clamp by using short detubulated skeletal muscle fibers and low external sodium. The principle observations were that the voltage dependence for activation and fast inactivation were shifted dramatically toward more hyperpolarized potentials (-53 mV and -88 mV respectively), as compared to heterologous expression studies of $\text{Na}_V1.4$ in HEK293 cells, and that slow inactivation occurred over a relatively depolarized range compared to fast inactivation.

The leftward shift for the voltage-dependence of fast gating was not anticipated, and so several controls were performed to exclude possible sources of artifact. Voltage-clamp error is not a likely cause for the following reasons. First, model simulations of a short cable with voltage-activated conductances (chapter two) demonstrated that our experimental conditions (fiber length $\sim 450 \mu\text{m}$, low external $[\text{Na}^+]$ of 10 mM with peak Na^+ current $< 150 \text{ nA}$) were conservative with regard to space clamp and clamp speed. Explicit simulations for the peak I-V curve showed only a minimal leftward shift of activation from distortions of the voltage clamp, about 1.5 mV for a 600 μm fiber in 22 mM Na^+ . Second, there was no correlation between the maximal peak amplitude of the Na^+ current and the midpoint of activation amongst a population of over 30 fibers. If series resistance had been significant, then an apparent left shift and steeper voltage dependence of activation would have been observed in fibers with larger current amplitudes. Third, the relative leftward shift of gating was not identical for activation and fast inactivation, which rules out an uncompensated junction potential or membrane surface charge effect. Three different leak subtraction techniques were used: conventional P/8, TTX-sensitive, slow inactivation with a prepulse and all yielded the same leftward shift of gating. The low external $[\text{Na}^+]$ of 10 mM used to minimize series resistance effects is not a likely cause since parallel studies on $\text{Na}_v1.4$ expressed in HEK293 cells did not show a concentration-dependent shift of gating. Finally, the possibility of an

upregulation of $\text{Na}_v1.5$ relative to $\text{Na}_v1.4$ was excluded by showing near complete block of currents with 200 nM TTX and by mRNA analysis with RT-PCR. Therefore, we conclude that the relatively hyperpolarized values for the voltage-dependence of gating reported herein are an intrinsic feature of $\text{Na}_v1.4$ when expressed in an intact fully-differentiated mouse fiber.

A survey of published reports for the voltage-dependence of $\text{Na}_v1.4$ gating reveals a rather broad range of values for the midpoint of activation or fast inactivation. In general, the observed voltage dependence of gating for $\text{Na}_v1.4$ is more depolarized when expressed heterologously in HEK293 cells (Bouhours et al., 2004; Takahashi and Cannon, 1999) than is observed for native current in skeletal muscle, regardless of whether the $\beta 1$ subunit is co-expressed (Webb et al., 2009). Moreover, the midpoint of activation is notoriously unstable in HEK293 cells. Over the course of a few minutes after attaining whole-cell access, the voltage dependence shifts by up to 20 mV to more hyperpolarized potentials. It is notable that we did not observe this progressive leftward shift in TEVC recordings lasting up to 20 minutes in muscle fibers. In HEK293 cells the midpoint of activation is -20 to -30 mV, and for fast inactivation is -60 to -70 mV. No consistent differences in voltage-dependence are observed between rat (Cummins et al., 1993; Hayward et al., 1996) and human (Takahashi and Cannon, 1999; Yang et al., 1994) $\text{Na}_v1.4$ expressed in HEK293 cells. To our knowledge, mouse $\text{Na}_v1.4$ has not been studied by expression in HEK293 cells. To study Na^+

currents in a muscle-cell context, recordings are often performed by whole-cell patch recording from myoballs that were differentiated from primary cultures of myoblasts. For human myoballs, the midpoint of activation and fast inactivation were -34 mV and -66 mV, respectively (Probstle et al., 1988). In mouse, cell-attached patch recordings from myoballs yielded values of -40 mV for activation and -75 mV for fast inactivation (Mille et al., 2009). An important caveat for the myoball studies is the high expression level of the fetal/cardiac isoform, $\text{Na}_v1.5$, which has a leftward shift of gating relative to $\text{Na}_v1.4$ and may account for 40% of the total Na^+ current (Mille et al., 2009). Finally, a variety of approaches have been used to record Na^+ currents from acutely dissociated fully-differentiated mammalian skeletal muscle. Adrian and Marshall developed a three-electrode technique for voltage-clamping intact fibers of physical lengths exceeding the length constant (Adrian and Marshall, 1977). Voltage control was approximate, at best, and the estimated midpoints for activation and fast inactivation in rat extensor digitorum longus muscle (EDL) were -47 mV and -80 mV, respectively. Pappone (Pappone, 1980) used a Vaseline gap voltage-clamp on cut fibers from rat fast twitch muscle (EDL or sternocleidomastoid). The midpoints for activation and fast inactivation were -52 mV and -90 mV, values that are identical to our findings herein. Almers and colleagues developed the loose-patch voltage-clamp method (Stuhmer and Almers, 1982) and recordings from biopsied human intercostal muscle showed midpoints for activation and fast inactivation of -46

mV and -86 mV, respectively (Almers et al., 1984). Taken together, these observations show a general trend that as the experimental preparation becomes more distant from fully differentiated intact muscle along a progression through disruption of muscle fiber integrity, cultured myotubes, or heterologous expression in non-muscle mammalian cell lines then there is a progressively larger depolarized shift in the voltage dependence of $\text{Na}_v1.4$ gating compared to the behavior in unperturbed muscle.

In addition to the experimental manipulations described above that result in shifts for the voltage dependence of $\text{Na}_v1.4$ gating, there are many examples whereby the voltage dependence of the Na^+ current is dynamically modulated in skeletal muscle. One of the strongest modulators is denervation, which results in upregulation of $\text{Na}_v1.5$ TTX-resistance channel expression (Yang et al., 1991) and therefore a leftward shift in the voltage dependence of current activation. Fiber type also influences Na^+ currents, with slow type I fibers having lower current density and a depolarized shift in gating as compared with fast type IIa or IIb (Duval and Leoty, 1980; Ruff, 1992), although also see (Rannou et al., 2009). We did not histologically assess fiber type in this study, but the intrinsic muscles of the footpad are primarily fast twitch muscles. Sodium currents may also be modified by acquired muscle diseases. In critical illness myopathy, excitability is decreased by a hyperpolarized shift of inactivation and activation with a net result of chronic inhibition at the resting potential (Rich and Pinter, 2003). More

recently, it has been observed in loose patch recordings that the midpoint of Na^+ current activation and fast inactivation in rat EDL will shift reversibly by tens of mV over minutes in response to sustained shifts in the holding potential (Filatov et al., 2005). This discovery raises questions about the impact of depolarizing high-K solutions used to nullify the resting potential for cell-attached patch studies on skeletal muscle. Genetic background can also affect Na^+ channel gating, as was observed for myoballs cultured from different strains of mice (Mille et al., 2009), although in agreement with our study there was no significant difference for C57BL/6 and 129-E mice. Much remains to be determined about the relative contributions of Na_v isoform switching, post translational modification, or trafficking as the mechanistic basis for the dynamic modulation of Na^+ current gating in skeletal muscle. Recognition of these effects, however, illustrates how it is possible for the gating behavior of $\text{Na}_v1.4$ channels to vary under different experimental contexts and supports our contention that the hyperpolarized shift of gating observed herein for TEVC recordings of detubulated mouse fibers, relative to the plethora of HEK293 cell expression studies, most likely represents the channel behavior when endogenously expressed in fast twitch muscle and not an artifact associated with the technical challenges for recording Na^+ currents in fibers.

Slow inactivation of $\text{Na}_v1.4$ in skeletal muscle may be important for setting Na^+ channel availability in response to slow shifts in the resting potential (Ruff et

al., 1988) , and if disrupted results in susceptibility to periodic paralysis (Cannon, 2006). As a result of the technical challenges to maintain a stable recording over several minutes required to characterize slow inactivation, prior studies of slow inactivation for endogenous Na^+ currents in mammalian muscle fibers are primarily based on the loose patch technique (Rich and Pinter, 2003; Ruff et al., 1988; Ruff and Whittlesey, 1992) and a few cell-attached patch studies (Desaphy et al., 2001). We found robust slow inactivation for Na^+ currents in mouse muscle fibers for which the kinetics of entry and recovery were about two-fold slower than observed when $\text{Na}_v1.4$ is expressed in HEK293 cells (Hayward et al., 1997), both at room temperature. Unlike the situation for fast inactivation where we observed ~ 20 mV leftward shift in muscle fibers compared to HEK293 cells (Fig. 3-2A), the voltage dependence for slow inactivation was comparable in muscle fibers and HEK293 cells, both being about -65 mV (Fig 3-4). Viewed in another way, our data for endogenous Na^+ currents in mouse muscle fibers showed a much larger separation in the voltage dependence of fast inactivation (-88 mV) and slow inactivation (-68 mV) than has been observed for $\text{Na}_v1.4$ expressed in HEK293 cells, typically -70 mV for fast and -64 mV for slow inactivation. Curiously, the inverse has been reported by two groups using loose patch recording (Rich and Pinter, 2003; Ruff and Whittlesey, 1992); that is slow inactivation occurred at more hyperpolarized potentials than fast inactivation. In one case (Ruff and Whittlesey, 1992), this may be partially explained by the use

of an unusually short conditioning pulse duration (20 msec) which would cause an apparent rightward shift of fast inactivation. Cell-attached patch recordings in rat fibers (Desaphy et al., 2001), both EDL and soleus, revealed a 30 mV depolarized shift for slow inactivation (-64 mV) compared to fast inactivation (-94 mV), similar to our TEVC studies in mouse fibers. The functional implication of our finding is that modulation of Na⁺ channel availability in skeletal muscle is tuned for regulation by fast inactivation at the resting potential of -90 mV corresponding to the steepest region of the fast inactivation curve. Slow inactivation, however, occurs at much more depolarized potentials (-68 mV). Therefore slow inactivation is more likely to have physiological relevance for limiting excitability during prolonged bursts of action potentials (use-dependent trapping in the slow inactivated state) or as a protective mechanism to prevent attacks of depolarization-induced periodic paralysis resulting from fast gating defects in mutant Nav1.4 channels.

The gating properties of Na⁺ currents reported herein provide an important benchmark. These data were recorded under conditions of minimal disruption of the internal milieu (by using sharp microelectrodes instead of cut fibers or patch pipette) in fully differentiated fibers and with excellent voltage-clamp control (detubulation and low external [Na⁺] to reduce series resistance errors). Moreover, slow inactivation was characterized in addition to the conventional measures of activation and fast inactivation. Model simulations of fiber excitability in

mammalian muscle and quantitative analyses to explore the functional impact of Na⁺ channel mutations in myotonia and periodic paralysis should be based on these data rather than the properties observed in HEK293 cells. Finally, these data provide normative controls for Na⁺ currents in the mouse which has become the preferred species for mammalian studies due to the opportunities for genetic manipulation.

**Chapter Four : Gating Defects for the Hyperkalemic Periodic Paralysis
Associated Sodium Channel Mutation M1592V in Fully Differentiated Mouse
Skeletal Muscle Fibers**

Introduction

The firing of action potentials in excitable cells such as nerve and muscle cells are triggered and regulated by the gating of the Na⁺ conductance. Five allelic inherited muscular diseases are caused by mutations in the gene *SCN4A* that encodes the α -subunit of skeletal muscle Na⁺ channel (Nav1.4). Hyperkalemic periodic paralysis (HyperPP) is an autosomal dominantly inherited disease associated with Nav1.4 mutations (Cannon, 2006). A characteristic feature of HyperPP is attacks of episodic weakness which is distinguished from other forms of periodic paralysis by association with elevations in the serum potassium concentration (Gamstorp, 1956). During attacks, the sarcolemmal excitability is transiently impaired due to the depolarized resting potentials and thereby causes the muscle weakness (Creutzfeldt et al., 1963). In addition to muscle weakness, HyperPP muscle may have pathologically enhanced excitability which results in muscle stiffness (myotonia) caused by abnormal repetitive firing of action potentials (Van Der Meulen et al., 1961).

In 1983, an aberrant persistent Na^+ current was detected in biopsied muscle fibers of patients with HyperPP (Lehmann-Horn et al., 1983). Subsequently, genetic evidence was obtained that showed HyperPP is linked to *SCN4A*, the gene encoding the α -subunit of $\text{Na}_v1.4$ (Fontaine et al., 1990). To date, eleven $\text{Na}_v1.4$ mutations have been identified among patients with HyperPP (Cannon, 2006; McClatchey et al., 1992; Ptacek et al., 1991; Rojas et al., 1991; Wagner et al., 1997). T704M and M1592V are the two commonly occurring mutations in HyperPP (Miller et al., 2004).

The substitution of M1592V is located near the cytoplasmic face of the S6 transmembrane segment of domain IV in the $\text{Na}_v1.4$ α -subunit (Figure 4-1). Functional studies of $\text{Na}_v1.4$ -M1592V by transient expression in HEK293 cells and *Xenopus laevis* oocytes have revealed gain-of-function defects. The voltage dependence of rM1585V (rat homologue, 92% identical to human isoform at the amino acid level) mutant channel was not changed, whereas the mutant channel displayed an increased non-inactivating steady-state Na^+ current compared to wild type (WT) channels ($I_{ss}/I_{peak} \sim 0.07$ compared to 0.01 for WT) (Cannon and Strittmatter, 1993). Slow inactivation was impaired for rM1585V, which exhibits a 12 mV depolarized shift of voltage dependence, a two-fold increase in the fraction of channels resistant to slow inactivation at strongly depolarized potentials and rapid recovery from slow inactivation (Hayward et al., 1997). Comparable defects were described for human M1592V mutant Na^+ Channel

expressed in HEK293 cells (Hayward et al., 1999). When expressed in *Xenopus laevis* oocytes, the voltage dependence of activation was 5~10mV shift toward the hyperpolarized direction for human M1592V mutant channels, resulted in a twofold increase in the persistent (window) current as compared to WT channels (Rojas et al., 1999). The hyperpolarized shift of activation for Nav1.4-M1592V was detected when expressed in human but not rat Nav1.4. This difference might be accounted for the subtle structure differences among these Na⁺ channel isoforms.

An additional source of discrepancy may be due to the potential variations of posttranslational modification among different cell types and species used for the studies. A mutation corresponding to the human M1592V substitution was introduced into the mouse Nav1.4 gene. The M1592V knock-in mutant mice exhibit a HyperPP phenotype including myotonia, K⁺-sensitive paralysis and muscle fiber-type switching (Hayward et al., 2008). The primary goal of this study is to determine whether similar gating defects of Nav1.4-M1592V channels found in heterologous expression systems occur endogenously in mouse skeletal muscle. Unfortunately, homozygous M1592V/M1592V mice had a very low survival rate (1.4%) (Hayward et al., 2008), and therefore all studies were performed in fibers dissociated from the footpad skeletal muscle in heterozygous WT/M1592V mice.

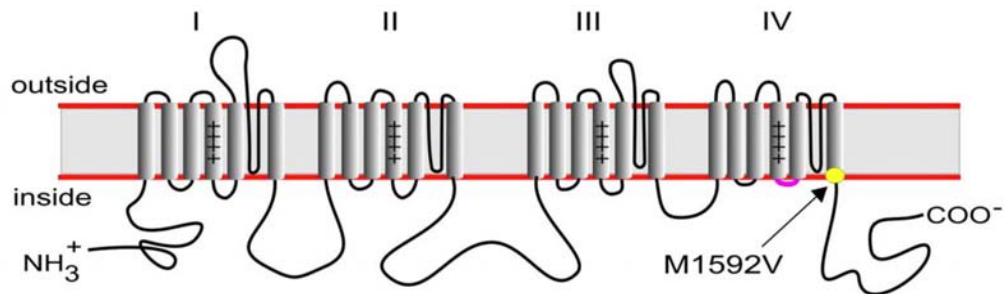


Figure 4-1. Location of M1592V HyperPP mutation. Topology of Na⁺ channel α-subunit and the location of the M1592V are shown. The M1592V mutation is located within the S6 transmembrane segment of domain IV. (Hayward et al., 2008)

Materials and Methods

Muscle Fiber Preparation

Individual muscle fibers were isolated by enzymatic digestion and mechanical disruption from mixed muscles of the hind foot of adult C57/B16 wild-type (WT) and M1592V Heterozygous mice (age 2 – 6 months). Animals were sacrificed by isoflurane inhalation and cervical dislocation, in accordance with guidelines by our Institutional Animal Care and Use Committee. The muscle was rapidly dissected free and placed in DMEM plus 1 mg/ml collagenase (Gibco, Grand Island, NY). The muscle was incubated at 37 °C for 90 minutes. Fibers were dissociated by trituration in a wide-bore pipette, pelleted by

centrifugation, and resuspended in DMEM plus 10% fetal bovine serum, 1% glutamine, 100U/ml Penicillin/streptomycin and 10mM HEPES. Approximately 100 fibers were plated in 35 mm culture dishes coated with rat tail collagen and matrigel (BD Biosciences, San Jose, CA). Cultures were maintained for 1 to 3 days in 5% CO₂ at 37 °C.

Two-Electrode Voltage Clamp Recording

Currents were recorded with the two-electrode voltage clamp (TEVC) technique, using an AxoClamp2B amplifier (Molecular Devices, Sunnyvale, CA) with the HS-2A headstage. Fibers were visualized on an inverted microscope (IMT-2 Olympus, Center Valley, PA) with Hoffman optics. Disruption of the T-tubule system from the sarcolemma was achieved by hyperosmolar shock in Ringer's solution plus 400 mM glycerol for 1 hr, and the fibers were then returned to isomolar Ringer's solution for 30min before recording (Dulhunty and Gage, 1973). Isolated fibers adherent to the collagen/matrigel coated dish and < 600 μm in length were selected for recording by impalement near their midpoint with both stimulating and recording sharp microelectrodes. The standard bath was a Cl-free low-Na⁺ solution containing NaOH 10 mM, tetraethylammonium hydroxide (TEAOH) 130 mM, Mg(OH)₂ 1 mM, Ca(OH)₂ 1 mM, 4-(2-hydroxyethyl)-1-piperazineethanesulfonic acid (HEPES) 10 mM, glucose 10 mM, 4-aminopyridine

(4-AP) 5 mM, anthracene-9-carboxylic acid (9-AC) 100 μ M, nifedipine 5 μ M, pH adjusted to 7.4 by methanesulfonic acid. Dantrolene 3 μ g/ml and the skeletal muscle myosin II inhibitor N-benzyl-p-toluene sulphonamide (BTS) 20 μ M (Cheung et al., 2002) were added to suppress depolarization-induced contraction in studies on fibers with intact T-tubules. The extracellular Na⁺ concentration was lowered to 10mM to reduce the current amplitude and thus to improve the voltage control. The current injection pipette was filled with 2 M Cs-Aspartate (resistance of 3-5M Ω) and the voltage sensing electrode contained 3 M CsCl (resistance 7-10 M Ω). All measurements were performed at room temperature.

Data Analysis

Voltage-clamp control, current recording, and analysis of traces were performed using pClamp9.2 (Axon Instruments, Foster City, CA). The data were analyzed by the using of computer programs: Excel (Microsoft Corporation) and Origin 6.0 (MicroCal, Northampton, MA).

Conductance was calculated as:

$$G(V) = I_{\text{peak}}(V)/(V-E_{\text{rev}})$$

where the reversal potential (E_{rev}) was measured experimentally for each cell. The voltage dependence of activation was quantified by fitting the current measure to a Boltzmann function:

$$I_{peak}(V)/(V-E_{rev}) = G_{max}/[1 + \exp(-(V - V_{1/2})/\kappa)]$$

The steady-state voltage dependence was measured for fast and for slow inactivation by using wither brief (300 msec) or long (30 sec) conditioning pulse respectively. The relative current availability (I_{test}/I_{max}) was fitted to a Boltzmann function with a non-zero pedestal (I_0), calculated as:

$$I_{test}/I_{max} = (1 - I_0)/[1 + \exp((V-V_{1/2})/\kappa)] + I_0$$

where $V_{1/2}$ is the half-maximum voltage and κ is the slope factor.

The kinetics of fast inactivation was quantified from single-exponential fits to the macroscopic current decay. The time constant of the decay (τ), was estimated by fitting macroscopic Na^+ currents (I) to a single exponential plus a constant term (I_0) as:

$$I=(I_{max}-I_0)*\exp^{-t/\tau}+I_0$$

where I_{max} is the maximal amplitude. A similar function was used to estimate the time constant for the entry to fast inactivation revealed by two-pulse protocols at conditioning voltage $-90mV \sim -60mV$.

$$I_{test}/I_{ref}=(1-I_0)*\exp^{-t/\tau}+I_0$$

In this case I_{test} is the peak current elicited by a test pulse to -40 mV after a conditioning inactivation pulse of varying duration (t). I_{test} was normalized to the peak amplitude of a reference current (I_{ref}), elicited by a -40mV pulse before application of the conditioning pulse. The same equation was used for the analysis of the kinetics of entry to slow inactivation.

To measure the time course of recovery from fast inactivation, a 30 msec conditioning pulse to -20 mV was applied to fast inactivate the channels fully, followed by a return to the recovery potential (between -120 and -90 mV) for a variable interval (t). The fraction of available (recovered) channels was assayed with a test pulse to -40 mV. The relative peak current (I_{test}/I_{ref}) was fit to the equation:

$$I_{test}/I_{ref} = A_1 * (1 - \exp(-t/\tau_1)) + A_2 * (1 - \exp(-t/\tau_2)) + I_0$$

A_1 and A_2 are the amplitudes of the two components, τ_1 and τ_2 are the time constants, t is the recovery time. The faster time constant was used to characterize the kinetics of recovery from fast inactivation.

The recovery of Na⁺ channel availability after prolonged depolarization is characterized by multiple exponential components (Cummins and Sigworth, 1996), including "intermediate" component (I_M , recovers within 100-300 msec), slow-inactivated component (I_S , recovers within 1-3 sec), and ultraslow-inactivated channels (I_U , recover over minutes). Recovery from intermediate (I_M)- and slow

(I_S)-inactivated states was measured by the use of a sequential recovery protocol in which a single conditioning pulse (up to 120 sec) was followed by a series of brief test pulses (7.5 msec) during the recovery interval. Peak current from each test pulse was normalized to a reference current (I_{ref}), measured as the mean peak value from five separate step depolarizations to -40 mV before the conditioning pulse. I_{test}/I_{ref} values were then fit with the same two-exponential equation as used for recovery from fast inactivation.

Measured values are presented as the mean \pm standard error of the mean unless otherwise noted. Statistical significance was determined by student t test. P values were noted in the text. Values of $P < 0.05$ were considered significant.

Mutant Sodium Channel Expression

A competitive RT-PCR assay was used to estimate the relative expression level of WT and M1592V mutant Na^+ channel in dissociated foot pad muscle fibers. Approximately 50 fibers were collected from each of three M1592V heterozygous mice after cell dissociation. After washing by PBS, cells were lysed in 0.25ml TRIZOL reagent (Sigma, St. Louis, MO) by trituration with needle. Total RNA was precipitated according to the chloroform/ isopropanol/ETOH method. Extracted RNA samples were treated with 4U RNase-free

Deoxyribonuclease I (DNaseI, 2 μ l, 2000U/ml, BioLabs, Ipswich, MA) to remove genomic DNA.

Total RNA from each sample was reverse transcribed in a 20 μ l reaction with Superscript III first strand kit (invitrogen, Carlsbad, CA). 20 μ l per sample RT reaction containing 1 \times RT buffer (2 μ l 10 \times buffer), 10mM DTT (2 μ l, 0.1M), 1mM dNTPs (2 μ l, 10mM), 5mM MgCl₂ (25mM 4 μ l), 40U RNAase inhibitor (1 μ l, 40u/ μ l), 100ng random hexamer (2 μ l 50ng/ μ l), 50U Superscript III (0.25 μ l, 200U/ μ l) and 10 μ l RNA sample, add DEPC water to make the final volume 20 μ l; keep mix on ice at all times. Reverse transcription was performed following the supplier recommended protocol. An "enzyme minus" negative control was set up side by side to test the contamination of genomic DNA.

To compare the expression levels of the WT and M1592V mutant transcripts, competitive RT-PCR was used to simultaneously amplify two Na⁺ channel fragments in a single reaction. Two rounds of PCR were used to amplify the signal. 5 μ l cDNA product from each sample was used for a conventional PCR reaction with Tag DNA polymerase (for each sample, 50 μ l PCR reaction containing 25 μ l choice tag mastermix (Denville scientific Inc., Metuchen, NJ), and 10 μ mol forward and reverse primers). The cycling parameters were denaturation at 94 $^{\circ}$ C for 30 sec, annealing at 55 $^{\circ}$ C for 30 sec, and extension at 72 $^{\circ}$ C for 45 sec, total 40 cycles. 5 μ l product from the first round of PCR was used

for secondary PCR reaction. Same protocol as the first PCR was used. The external primer pairs used for first PCR were:

forward 5'- TCTTCGGCATGTCTAACTTCGCCT-3'

reverse 5'-AAAGAGGATGTCCAGGCAGTGGAT-3'

the nested internal primers used for second PCR were:

forward 5'- AGACTGTGACCCGACATTGGAGAA-3'

reverse 5'- AGAAAGGCGGCTGTAGTCGATGAA -3'

Because the WT and M1592V mutant templates differ by only two base pairs (Hayward et al., 2008), the two transcripts should be amplified with equivalent efficiencies.

The PCR products after the second round PCR reaction for WT and M1592V mutant Na⁺ channel both are 271bp. TA-cloning and restriction enzyme digestion were used to distinguish WT and mutant amplicon abundance (Mankodi et al., 2002) because this method has higher sensitivity than simple gel intensity measurements. Products were cloned in pCR2.1 vector using the original TA-cloning kit (Invitrogen, Carlsbad, CA). Clones expressing inserted cDNA fragment were selected and plasmid DNA was isolated by miniprep. 10µl plasmid DNA was processed by specific restriction endonuclease treatment using *pflFI* and *HpaI*, 37°C overnight. For plasmid DNA inserted with mutant channel,

there are two fragments after enzyme treatment, 2777 bp and 1423 bp, whereas the WT channel fragment remained one 4200 bp band. Enzyme treated products were analyzed on a 1% agarose gel. The numbers of clones containing WT or mutant channel were counted for each sample. Total 5 samples from 3 mice were included in the statistics.

Results

Activation

Na⁺ channel activation was determined by measuring the peak Na⁺ current elicited by 15 msec step depolarizations from a holding potential of -100mV (Figure 4-2). Test depolarizations from -100 to +45mV were applied in 5mV increments. Leak subtraction was performed by using a 30 msec conditioning pulse to inactivate Na⁺ channels, after which the pulse protocol was repeated to measure the residual background currents (capacitive and ionic) (chapter two). The peak Na⁺ current density (at test potential -45mV) was greater for muscle fibers from WT mice (-14.9 ± 0.88 nA/nF) compared to M1592V heterozygous mice (-10.4 ± 1.01 nA/nF), $p < 0.05$ (Figure 4-2B). The Na⁺ conductance was estimated from the peak current and the measured reversal potential for each fiber. The G-V relation was fit well by a Boltzmann function as plotted in Figure 4-3A (right). The voltage for half-activation and steepness were comparable for WT

and M1592V heterozygous mice. The activation midpoints were -53.3 ± 0.45 mV (WT, $n = 41$) and -51.5 ± 0.91 mV (M1592V, $n = 10$) and steepness factors were 4.2 ± 0.17 mV (WT) and 4.6 ± 0.30 mV (M1592V).

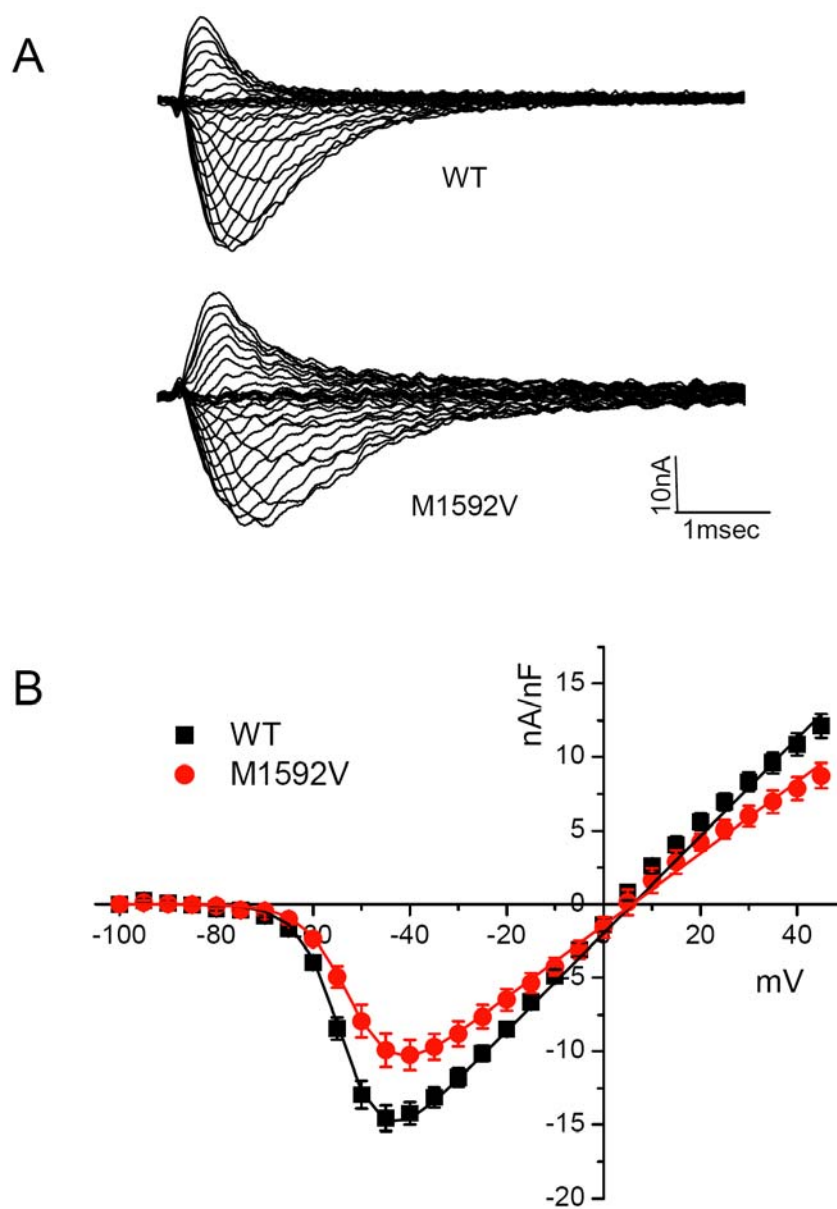


Figure 4-2. Representative currents and voltage dependence of activation. (A) Representative currents of muscle fibers from WT (top) and M1592V heterozygous (bottom) mice. Currents were elicited by a series of 15 msec voltage steps from a holding potential of -100 mV to voltages ranging from -100 to +45 mV in 5 mV increments. (B) Peak Na⁺ current was normalized to fiber capacitance and plotted as the average for fibers from WT mice or M1592V heterozygous mice. Error bars show SEM.

Fast inactivation

The steady-state voltage dependence of fast inactivation was measured as the relative Na⁺ current elicited by a test depolarization to -40 mV, following a 300 msec conditioning pulse from -100mV to 0mV in 5mV increments (Figure 4-3A, left). A standard P/8 leak subtraction method was used to remove background leak current. The steady-state voltage dependence was not different between fibers from WT and M1592V heterozygous mice. Quantified by fitting to a Boltzmann function, the half-inactivation midpoints are -87.7 ± 0.59 mV (WT, n = 36) and -87.0 ± 1.3 mV (M1592V, n = 20), and the steepness factors are 6.8 ± 0.1 mV (WT) and 6.8 ± 0.2 (M1592V).

The time course of recovery from and entry to fast inactivation was quantified and used to characterize the kinetics of fast inactivation. Recovery from inactivation was measured after a 30 msec conditioning pulse to -20 mV to fully fast inactivate Na⁺ channel. After an increasing duration of recovery (0.2-300 msec) at potentials ranged from -120 mV to -90 mV msec, the Na⁺ current

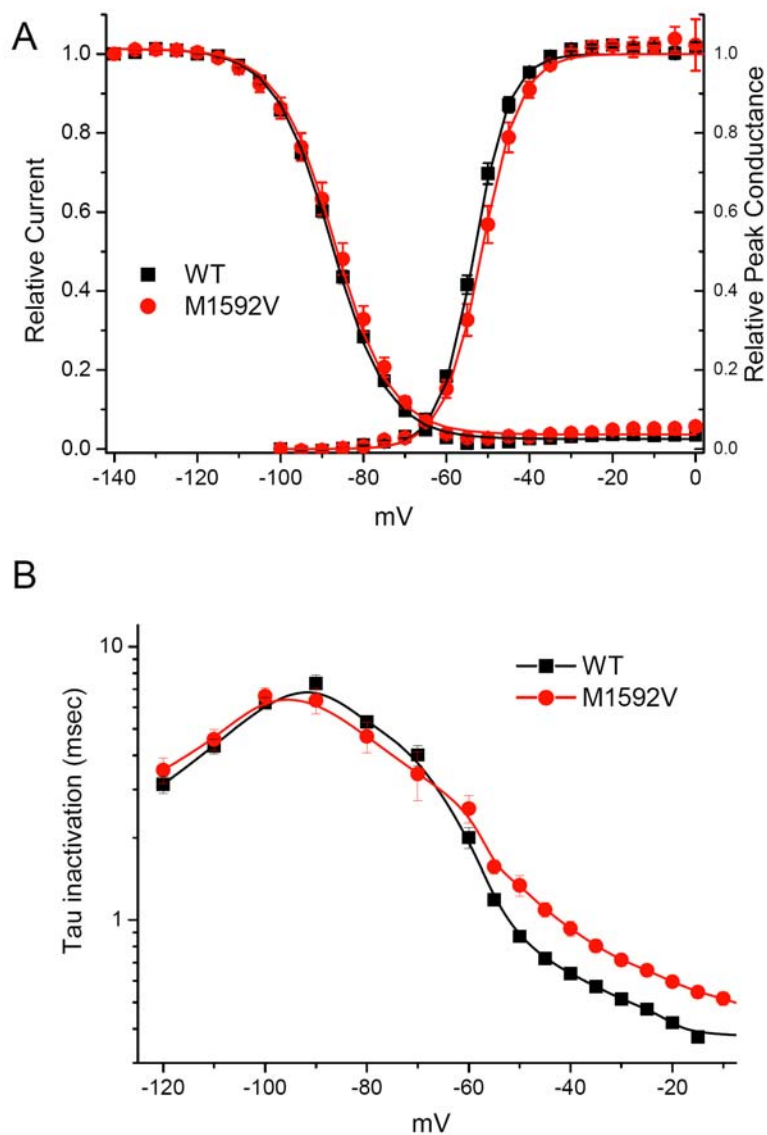


Figure 4-3. Fast inactivation properties. (A) Boltzmann fits of relative peak conductance were indistinguishable for WT and M1592V fibers. Voltage-dependence of fast inactivation was measured as the relative current after a 300 msec conditioning pulse. Boltzmann fits was not altered by M1592V. (B) Kinetics of fast inactivation is displayed as the time constant for recovery, entry from closed states or the open state. Kinetic properties were slightly slower for M1592V fibers compared to WT at depolarized potential. Parameters for voltage dependence of activation and steady state fast inactivation were listed in Table 4-1.

was elicited by a second pulse to -40mV. The recovery of relative peak Na⁺ current was fit by a double exponential, with the faster component used to characterize the kinetics of recovery from fast inactivation. The kinetics for entry to fast inactivation from the open state (-55 to -20 mV range) was determined by a single exponential fit to the macroscopic Na⁺ current decay. Finally, the rate of closed-state entry to fast inactivation (-90 to -60 mV range) was determined with a two-pulse protocol. In the protocol, the conditioning pulse duration was progressively increased from 0.2 to 300 msec, and the decay of peak Na⁺ current elicited by the second pulse to -40 mV was fitted by a single exponential. A summary for all three measures of fast inactivation kinetics is shown in Figure 4-3B. The time constants were plotted against the voltage. The time constants at depolarized potential (from -55 to -15 mV) were slightly increased for muscle fibers dissociated from M1592V heterozygous mice compared to WT.

	Activation		Fast Inactivation		Slow Inactivation		
	V _{0.5} (mV)	κ (mV)	V _{0.5} (mV)	κ (mV)	V _{0.5} (mV)	κ (mV)	I _o
WT	-53.3 ± 0.5 (41)	4.2 ± 0.2	-87.7 ± 0.6 (36)	6.8 ± 0.1	-62.9 ± 3.28 (4)	11.3 ± 0.87	0.18 ± 0.051
M1592V Het	-51.5 ± 0.9 (10)	4.6 ± 0.3	-87.0 ± 1.3 (20)	6.8 ± 0.2	-68.1 ± 1.88 (7)	11.4 ± 0.28	0.15 ± 0.012

Slow inactivation

A recovery gap of 100 msec duration was used to distinguish the two non-conducting states, fast inactivation and slow inactivation (see chapter three). For recovery from slow inactivation, the control response was measured as the peak Na^+ current elicited at a depolarization of 20 mV from a holding potential of -100 mV. A 30 sec conditioning pulse to 0 mV was then applied to inactivate channels and recovery at -100 mV was monitored as the peak Na^+ current elicited by 7.5 msec test depolarizations to 20 mV applied at a series of progressively longer intervals (see inset, Figure 4-4A). Recovery is plotted as the relative amplitude of the Na^+ current elicited by the test pulse compared to control current. Approximately 10% of the available current recovered within the first 20 msec and little additional recovery occurs by 50 msec for WT muscle fibers, indicating that 90% of WT channels were slow inactivated by the 30 sec conditioning pulse. For fibers from M1592V mutant mice, ~20% ($p < 0.01$) of the available current recovered within the first 50 msec, indicating that a smaller proportion of M1592V channels (80%) were slow inactivated at the end of the 30 sec conditioning pulse. The time course of recovery was best fit by a two-exponential curve (solid lines, Fig. 4-4A). The two components had time constants of about 0.7 sec and 5 sec for WT, whereas 0.4 sec ($P < 0.05$) and 4 sec for mutant muscle fibers. The magnitudes of the two components were comparable, around 0.4 (Table 4-2) for both WT and M1592V fibers. The faster

component of recovery from slow inactivation in M1592V mutant muscle fibers was about two-fold accelerated than was observed in WT muscles (Fig. 4-4A).

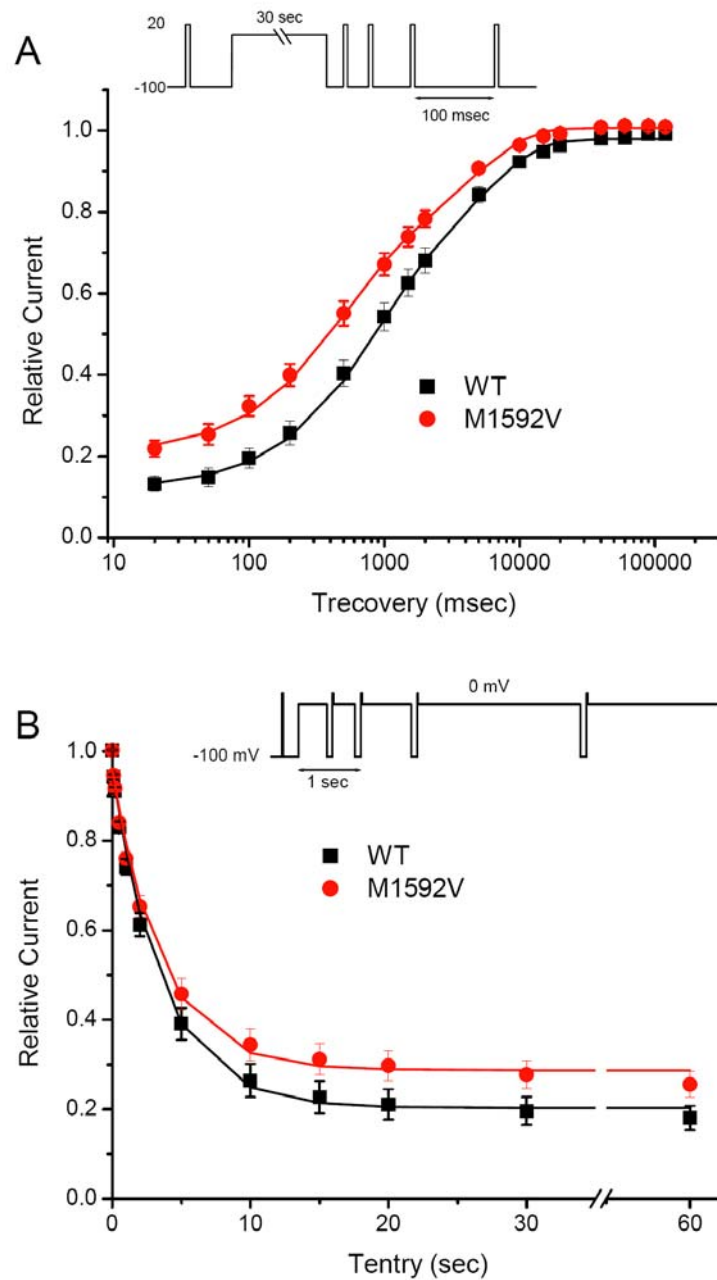


Figure 4-4. Kinetics of slow inactivation. (A) Recovery from slow inactivation at -100 mV was measured as the relative Na⁺ current elicited by 7.5 msec test pulses at varying times after a 30 sec conditioning pulse to 0 mV. Solid lines show double exponential fits to the recovery time course. The fast component of recovery from slow inactivation in M1592V mutant muscle fibers ($\tau \approx 0.4$ sec) was about two-fold faster than it is observed in WT muscle fibers ($\tau \approx 0.7$ sec), $p < 0.05$. The fraction of channels resistant to slow inactivation at depolarized potentials was increased for M1592V (0.21 ± 0.018) compare to WT (0.12 ± 0.015), $p < 0.01$. (B) Entry to slow inactivation at 0 mV was monitored as the relative Na⁺ current measured from a series of test pulses that were preceded by a 100 msec recovery gap to -100 mV. Single exponential fits demonstrated a comparable kinetics for M1592V fibers (3.08 sec) and WT (3.51 sec). The fraction of channels resistant to slow inactivation showed a trend to increase in mutant fibers. Parameters were listed in Table 4-2.

The time course for entry to slow inactivation was measured by depolarizing the membrane potential to 0 mV, and then interjecting a series of 100 msec recovery intervals at -100 mV immediately followed by a test depolarization at 20 mV (Figure 4-4B, inset). The peak currents at these test depolarizations, normalized to the control response elicited at 20 mV from a holding potential of -100 mV, provided a measure for the onset of slow inactivation at 0 mV. The onset of slow inactivation occurred over a course of seconds. The residual current after 120 sec depolarization to 0mV is around 20% and 29% ($p = 0.06$) for WT and mutant muscle fibers respectively. The time course for entry to slow inactivation was fit well by a single exponential with time constants of 3.28 ± 0.21 sec for WT ($n = 9$) and 3.5 ± 0.23 sec for mutant muscle fibers ($n = 11$).

Table 4-2 Slow Inactivation Kinetics

	WT	M1592V Het
Entry Kinetics		
<i>Amp</i>	0.80 ± 0.02	0.68 ± 0.03
<i>Tau</i> (sec)	3.08 ± 0.16	3.51 ± 0.23
	(9)	(11)
Recovery Kinetics		
<i>Amp_0</i>	0.12 ± 0.02	0.21 ± 0.02**
<i>Amp_1</i>	0.46 ± 0.03	0.44 ± 0.02
<i>Tau_1</i> (sec)	0.73 ± 0.09	0.44 ± 0.06*
<i>Amp_2</i>	0.40 ± 0.03	0.36 ± 0.02
<i>Tau_2</i> (sec)	5.0 ± 0.6	4.1 ± 0.4
	(12)	(10)

* p<0.05, **
p<0.01

The steady-state voltage-dependence of slow inactivation is shown in Figure 4-5. Na⁺ current was measured after 20 msec gap at -100 mV to allow >80% recovery from fast inactivation, following a series of 30 sec conditioning pulses ranged from -120 to 0mV (Figure 4-5). The relative amplitude of Na⁺ current was plotted against the potential of conditioning pulsed and the curve was fitted by a Boltzmann function. The maximal extent of slow inactivation reached a plateau of

85% (0.15 relative current) at depolarized potentials, and the midpoint for the voltage dependence was about -65 mV for Na⁺ channels in both WT and M1592V fibers (see Table 4-1).

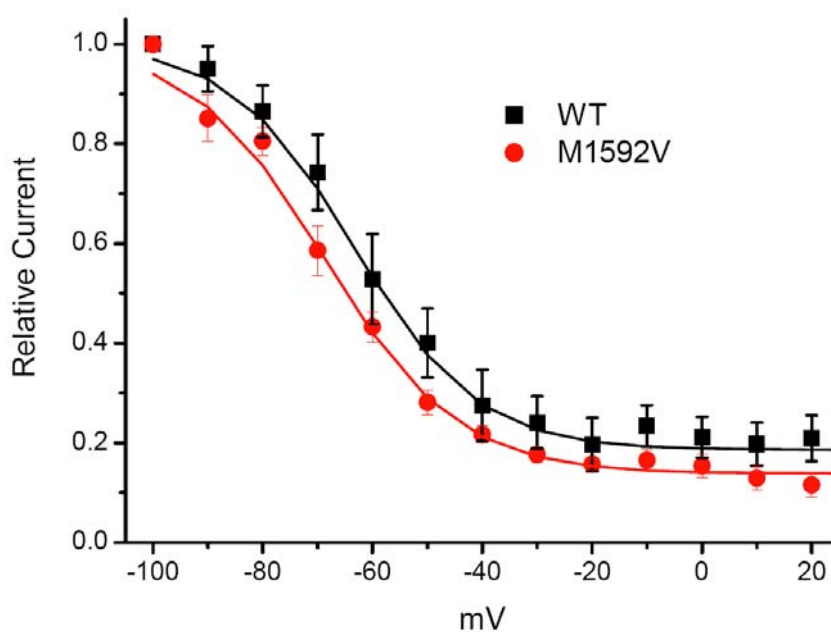


Figure 4-5. Voltage dependence of slow inactivation. Slow inactivation was measured as the relative Na⁺ current that recovered within 100 msec at -100 mV, after 30 sec conditioning pulses at varying potentials. Responses from WT and M1592V fibers were similar. Solid lines show Boltzmann fits with the parameters listed in Table 4-1.

Persistent Na⁺ current

Previous studies of HyperPP mutants expressed in HEK293 cells showed that a common functional defect among these mutants was an anomalous persistent Na⁺ current that lasted for several tens of milliseconds after the onset of depolarization (Cannon et al., 1991). The persistent current is small for WT channels, on the order of 0.1% compared to the inward peak transient, but a relative increase of 2 to 5-fold can significantly alter muscle excitability (Cannon and Corey, 1993).

Persistent current was measured by two methods. First, a tetrodotoxin-subtraction protocol was used to isolate the TTX-sensitive current. A longer step depolarization (50 msec) from -100mV to 45mV was used to elicit Na⁺ current. The current was measured in control bath solution and after adding 3 μ M TTX. By subtraction of current measured in TTX containing solution from control current, a TTX sensitive Na⁺ current was isolated. This method is more sensitive for the detection of the small persistent Na⁺ current, as opposed to standard P/N leak subtraction which may be contaminated by nonlinear background currents, especially in skeletal muscle fibers. The amplitude of the steady-state current was averaged during the last 5 msec of 50 msec depolarization and normalized by membrane capacitance (Figure 4-6A). The persistent current observed at -40mV testing potential for WT and mutant muscle fibers are -2.4 ± 0.24 (n = 21) and -

3.0 ± 0.26 nA/nF ($n = 14$) respectively. There is a slight increase for mutant muscle fibers, but no significant difference ($p=0.11$). However, because the peak current density is about 30% smaller for M1592V mutant channel (Figure 4-2), it is quite remarkable that the persistent current normalized to capacitance is underestimated for M1592V. The ratios of persistent current (averaged) to peak current (averaged, in 10mM[Na⁺]) (I_{ss}/I_{peak}) were 16 % and 30% for WT and mutant muscle fibers respectively. This normalization suggested a ~ twofold increased persistent current for mutant muscle.

Another method used to measure persistent current is slow voltage ramp protocol. Membrane potential was gradually depolarized from -100mV to 60mV with a linear ramp over 500 msec. As the membrane potential was slowly depolarized, most Na⁺ channels were inactivated from closed states and therefore never conducted current. The background leakage current was removed by subtracting the linear fitted curve from the ramp current recorded over 500 msec, which improved the separation and visualization of the noninactivating component. The averaged ramp currents of multiple muscle fibers (after linear leak subtraction) are shown in Figure 4-6B. Both WT and mutant muscle fibers displayed a noninactivating component starting from -80mV, as illustrated in Figure 4-6. The peak current density at -40 mV was -2.19 ± 0.23 nA/nF for WT ($n = 35$) and -2.87 ± 0.24 nA/nF for M1592V heterozygotes ($n = 26$) (Figure 4-6C). The persistent current of mutant muscle fibers is ~30% bigger compared to WT

($p < 0.05$). Same normalization to averaged peak current suggested a \sim twofold increased persistent current for mutant muscle (28%) compared to WT (15%) (Figure 4-6C inset).

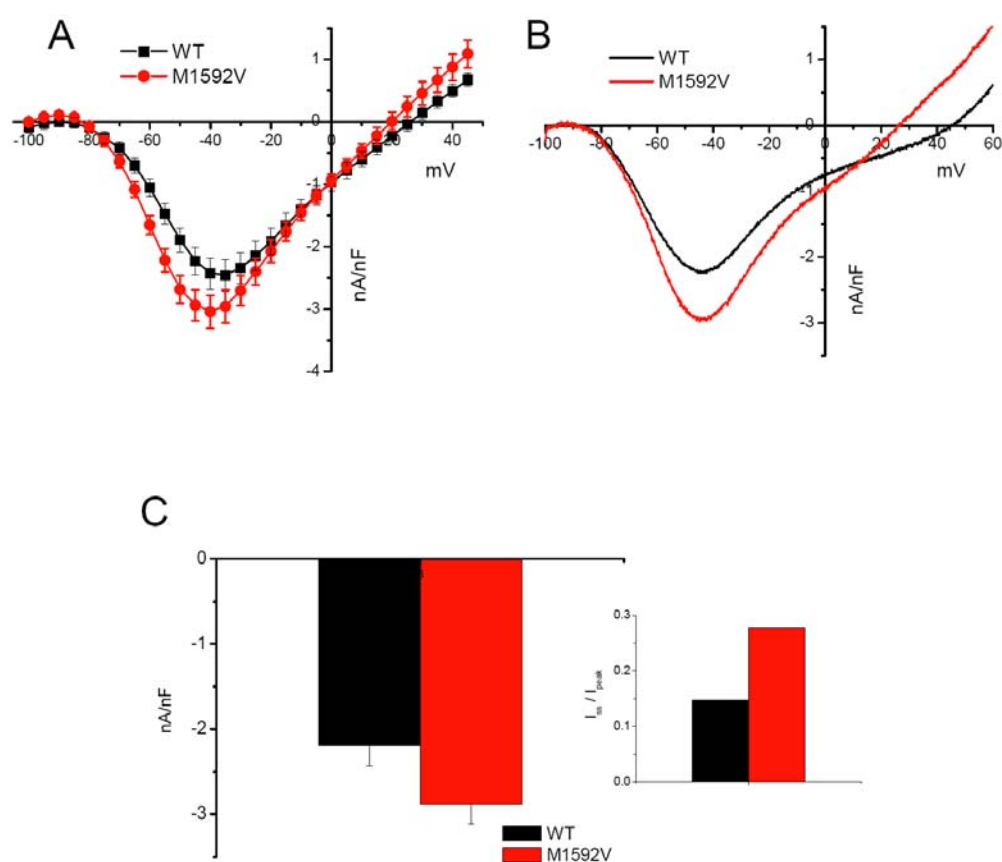


Figure 4-6. Persistent currents (A) Persistent Na^+ current, measured as the TTX-sensitive component during the final 5 msec of a 50 msec test depolarization. The peak current showed slightly increase for M1592V heterozygotes. (B) Average of currents recorded during a slow voltage ramp from -100 mV to +60 mV over 500

msec. Linear leak component was subtracted off-line. (C) The peak of the inward current at -40 mV was increased for M1592V mutant mice, the peak current density was -2.19 ± 0.23 nA/nF for WT (n = 35) and -2.87 ± 0.24 nA/nF for M1592V heterozygotes (n = 26), $p < 0.05$. Inset, the persistent currents were normalized by averaged transient peak current (I_{ss}/I_{peak}) (Figure 4-2). After normalization, M1592V mutant fibers have twofold increased persistent current compared to WT.

Expression of mutant channel

Overall, the gating defects of Na⁺ currents in WT/M1592V heterozygous muscle are much less pronounced than the changes reported for M1592V expressed as a pure population of channels in HEK293 cells. One hypothesis is the reduced expression of the mutant allele at the mRNA level contributes to this change.

Competitive RT-PCR and TA-cloning were used to analyze the expression pattern of M1592V mutant Na⁺ channel at mRNA level. Clones were isolated from cDNA amplified from foot skeletal muscle fibers harvested from 3 separate WT/M1592V heterozygous mice. Mutant channel cDNAs were distinguished from WT by specific restriction endonuclease treatment using *pflFI* and *HpaI*. For plasmids containing the mutant channel, the digest resulted in two bands, 2777 bp and 1423 bp, whereas the digest for a plasmid with the WT channel yielded a single linearized fragment of 4200 bp (Figure 4-7). The M1592V mutation was

found in 44 of 147 colonies, suggesting the expression level of M1592V is about 30%.

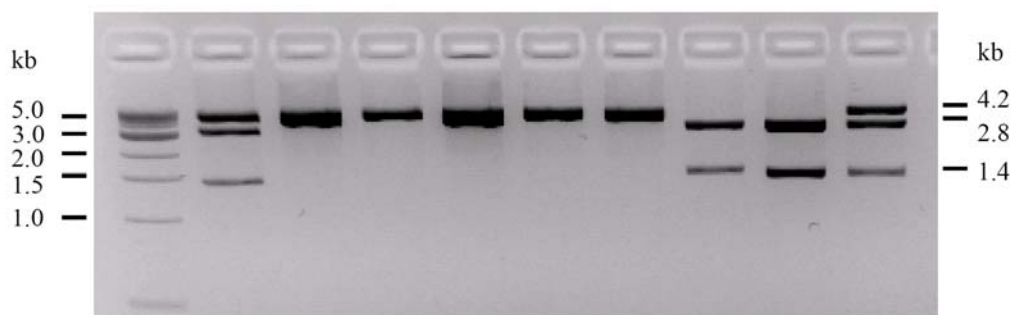


Figure 4-7. Gel photo of the enzymatic treatment. After enzymatic digestion, M1592V (Mut) inserted plasmid DNA has two band, whereas WT inserted DNA has single band. Three bands represents mutant channel after incomplete enzyme cutting.

Resurgent current

Resurgent Na^+ currents occur in specialized cellular contexts, such as Purkinje cells of the cerebellum, and are manifest as channel reopenings during the repolarization phase of the action potential. Resurgent Na^+ currents increase cellular excitability and may be aberrantly present or enhanced in a variety of Na^+ channelopathies, including myotonia (Cannon and Bean, 2010; Jarecki et al.,

2010). The M1592V Na⁺ channel mutation associated with HyperPP causes myotonia as well as periodic paralysis, which raises the question of whether mutant channels have an enhanced resurgent current that contributes to the disease phenotype. Resurgent Na⁺ currents have not been reported in studies of skeletal muscle, but the pulse protocols may not have been optimized to detect this property. Moreover, it has not been possible to reconstitute resurgent Na⁺ current properties in heterologous expression systems using the neuronal channel Nav1.6. The M1592V knock-in mouse model provides a unique opportunity to test whether a resurgent current is present for M1592V mutant channels expressed in native skeletal muscle.

A pulse protocol with a tail voltage in the range of -80mV to 0 mV, following a 20mS conditioning step to 30mV, was used to optimize the detection of resurgent current behavior. TTX (1μM) leak subtraction was used to remove the nonlinear background and capacitance transient (Figure 4-8).

We did not observe a transient reopening of Na⁺ channels with a distinct rising phase after membrane repolarization for either WT or mutant muscle fibers. The amplitude of the TTX-sensitive currents for mutant muscle fibers was increased compared to WT. The kinetics are too slow, however to be typical of resurgent current detected in cerebellar Purkinje neurons (rises in 5–6 msec) (Raman and Bean, 2001).

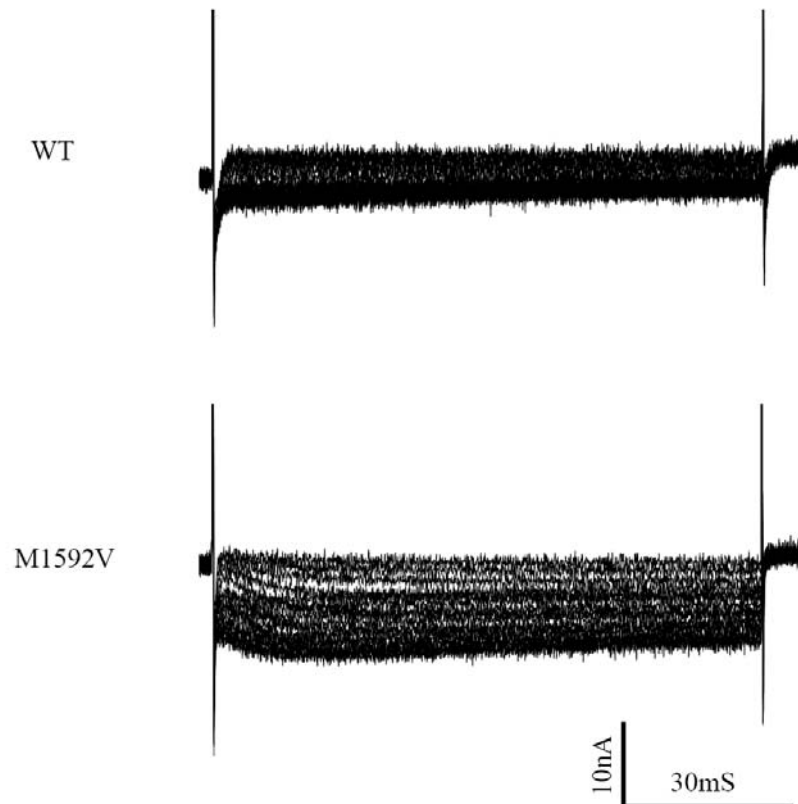


Figure 4-8. Detection of resurgent current in mouse skeletal muscle fibers. Resurgent current were recorded from -80mV to 0mV after a 20mS conditioning step to 30mV to allow Na^+ channel inactivated. The Background leak and capacitance transient were removed by subtracting remaining current in $1\mu\text{M}$ TTX. The currents after membrane was repolarized to resting potential were displayed. There were not resurgent current detected in WT (top) and M1592V (bottom) muscle fibers.

Discussion

In this study, we have obtained the first characterization of Na_v1.4-M1592V mutant channels expressed in vivo in fully-differentiated mouse skeletal muscle fibers.

Consistent with previous expression studies in HEK293 cells, the fast inactivation properties (both voltage-dependence and kinetics) were not altered by the M1592V mutation. Analysis of Na⁺ channel activation showed a similar voltage dependence for WT and M1592V fibers. The activation was not enhanced by a hyperpolarized leftward shift, as was detected in *Xenopus* oocytes expressing human Na_v1.4-M1592V channel (Rojas et al., 1999), but was not found in HEK293 cells expressing rat homologue rM1585V mutation (Cannon and Strittmatter, 1993).

The gating defects of Na_v1.4-M1592V channels identified in heterologous expression systems were also detected for channels expressed in mouse skeletal muscle. First, at potentials near -40 mV the amplitude of the persistent current at the end of a 50 msec pulse showed a significant increase for M1592V compared to WT muscle fibers. The increase of the persistent current for M1592V mutant mice is about 30% in comparison to WT channels (~ twofold as normalized by peak current). This gain-of-function defect is of considerably smaller magnitude than was observed in expression studies. Cannon and

Strittmatter expressed rM1585V in HEK293 cells and detected an approximately five fold increase of persistent Na⁺ current for mutant channels (7.5% for mutant vs. 1.4% for WT) (Cannon and Strittmatter, 1993). If normalized by peak current, the twofold increased persistent current for mutant channel is consistent with the observation in *Xenopus* oocytes (Rojas et al., 1999). Second, the M1592V substitution disrupted Na⁺ channel slow inactivation, which exhibited a faster recovery and a twofold increase in the fraction of Na⁺ channels resistant to slow inactivation at depolarized potentials. The steady state properties of slow inactivation, however, were comparable or even slightly enhanced for M1592V fibers. Defects in slow inactivation have been observed for M1592V expressed in HEK293 cells, with a 12 mV right shift in voltage dependence and a reduction in the maximal extent of slow inactivation, and an accelerated recovery rate, either in the rat background (rM1585V; Hayward et al. 1997) or the human isoform (hM1592V, Hayward et al. 1999).

These gain-of-function defects are predicted to cause the phenotypes observed in HyperPP patients with the M1592V mutation. The increased persistent Na⁺ current increases the susceptibility to after-discharges and thereby produces myotonia. In combination with hyperkalemia, the persistent Na⁺ current can also cause a large depolarized shift in resting potential (V_{rest}), which inactivates the majority of Na⁺ channels and thereby renders the fiber inexcitable and unable to generate force. Slow inactivation is a distinct inactivation process,

temporally and mechanistically separate from fast inactivation. The gain-of-function produced by impairment of slow inactivation increases the susceptibility to depolarized shifts in V_{rest} with attendant paralysis (Cannon et al., 1991; Hayward et al., 1997).

The defects of M1592V mutant channel in mouse skeletal muscle fibers were less pronounced than has been previously reported in studies using heterologous expression systems. The persistent current only increased 30% (~ twofold as normalized by peak current) in mutant muscle fibers and a depolarized shift in the voltage dependence of slow inactivation was not detected. One possible explanation is that HEK293 cells or *Xenopus* oocyte systems over express a pure population of mutant channels, whereas in our study only heterozygous WT/M1592V mice are available. RT-PCR and TA-cloning were used to analyze the expression pattern of M1592V mutant Na^+ channel at the mRNA level, and suggested only about 30% expression level for the M1592V mutant channels. Because there is just one amino acid difference, currently we do not have a suitable method to analyze the expression of WT and mutant channel at the protein level.

**Chapter Five : Gating Defects for the Hypokalemic Periodic Paralysis
Associated Sodium Channel Mutation R663H in Fully Differentiated Mouse
Skeletal Muscle Fibers**

Introduction

Gating behavior of skeletal muscle sodium channel Na_v1.4 is critical for the regulation of sarcolemmal excitability. Several inherited muscular diseases are associated with the mutations in the gene that encodes the α -subunit of Na_v1.4. Familial hypokalemic periodic paralysis (HypoPP) is a rare autosomal-dominant disorder. Mutations in skeletal muscle calcium channel Cav1.1 and Na_v1.4 both are established cause of HypoPP. In total, Cav1.1 mutations are found in ~70% and Na_v1.4 mutations in ~10% of the epidemiological analysis. The genetics basis of the remaining ~20% is still unclear (Sternberg et al., 2001).

HypoPP is characterized by attacks of muscle flaccid weakness in the setting of hypokalemia (Rudel et al., 1984). The onset of HypoPP usually starts in the second decade of life. The attacks of weakness are precipitated by rest after exercise, heavy carbohydrate ingestion, insulin administration and often last for hours to days (Vicart et al., 2005). Unlike HyperPP, myotonic stiffness does not occur in HypoPP patients.

Until 1999, the general consensus was that mutations of $Na_v1.4$ were associated with disorders in the Myotonia – HyperPP spectrum, whereas HypoPP was caused by missense mutations of $Ca_v1.1$. Bulman and colleagues identified the first missense mutation in $Na_v1.4$, R669H, that cosegregated with the HypoPP phenotype (Bulman et al., 1999). This mutation substitutes the outermost arginine in the domain II S4 voltage sensor of $Na_v1.4$ by histidine, thus alters the positive charge of channel voltage sensor (Figure 5-1).

As with other forms of periodic paralysis, in HypoPP the paralytic attacks are caused by aberrant sustained depolarization of the sarcolemmal resting potential (Rudel et al., 1984). However, the basis for this depolarization remains unclear, and does not appear to involve incomplete inactivation of the Na^+ current as was detected in Na^+ channel mutations associated with HyperPP (Cannon et al., 1993; Cummins and Sigworth, 1996; Hayward et al., 1997; Hayward et al., 1999). In contrast, the R669H mutation was studied in HEK293 cells and found to cause loss-of-function changes from enhanced slow inactivation, exhibits a hyperpolarized shift in the voltage dependence of slow inactivation and prolonged recovery from slow inactivation (Struyk et al., 2000). Enhanced fast inactivation was reported for other two HypoPP associated $Na_v1.4$ mutations, R672G/H (Jurkat-Rott et al., 2000) expressed in tsA201 mammalian cell line. It has been suggested that this enhanced inactivation might predispose patients to paralytic attacks by reducing Na^+ channel availability.

Although the studies of mutant $\text{Na}_v1.4$ gating in heterologous expression systems have provided invaluable insights into the mechanism of HypoPP, the basis of membrane depolarization, which is the core feature of HypoPP, remains speculative. The potential variation of posttranslational modifications in different cellular contexts may introduce variations in the behavior of mutant $\text{Na}_v1.4$ that are not studied in the endogenous cellular milieu of skeletal muscle fibers. Studies of HypoPP associated $\text{Na}_v1.4$ mutations in intact muscle fibers may help to shed light on these persistent questions.

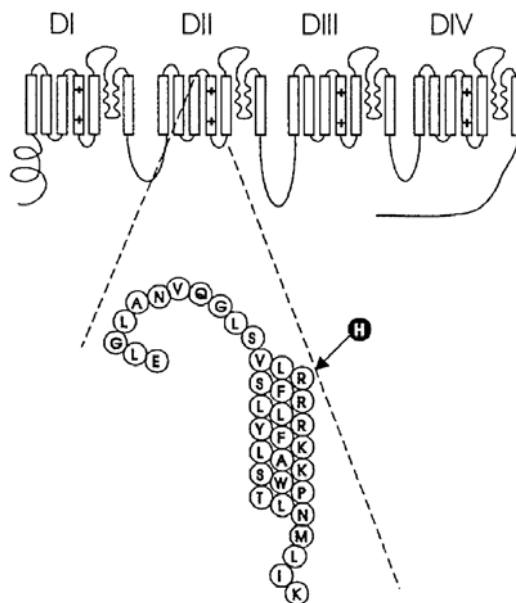


Figure 5-1. Location of R663H HypoPP mutation. Schematic representation of a sodium channel α -subunit. The arginine (R) is replaced by a histidine (H) in the region of DIIS4. [From (Bulman et al., 1999)]

A Nav1.4-R663H (the ortholog of human R669H) knock-in mutant mouse was established. Homozygous mutant Nav1.4-R663H mice are viable, providing an opportunity to study the properties of mutant R663H channels without a contribution from wild type (WT) Nav1.4.

Materials and Methods

Muscle Fiber Preparation

Individual muscle fibers were isolated by enzymatic digestion and mechanical disruption from mixed muscles of the hind foot of adult C57/B16 wild-type (WT) and M1592V Heterozygous mice (age 2 – 6 months). Animals were sacrificed by isoflurane inhalation and cervical dislocation, in accordance with guidelines by our Institutional Animal Care and Use Committee. The muscle was rapidly dissected free and placed in DMEM plus 1 mg/ml collagenase (Gibco, Grand Island, NY). The muscle was incubated at 37 °C for 90 minutes. Fibers were dissociated by trituration in a wide-bore pipette, pelleted by centrifugation, and resuspended in DMEM plus 10% fetal bovine serum, 1% glutamine, 100U/ml Penicillin/streptomycin and 10mM HEPES. Approximately 100 fibers were plated in 35 mm culture dishes coated with rat tail collagen and matrigel (BD Biosciences, San Jose, CA). Cultures were maintained for 1 to 3 days in 5% CO₂ at 37 °C.

Two-Electrode Voltage clamp Recording

Currents were recorded with the two-electrode voltage clamp (TEVC) technique, using an AxoClamp2B amplifier (Molecular Devices, Sunnyvale, CA) with the HS-2A headstage. Fibers were visualized on an inverted microscope (IMT-2 Olympus, Center Valley, PA) with Hoffman optics. Disruption of the T-tubule system from the sarcolemma was achieved by hyperosmolar shock in Ringer's solution plus 400 mM glycerol for 1 hr, and the fibers were then returned to isomolar Ringer's solution for 30min before recording (Dulhunty and Gage, 1973). Isolated fibers adherent to the collagen/matrigel coated dish and < 600 μm in length were selected for recording by impalement near their midpoint with both stimulating and recording sharp microelectrodes. The standard bath was a Cl-free low- Na^+ solution containing NaOH 10 mM, tetraethylammonium hydroxide (TEAOH) 130 mM, $\text{Mg}(\text{OH})_2$ 1 mM, $\text{Ca}(\text{OH})_2$ 1 mM, 4-(2-hydroxyethyl)-1-piperazineethanesulfonic acid (HEPES) 10 mM, glucose 10 mM, 4-aminopyridine (4-AP) 5 mM, anthracene-9-carboxylic acid (9-AC) 100 μM , nifedipine 5 μM , pH adjusted to 7.4 by methanesulfonic acid. Dantrolene 3 $\mu\text{g}/\text{ml}$ and the skeletal muscle myosin II inhibitor N-benzyl-p-toluene sulphonamide (BTS) 20 μM (Cheung et al., 2002) were added to suppress depolarization-induced contraction in studies on fibers with intact T-tubules. The extracellular Na^+ concentration

was lowered to 10mM to reduce the current amplitude and thus to improve the voltage control. The current injection pipette was filled with 2 M Cs-Aspartate (resistance of 3-5M Ω) and the voltage sensing electrode contained 3 M CsCl (resistance 7-10 M Ω). All measurements were performed at room temperature.

Data Analysis

Voltage-clamp control, current recording, and analysis of traces were performed using pClamp9.2 (Axon Instruments, Foster City, CA). The data were analyzed by the using of computer programs: Excel (Microsoft Corporation) and Origin 6.0 (MicroCal, Northampton, MA).

Conductance was calculated as:

$$G(V) = I_{\text{peak}}(V)/(V-E_{\text{rev}})$$

where the reversal potential (E_{rev}) was measured experimentally for each cell. The voltage dependence of activation was quantified by fitting the current measure to a Boltzman function:

$$I_{\text{peak}}(V)/(V-E_{\text{rev}}) = G_{\text{max}}/[1 + \exp(-(V - V_{1/2})/\kappa)]$$

The steady-state voltage dependence was measured for fast and for slow inactivation by using wither brief (300 msec) or long (30 sec) conditioning pulse

respectively. The relative current availability (I_{test}/I_{max}) was fitted to a Boltzmann function with a non-zero pedestal (I_0), calculated as:

$$I_{test}/I_{max} = (1 - I_0)/[1 + \exp((V-V_{1/2})/\kappa)] + I_0$$

where $V_{1/2}$ is the half-maximum voltage and κ is the slope factor.

The kinetics of fast inactivation was quantified from single-exponential fits to the macroscopic current decay. The time constant of the decay (τ), was estimated by fitting macroscopic Na^+ currents (I) to a single exponential plus a constant term (I_0) as:

$$I = (I_{max} - I_0) * \exp^{-t/\tau} + I_0$$

where I_{max} is the maximal amplitude. A similar function was used to estimate the time constant for the entry to fast inactivation revealed by two-pulse protocols at conditioning voltage $-90mV \sim -60mV$.

$$I_{test}/I_{ref} = (1 - I_0) * \exp^{-t/\tau} + I_0$$

In this case I_{test} is the peak current elicited by a test pulse to $-40 mV$ after a conditioning inactivation pulse of varying duration (t). I_{test} was normalized to the peak amplitude of a reference current (I_{ref}), elicited by a $-40mV$ pulse before application of the conditioning pulse. The same equation was used for the analysis of the kinetics of entry to slow inactivation.

To measure the time course of recovery from fast inactivation, a 30 msec conditioning pulse to -20 mV was applied to fast inactivate the channels fully, followed by a return to the recovery potential (between -120 and -90 mV) for a variable interval (t). The fraction of available (recovered) channels was assayed with a test pulse to -40 mV. The relative peak current (I_{test}/I_{ref}) was fit to the equation:

$$I_{test}/I_{ref} = A_1 * (1 - \exp(-t/\tau_1)) + A_2 * (1 - \exp(-t/\tau_2)) + I_0$$

A_1 and A_2 are the amplitudes of the two components, τ_1 and τ_2 are the time constants, t is the recovery time. The faster time constant was used to characterize the kinetics of recovery from fast inactivation.

The recovery of Na⁺ channel availability after prolonged depolarization is characterized by multiple exponential components (Cummins and Sigworth, 1996), including "intermediate" component (I_M , recovers within 100-300 msec), slow-inactivated component (I_S , recovers within 1-3 sec), and ultraslow-inactivated channels (I_U , recover over minutes). Recovery from intermediate (I_M)- and slow (I_S)-inactivated states was measured by the use of a sequential recovery protocol in which a single conditioning pulse (up to 120 sec) was followed by a series of brief test pulses (7.5 msec) during the recovery interval. Peak current from each test pulse was normalized to a reference current (I_{ref}), measured as the mean peak value from five separate step depolarizations to -40 mV before the conditioning

pulse. $I_{\text{test}}/I_{\text{ref}}$ values were then fit with the same two-exponential equation as used for recovery from fast inactivation.

Measured values are presented as the mean \pm standard error of the mean unless otherwise noted. Statistical significance was determined by student *t* test. *P* values were noted in the text. Values of $P < 0.05$ were considered significant.

Results

Activation

Na⁺ channel activation was determined by measuring the peak Na⁺ current elicited by 15 msec step depolarizations from a holding potential of -100mV (Figure 5-2). Test depolarizations from -100 to +45mV were applied in 5 mV increments. Leak subtraction was performed by using a 30 msec conditioning pulse to inactivate Na⁺ channels, after which the pulse protocol was repeated to measure the residual background currents (capacitive and ionic) (chapter Two). Peak current density was compared between WT and R663H mutant mice. The peak Na⁺ current densities (at test potential -45mV) were -21.0 ± 1.2 nA/nF, -19.9 ± 1.7 nA/nF and -9.0 ± 0.8 nA/nF for WT (n = 18), R663H heterozygotes (n = 6) and R663H homozygotes (n = 7) respectively. The current density was significantly decreased in R663H homozygote, $p < 0.01$ (Figure 5-2B). Channel

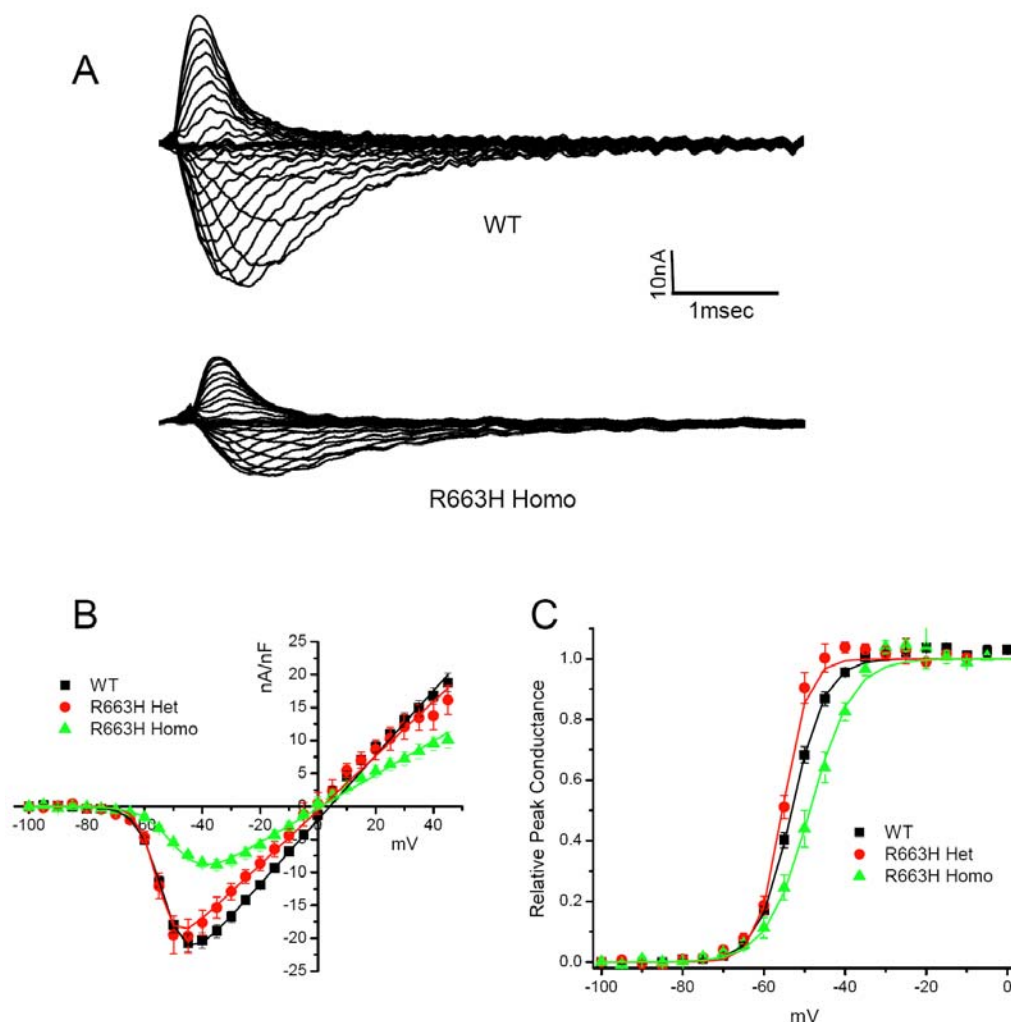


Figure 5-2. Representative currents and voltage dependence of activation. (A) Representative currents for muscle fibers from WT (top) and R663H homozygous (bottom) mice. Currents were elicited by a series of 15 msec voltage steps from a holding potential of -100 mV to voltages ranging from -100 to +45 mV in 5 mV increments. (B) Peak Na⁺ current was normalized to fiber capacitance and plotted as the average for fibers from WT (n = 18), R663H heterozygous (n = 6) and R663H homozygous (n = 7) mice. The peak current density is significantly decreased for R663H homozygous mice (C) The data from (A) are replotted as relative peak conductance. Boltzmann fits revealed a significant rightward shift for C57BL/6 and R663H homozygous muscle fibers. Error bars show SEM.

conductance was estimated from the peak current and the measured reversal potential for each fiber. The Boltzmann fitted G-V relation is plotted in Figure 5-2C. The midpoints of G-V relation are -53.1 ± 0.5 mV, -55.4 ± 0.4 mV and -48.7 ± 1.2 mV, the steepness factors are 4.2 ± 0.2 mV and 3.1 ± 0.5 mV and 5.2 ± 0.2 mV for WT, R663H heterozygotes and R663H homozygotes respectively. The voltage-dependence of activation showed a significant reduced steepness and rightward shift for R663H homozygous mice ($p < 0.01$). Parameters were listed in Table5-1.

Fast inactivation

The steady-state voltage dependence of fast inactivation was measured as the relative Na^+ current elicited by a test depolarization to -40 mV, following 300 msec conditioning pulses from -100 mV to 10 mV in 5 mV increments (Figure 5-3A). A standard P/8 leak subtraction method was used to remove background leak current. The voltage-dependence of fast inactivation was leftward shifted and the steepness was decreased for R663H homozygote compared to WT. Estimated by fitting to a Boltzmann function, the half-inactivation midpoints are -88.7 ± 1.0 mV, -92.1 ± 2.6 mV and -98.2 ± 1.1 mV, and the steepness factors are 6.3 ± 0.1 mV, 7.5 ± 0.3 mV and 9.5 ± 0.4 mV for WT ($n = 13$), R663H heterozygotes ($n =$

8) and R663H homozygotes (n = 24) respectively. Parameters were listed in Table5-1.

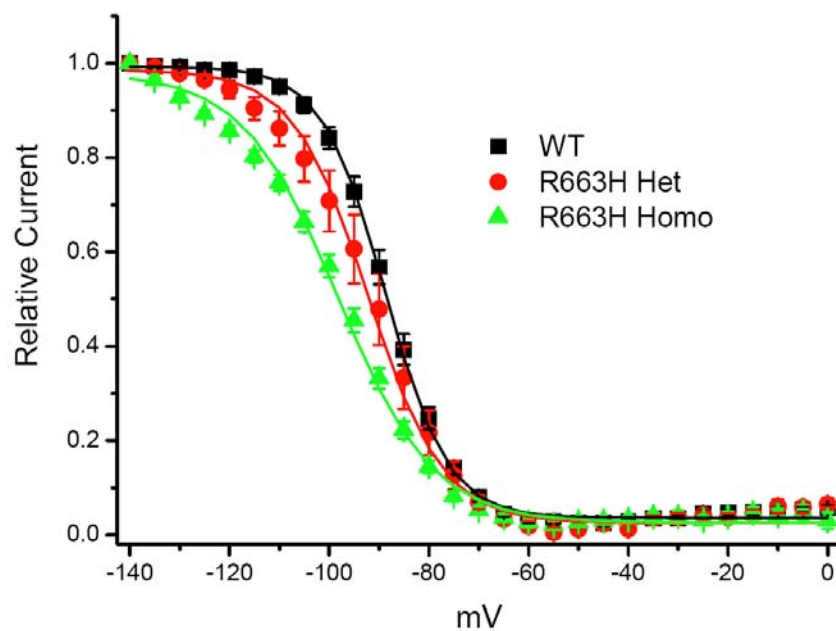


Figure 5-3. Fast inactivation properties. The voltage-dependence of fast inactivation was measured as the residual current that remained after a 300 msec conditioning pulse to voltages from -140 to 0 mV. The $V_{1/2}$ is -88.7 ± 1.0 , -92.1 ± 2.6 and -98.2 ± 1.1 mV, κ is 6.3 ± 0.1 and 7.5 ± 0.3 and 9.5 ± 0.4 for WT, R663H heterozygote and R663H homozygote respectively. The voltage-dependence of fast inactivation was leftward shifted and the steepness was decreased for R663H homozygote compared to WT, $p < 0.01$.

	Activation		Fast Inactivation		Slow Inactivation		
	$V_{0.5}$ (mV)	κ (mV)	$V_{0.5}$ (mV)	κ (mV)	$V_{0.5}$ (mV)	κ (mV)	I_o
WT	-53.1 ± 0.5 (18)	4.2 ± 0.2	-88.7 ± 1.0 (13)	6.3 ± 0.1	-67.6 ± 1.5 (10)	10.8 ± 0.44	0.17 ± 0.019
R663H Het	-55.4 ± 0.4 (6)	$3.1 \pm 0.5^*$	-92.1 ± 2.6 (8)	$7.5 \pm 0.3^{**}$	-64.2 ± 1.4 (6)	9.8 ± 0.41	0.23 ± 0.019
R663H Homo	$-48.7 \pm 1.3^{**}$ (7)	$5.2 \pm 0.2^{**}$	$-98.2 \pm 1.1^{**}$ (24)	$9.5 \pm 0.4^{**}$	$-75.5 \pm 1.4^{**}$ (7)	10.6 ± 0.47	$0.11 \pm 0.017^*$

* $p < 0.05$, ** $p < 0.01$

Slow inactivation

A recovery gap of 100 msec duration was used to distinguish the two non-conducting states, fast inactivation and slow inactivation (see chapter three). For recovery from slow inactivation, the control response was measured as the peak Na^+ current elicited by a depolarization of 20 mV from a holding potential of -100 mV. A 30 sec conditioning pulse to 0 mV was then applied to inactivate channels and recovery at -100 mV was monitored as the peak Na^+ current elicited by 7.5 msec test depolarizations to 20 mV applied at a series of progressively longer intervals (see inset, Figure 5-4A). Recovery is plotted as the relative amplitude of the Na^+ current elicited by the test pulse compared to control current. The time course of recovery was best fit by a two-exponential curve (solid lines, Fig. 5-4A). The faster time constants are 0.87 ± 0.12 sec, 0.85 ± 0.08 sec and 2.76 ± 0.30 sec, the slower time constants are 7.1 ± 1.0 sec, 5.1 ± 0.7

sec and 17.3 ± 2.3 sec for WT (n=11), R663H heterozygote (n=10) and R663H homozygote (n=11), respectively. The recovery from slow inactivation was prolonged for R663H homozygous mice, $p < 0.01$ for both time constants. Channels resistant to slow inactivation at the end of the 30 sec conditioning pulse was decreased for R663H homozygote (0.06 ± 0.009) compare to WT (0.12 ± 0.017), $p < 0.05$. The time course for entry to slow inactivation was measured by depolarizing the membrane potential to 0 mV, and then interjecting a series of 100 msec recovery intervals at -100 mV immediately followed by a test depolarization at 20 mV (Figure 4-4B, inset). The peak current at these test depolarizations, normalized to the control response elicited at 20 mV from a holding potential of -100 mV, provided a measurement for the onset of slow inactivation at 0 mV. The onset of slow inactivation occurred over a course of seconds and was faster for currents in R663H fibers.

The time course for the entry to slow inactivation was fit well by a single exponential with time constants of 5.93 ± 0.35 sec, 3.43 ± 0.27 sec and 2.49 ± 0.13 sec for muscle fibers from WT (n = 8), R663H heterozygous (n = 7) and homozygous (n = 15) mice. The time constant for entry to slow inactivation was reduced for both heterozygous and homozygous mutant fibers compared to WT ($p < 0.01$). The final asymptotic value for the fraction of channels that were not slow inactivated was significantly reduced for R663H homozygote (0.13 ± 0.01) compare to WT (0.17 ± 0.01), $p < 0.01$.

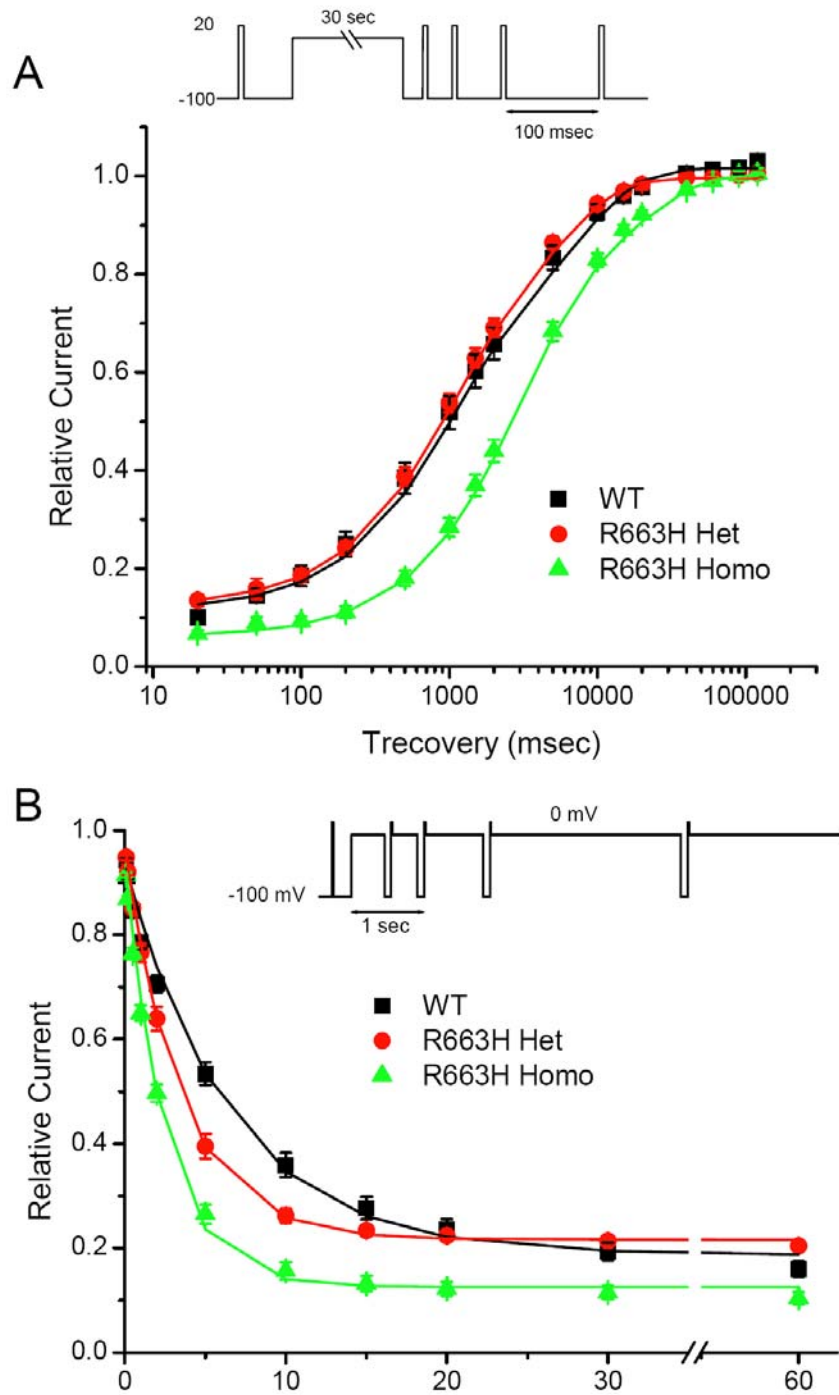


Figure 5-4. Kinetics of slow inactivation. (A) Recovery from slow inactivation at -100 mV was measured as the relative Na⁺ current elicited by 7.5 msec test pulses at varying times after a 30 sec conditioning pulse to 0 mV. Solid lines show double exponential fits to the recovery time course. The recovery from slow inactivation was prolonged for R663H homozygous mice for both time constants. The fraction of channels resistant to slow inactivation at depolarized potentials was decreased for R663H homozygote (0.06 ± 0.009) compare to WT (0.12 ± 0.017), $p < 0.05$. (B) Entry to slow inactivation at 0 mV was monitored as the relative Na⁺ current measured for a series of test pulses that were preceded by a 100 msec recovery gap to -100 mV. Single exponential fits demonstrated decreased time constants of mutant mice (Het 3.43 ± 0.27 sec; Homo 2.49 ± 0.13 sec) compared to WT (5.93 ± 0.35 sec). The fraction of channels resistant to slow inactivation showed a significantly reduction for R663H homozygote (0.13 ± 0.01) compare to WT (0.17 ± 0.01), $p < 0.01$. Parameters were summarized in Table 5-2

Table 5-2 Slow Inactivation Kinetics

	WT	R663H Het	R663H Homo
Entry Kinetics			
<i>Amp</i>	0.77 ± 0.01	0.76 ± 0.01	$0.83 \pm 0.01^{**}$
<i>Tau</i> (sec)	5.93 ± 0.35	$3.43 \pm 0.27^{**}$	$2.49 \pm 0.13^{**}$
	(8)	(7)	(15)
Recovery Kinetics			
<i>Amp_0</i>	0.12 ± 0.02	0.12 ± 0.01	$0.06 \pm 0.01^*$
<i>Amp_1</i>	0.48 ± 0.03	0.47 ± 0.03	$0.64 \pm 0.04^{**}$
<i>Tau_1</i> (sec)	0.87 ± 0.12	0.85 ± 0.08	$2.76 \pm 0.30^{**}$
<i>Amp_2</i>	0.42 ± 0.02	0.40 ± 0.02	$0.30 \pm 0.03^{**}$
<i>Tau_2</i> (sec)	7.1 ± 1.0	5.1 ± 0.7	$17.3 \pm 2.3^{**}$
	(11)	(10)	(11)

* $p < 0.05$, ** $p < 0.01$

The steady-state voltage-dependence of slow inactivation is shown in Figure 5-5. Na^+ current was measured following a series of 30 sec conditioning pulses ranged from -120 to 0mV. A 100 msec gap at -100 mV was used after the conditioning pulse to allow the fully recovery from fast inactivation before measuring the fraction of the available channels with a test pulse to 20 mV. The relative amplitude of Na^+ current was plotted against the conditioning potential and the curve was fitted by a Boltzmann function. The maximal extent of slow inactivation reached a plateau of 17% and 11% relative residual current at depolarized potentials for WT (n = 10) and R663H homozygote (n=7). The midpoints for the voltage dependence were -67.6 ± 1.5 mV for WT and -75.5 ± 1.4 mV for R663H homozygotes. (Table 5-1).

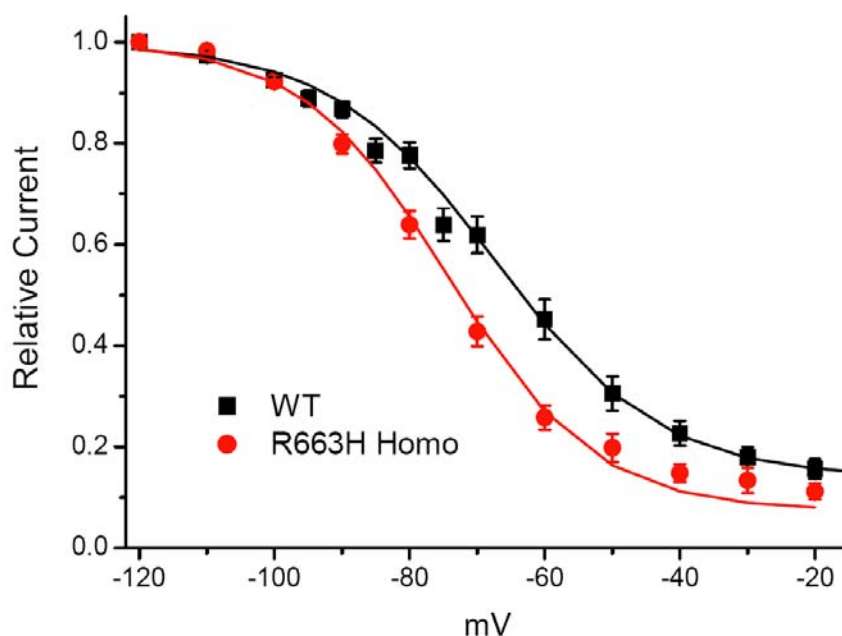


Figure 5-5. Voltage dependence of slow inactivation. Slow inactivation was measured as the relative Na^+ current that recovered within 100 msec at -100 mV, after 30 sec conditioning pulses at varying potentials. The voltage-dependence of slow inactivation for R663H channels was shifted in the hyperpolarized direction and the maximal extent of slow inactivation was increased at depolarized potentials. Solid lines show Boltzmann fits with the parameters listed in Table 5-1.

Discussion

Based on Na^+ current measurements from homozygous R663H fibers, the major functional defect for mutant channels was an enhancement of inactivation, both fast and slow. The enhancement of fast inactivation was manifest as a 10 mV hyperpolarized (leftward) shift in steady-state voltage dependence compared to WT. For slow inactivation, enhancement was reflected by a decrease in the Na^+ current availability at the end of a 30 sec conditioning pulse from 17% for WT to 11% for homozygous R663H fibers. In addition, there was an 8 mV leftward shift for the voltage dependence of slow inactivation. The kinetics of slow inactivation also showed evidence of enhancement. Onset of slow inactivation was accelerated and the rate of recovery was decreased for Na^+ currents in R663H fibers compared to WT. Taken together, all three phenomena – maximal extent of slow inactivation, voltage dependence, and kinetics of entry / recovery – had changes that were consistent with an enhancement of slow inactivation for R663H mutant channels.

The observation of enhanced slow inactivation is in agreement with our prior study of hR669H in the HEK293 cell expression system (Struyk et al., 2000), although we did not previously detect a faster entry to slow inactivation. The enhancement of fast inactivation observed for R663H in muscle fibers was not detected in our studies of hR669H in HEK293 cells. A similar 10mV left shift, however, was reported for neighboring HypoPP mutations at R672H/G. Beside the enhanced inactivation, we also observed impaired activation with a 5mV rightward shifted in voltage dependence. The steepness for G-V relation was also reduced, as would be anticipated for partial neutralization of a gating charge caused by substitution of arginine to histidine. Overall, the enhanced inactivation and impaired activation are predicted to cause a loss-of-function defect. This study provides an important confirmation of our prior work in HEK293 cells. Indeed, microelectrode studies in biopsied fibers from $\text{Na}_v1.4$ -HypoPP patients (Jurkat-Rott, et al. 2000) show a sluggish rising phase of the action potential and smaller spike amplitude consistent with the notion that a loss-of-function defect of $\text{Na}_v1.4$ occurs in human muscle.

An additional anomaly has been detected for $\text{Na}_v1.4$ -rR663H channels expressed in Oocytes. The disruption in the S4 voltage-sensor produces an alternative ionic current pathway that supports an inward gating-pore current conducted by protons at hyperpolarized potentials when the S4 segment is in the closed conformation (Struyk et al., 2007). This gating pore current increases the

susceptibility to paradoxical membrane depolarization in low external $[K^+]$ (Struyk et al. 2008), which inactivates Na^+ channels and renders the fiber inexcitable. The loss-of-function changes to R663H produced by enhanced inactivation (fast and slow, as reported herein) would exacerbate the loss of excitability that occurs with depolarization of V_{rest} and thereby would contribute to the pathogenesis of HypoPP.

Chapter Six : Summary and Future Directions

We have developed an improved method to record sodium currents from intact mouse skeletal muscle fibers. Using this technique, we have characterized the gating properties of $\text{Na}_V1.4$ channels in their native environment and performed a survey of fast and slow gating properties for the HyperPP-associated $\text{Na}_V1.4$ channel mutation M1592V and the HypoPP-associated $\text{Na}_V1.4$ channel mutation R663H in situ. Our primary observations were:

1. Gating behavior of WT $\text{Na}_V1.4$ channels in mouse footpad muscle fibers, with a comparison of currents from two mouse strains, C57BL/6 and 129-E.

The most dramatic finding was a hyperpolarized shift in the voltage dependence of activation (-25 mV) and fast inactivation (-18 mV) as compared to heterologous expression studies of $\text{Na}_V1.4 \pm \beta_1$ subunit in HEK293 cells. We have extensively considered and excluded sources of artifact (Rs, cable behavior, extracellular Na^+ concentration, stability, junction potentials) or contribution from other Na_V isoforms ($\text{Na}_V1.5$) as a potential cause for this difference.

The Na^+ channel behavior in skeletal muscle fibers was compared between two mouse strains, C57BL/6 and 129-E. There was no significant difference in

voltage dependence of fast gating. We found the entry to slow inactivation was slower in fibers from the 129-E mice, whereas the recovery from slow inactivation was comparable between two mouse strains.

2. Survey of gating behavior for the HyperPP mutant $\text{Na}_v1.4\text{-M1592V}$ studied in fibers from knock-in mutant mice.

Overall, the differences in Na^+ currents between WT and M1592V-mutant mice were very subtle, with the major change being a slight increase in the persistent current and moderately disrupted slow inactivation.

Our studies of M1592V mutant channels were limited by the inability to generate viable homozygous mutant mice to study a pure population of mutant channels. Because M1592V is a point mutation in a predicted transmembrane segment, we did not pursue an antibody approach to measure the relative abundance of mutant channel at the protein level. Although successful expression of the mutant allele at the surface membrane has been verified (Hayward et al., 2008), an estimate for the relative expression level of WT and mutant channels in muscle fibers has not previously been reported. By RT-PCR, we estimate that the stable mRNA level of M1592V is approximately 30% of the total $\text{Na}_v1.4$ transcript. Decreased expression of M1592V relative to WT $\text{Na}_v1.4$ may account

for the difficulties in detecting the gain-of-function alterations in gating behavior that have been reported in heterologous expression systems.

3. To characterize the gating defects for $\text{Na}_v1.4$ point mutation R663H associated with HypoPP

The main advantage of the R663H mutant mouse model compared to M1592V is the availability of homozygous mutant animals. Based on Na^+ current measurements from homozygous R663H fibers, the major change was an enhancement of inactivation, both fast and slow. This observation is consistent with prior reports on heterologous expression studies of HypoPP- $\text{Na}_v1.4$ mutants (Struyk et al., 2000). We also observed impaired activation, with leftward shifted voltage dependence and a reduction in the steepness, as would be anticipated for partial neutralization of a gating charge. While these observations provide important confirmation of prior work using expression systems, the current focus of interest lies in determining whether this missense mutation of an arginine in DII S4 produces a gating pore current when expressed in muscle and in determining how large this anomalous conductance is in comparison to the endogenous conductances in WT fibers that set the resting potential.

Future Directions:

Characterization of gating pore currents for Na_v1.4-R663H

The latest advance in studies of HypoPP-associated mutations is the discovery of gating pore currents from R/X missense mutations in S4 voltage sensors of Na_v1.4 (Cannon, 2010; Sokolov et al., 2007; Struyk and Cannon, 2007; Struyk et al., 2008). Using high-expression studies in the cut-open oocyte configuration, our lab has shown that the R663H HypoPP mutation produces gating pore currents that is active at hyperpolarized potentials (“inward” position of the voltage sensor) and is selective for protons (Struyk and Cannon, 2007). A key question in determining the relevance of this current to the pathogenesis of HypoPP is the magnitude of the gating pore conductance in relation to other conductances in skeletal muscle. The opportunity to investigate the gating pore currents in homozygous R663H knock-in mice is a unique tool to make this determination. We know the gating pore current amplitude will be very small, on the order of 1/100th ~ 1/1000th of the Na⁺ current through the central pore. Presently, we are working on methods to optimize the block of endogenous conductances in mouse muscle fibers, which will be required to obtain the resolution necessary to observe gating pore currents.

Detection of a gating pore current for the HypoPP mutation CaV1.1-R528H

A related project is to screen for gating pore currents in the $Ca_v1.1$ -R528H mutant mice. This mutation is in the homologous location of $Ca_v1.1$ to the R663H mutation in $Na_v1.4$. No lab has been able to test gating pore currents in HypoPP-associated $Ca_v1.1$ mutant channels, because the expression level is very poor in heterologous systems. If we detect gating pore currents for $Ca_v1.1$ -R528H, it would be a major finding, as it would establish a common pathophysiological link for $Na_v1.4$ and $Ca_v1.1$ mutations that both cause HypoPP.

APPENDIX A Parameter Estimates for Na⁺ channel Gating

The time and voltage dependence for the Na⁺ conductance were simulated with a modified form of the rate relations for the Hodgkin-Huxley equations. Conduction through the open pore was assumed to be Ohmic, and the Na⁺ current, I_{Na} , was computed as:

$$I_{Na} = G_{Na} m^3 h (V - E_{Na}) \quad , \quad \text{Eq. A1}$$

where G_{Na} is the maximal conductance and E_{Na} is the equilibrium potential for Na⁺. The gating variables, m and h , were modeled by the usual first-order rate relations, described in terms of the steady-state and kinetic properties measured experimentally:

$$\dot{m}(V, t) = [m_{\infty}(V) - m] / \tau_m(V) \quad \text{Eq. A2a}$$

$$\dot{h}(V, t) = [h_{\infty}(V) - h] / \tau_h(V) \quad \text{Eq. A2b}$$

First, the steady-state values for $m_\infty(V)$ and $h_\infty(V)$ were determined by fitting representative data from Na^+ currents measured in muscle fibers to Boltzmann functions (Eq. A3) for the $G_{peak}(V)^{1/3}$ and steady-state availability data “ H_∞ curve”, respectively.

$$m_\infty(V) = \frac{1}{1 + e^{-(V-V_m)/k_m}} ; \quad h_\infty(V) = \frac{1}{1 + e^{(V-V_h)/k_h}} \quad \text{Eq. A3}$$

This approach assumes $h = 1$ at the peak I_{Na} , which is an approximation. Next, the rate relations in Eq. A4 were used to fit the voltage dependence for $\tau_h(V)$, measured experimentally as the time constant for Na^+ current decay or as the time constant of pre-pulse inactivation.

$$\tau_h(V) = \frac{1}{a_h + b_h} ; \quad a_h(V) = \bar{a}_h e^{-V/k_{ah}} ;$$

$$b_h(V) = \frac{\bar{b}_{h1} + \bar{b}_{h2}V}{1 + e^{-(V-V_{bh})/k_{bh}}} \quad \text{Eq. A4}$$

To extract the time constant for activation, $\tau_m(V)$, the Na^+ current was divided by the driving force $(V-E_{Na})$ and by the inactivation variable $h(V, t) = h_\infty(V) + (h_0 - h_\infty(V)) \exp[-t/\tau_h(V)]$ to yield $m(V, t)^3$ as derived from Eq. A1. This scaled current

trace was fit, in turn, by $(1-\exp[-t/\tau_m])^3$ to determine τ_m . Finally, activation time constants measured at a series of voltages were fit by the rate relations in Eq. A5 to establish the parameter values for simulating $\tau_m(V)$.

$$\tau_m(V) = \frac{1}{a_m + b_m}; \quad a_m(V) = \frac{\bar{a}_m}{1 + e^{-(V-V_{am})/k_{am}}};$$

$$b_m(V) = \bar{b}_m e^{-V/k_{bm}} \quad \text{Eq. A5}$$

Values for the model parameters, determined from Na^+ currents measured in a representative foot pad muscle fiber, are listed in Table A1.

Table A.1 Gating Parameters¹				
	Steady State		Kinetic	
Activation	$V_m = -57$	$k_m = 4.7$	$\bar{a}_m = 6.0 \text{ ms}^{-1}$	$V_{am} = 37 \quad k_{am} = 10$
			$\bar{b}_m = 11 \text{ s}^{-1}$	$k_{bm} = 13$
Inactivation	$V_h = -97$	$k_h = 7.1$	$\bar{a}_h = 0.06 \text{ s}^{-1}$	$k_{ah} = 8.6$
			$\bar{b}_{h1} = 1.8 \text{ ms}^{-1}$	$\bar{b}_{h2} = 0.0049$
			$V_{bh} = 50$	$k_{bh} = 12$

¹ Values in mV unless otherwise noted.

BIBLIOGRAPHY

- Adrian, R.H., Chandler, W.K., and Hodgkin, A.L. (1970). Voltage clamp experiments in striated muscle fibres. *The Journal of physiology* 208, 607-644.
- Adrian, R.H., and Marshall, M.W. (1976). Action potentials reconstructed in normal and myotonic muscle fibres. *The Journal of physiology* 258, 125-143.
- Adrian, R.H., and Marshall, M.W. (1977). Sodium currents in mammalian muscle. *The Journal of physiology* 268, 223-250.
- Adrian, R.H., and Peachey, L.D. (1973). Reconstruction of the action potential of frog sartorius muscle. *The Journal of physiology* 235, 103-131.
- Akopian, A.N., Souslova, V., England, S., Okuse, K., Ogata, N., Ure, J., Smith, A., Kerr, B.J., McMahon, S.B., Boyce, S., *et al.* (1999). The tetrodotoxin-resistant sodium channel SNS has a specialized function in pain pathways. *Nat Neurosci* 2, 541-548.
- Aldrich, R.W., Corey, D.P., and Stevens, C.F. (1983). A reinterpretation of mammalian sodium channel gating based on single channel recording. *Nature* 306, 436-441.
- Almers, W., Roberts, W.M., and Ruff, R.L. (1984). Voltage clamp of rat and human skeletal muscle: measurements with an improved loose-patch technique. *The Journal of physiology* 347, 751-768.
- Almers, W., Stanfield, P.R., and Stuhmer, W. (1983). Slow changes in currents through sodium channels in frog muscle membrane. *The Journal of physiology* 339, 253-271.
- Anderson, P.A.V., and Greenberg, R.M. (2001). Phylogeny of ion channels: clues to structure and function. *Comparative Biochemistry and Physiology Part B: Biochemistry and Molecular Biology* 129, 17-28.
- Armstrong, C.M. (1981). Sodium channels and gating currents. *Physiol Rev* 61, 644-683.
- Beam, K.G., and Knudson, C.M. (1988). Calcium currents in embryonic and neonatal mammalian skeletal muscle. *J Gen Physiol* 91, 781-798.
- Bendahhou, S., Cummins, T.R., Hahn, A.F., Langlois, S., Waxman, S.G., and Ptacek, L.J. (2000). A double mutation in families with periodic paralysis defines new aspects of sodium channel slow inactivation. *J Clin Invest* 106, 431-438.
- Biemond, A., and Daniels, A.P. (1934). Familial periodic paralysis and its transition into spinal muscular atrophy. *Brain* 57, 91-108.
- Bouhours, M., Sternberg, D., Davoine, C.S., Ferrer, X., Willer, J.C., Fontaine, B., and Tabti, N. (2004). Functional characterization and cold sensitivity of T1313A, a new mutation of the skeletal muscle sodium channel causing paramyotonia congenita in humans. *The Journal of physiology* 554, 635-647.

- Bulman, D.E., Scoggan, K.A., van Oene, M.D., Nicolle, M.W., Hahn, A.F., Tollar, L.L., and Ebers, G.C. (1999). A novel sodium channel mutation in a family with hypokalemic periodic paralysis. *Neurology* 53, 1932-1936.
- Buruma, O.J.S., and Schipperheyn, J.J. (1979). Periodic paralysis. In *Diseases of Muscle, Part 2 Handbook of Clinical Neurology*, P.J. Vinken, G.W. Bruyn, and S.P. Ringel, eds. (New York, Elsevier/North Holland), pp. 147-147.
- Cannon, S.C. (1997). From mutation to myotonia in sodium channel disorders. *Neuromuscular Disorders* 7, 241-249.
- Cannon, S.C. (2002). An expanding view for the molecular basis of familial periodic paralysis. *Neuromuscular Disorders* 12, 533-543.
- Cannon, S.C. (2006). Pathomechanisms in channelopathies of skeletal muscle and brain. *Annu Rev Neurosci* 29, 387-415.
- Cannon, S.C. (2010). Voltage-sensor mutations in channelopathies of skeletal muscle. *The Journal of physiology* 588, 1887-1895.
- Cannon, S.C., and Bean, B.P. (2010). Sodium channels gone wild: resurgent current from neuronal and muscle channelopathies. *J Clin Invest* 120, 80-83.
- Cannon, S.C., Brown Jr, R.H., and Corey, D.P. (1993). Theoretical reconstruction of myotonia and paralysis caused by incomplete inactivation of sodium channels. *Biophysical Journal* 65, 270-288.
- Cannon, S.C., Brown, R.H., Jr., and Corey, D.P. (1991). A sodium channel defect in hyperkalemic periodic paralysis: potassium-induced failure of inactivation. *Neuron* 6, 619-626.
- Cannon, S.C., and Corey, D.P. (1993). Loss of Na⁺ channel inactivation by anemone toxin (ATX II) mimics the myotonic state in hyperkalaemic periodic paralysis. *The Journal of physiology* 466, 501-520.
- Cannon, S.C., and Strittmatter, S.M. (1993). Functional expression of sodium channel mutations identified in families with periodic paralysis. *Neuron* 10, 317-326.
- Catterall, W.A. (2000). From Ionic Currents to Molecular Mechanisms: The Structure and Function of Voltage-Gated Sodium Channels. *Neuron* 26, 13-25.
- Chahine, M., Deschene, I., Chen, L.Q., and Kallen, R.G. (1996). Electrophysiological characteristics of cloned skeletal and cardiac muscle sodium channels. *Am J Physiol* 271, H498-506.
- Chahine, M., George, A.L., Jr., Zhou, M., Ji, S., Sun, W., Barchi, R.L., and Horn, R. (1994). Sodium channel mutations in paramyotonia congenita uncouple inactivation from activation. *Neuron* 12, 281-294.
- Chandler, W.K., and Meves, H. (1970). Slow changes in membrane permeability and long-lasting action potentials in axons perfused with fluoride solutions. *The Journal of physiology* 211, 707-728.

- Chen, C.F., and Cannon, S.C. (1995). Modulation of Na⁺ channel inactivation by the β_1 subunit: a deletion analysis. *Pflügers Archiv* *431*, 186-195.
- Cheung, A., Dantzig, J.A., Hollingworth, S., Baylor, S.M., Goldman, Y.E., Mitchison, T.J., and Straight, A.F. (2002). A small-molecule inhibitor of skeletal muscle myosin II. *Nat Cell Biol* *4*, 83-88.
- Chua, M., and Betz, W.J. (1991). Characterization of ion channels on the surface membrane of adult rat skeletal muscle. *Biophys J* *59*, 1251-1260.
- Creutzfeldt, O.D., Abbott, B.C., Fowler, W.M., and Pearson, C.M. (1963). Muscle Membrane Potentials in Episodic Adynamia. *Electroencephalogr Clin Neurophysiol* *15*, 508-519.
- Cummins, T.R., and Sigworth, F.J. (1996). Impaired slow inactivation in mutant sodium channels. *Biophys J* *71*, 227-236.
- Cummins, T.R., Zhou, J., Sigworth, F.J., Ukomadu, C., Stephan, M., Ptacek, L.J., and Agnew, W.S. (1993). Functional consequences of a Na⁺ channel mutation causing hyperkalemic periodic paralysis. *Neuron* *10*, 667-678.
- Desaphy, J.F., Pierno, S., Leoty, C., George, A.L., Jr., De Luca, A., and Camerino, D.C. (2001). Skeletal muscle disuse induces fibre type-dependent enhancement of Na(+) channel expression. *Brain* *124*, 1100-1113.
- Dib-Hajj, S., Black, J.A., Cummins, T.R., and Waxman, S.G. (2002). NaN/Nav1.9: a sodium channel with unique properties. *Trends in Neurosciences* *25*, 253-259.
- Dice, M.S., Abbruzzese, J.L., Wheeler, J.T., Groome, J.R., Fujimoto, E., and Ruben, P.C. (2004). Temperature-sensitive defects in paramyotonia congenita mutants R1448C and T1313M. *Muscle & nerve* *30*, 277-288.
- DiFranco, M., Capote, J., and Vergara, J.L. (2005). Optical imaging and functional characterization of the transverse tubular system of mammalian muscle fibers using the potentiometric indicator di-8-ANEPPS. *J Membr Biol* *208*, 141-153.
- Dulhunty, A.F., and Gage, P.W. (1973). Differential effects of glycerol treatment on membrane capacity and excitation-contraction coupling in toad sartorius fibres. *The Journal of physiology* *234*, 373-408.
- Duval, A., and Leoty, C. (1978). Ionic currents in mammalian fast skeletal muscle. *The Journal of physiology* *278*, 403-423.
- Duval, A., and Leoty, C. (1980). Ionic currents in slow twitch skeletal muscle in the rat. *The Journal of physiology* *307*, 23-41.
- Eaholtz, G., Scheuer, T., and Catterall, W.A. (1994). Restoration of inactivation and block of open sodium channels by an inactivation gate peptide. *Neuron* *12*, 1041-1048.
- Elbaz, A., Vale-Santos, J., Jurkat-Rott, K., Lapie, P., Ophoff, R.A., Bady, B., Links, T.P., Piussan, C., Vila, A., Monnier, N., *et al.* (1995). Hypokalemic periodic paralysis and the dihydropyridine receptor (CACNL1A3): genotype/phenotype correlations for two

predominant mutations and evidence for the absence of a founder effect in 16 caucasian families. *Am J Hum Genet* 56, 374-380.

Engel, A.G., Ohno, K., and Sine, S.M. (2003). Sleuthing molecular targets for neurological diseases at the neuromuscular junction. *Nat Rev Neurosci* 4, 339-352.

Featherstone, D.E., Richmond, J.E., and Ruben, P.C. (1996). Interaction between fast and slow inactivation in Skm1 sodium channels. *Biophys J* 71, 3098-3109.

Filatov, G.N., Pinter, M.J., and Rich, M.M. (2005). Resting potential-dependent regulation of the voltage sensitivity of sodium channel gating in rat skeletal muscle in vivo. *J Gen Physiol* 126, 161-172.

Fleischhauer, R., Mitrovic, N., Deymeer, F., Lehmann-Horn, F., and Lerche, H. (1998). Effects of temperature and mexiletine on the F1473S Na⁺ channel mutation causing paramyotonia congenita. *Pflügers Archiv* 436, 757-765.

Fontaine, B. (2008). Periodic paralysis. *Adv Genet* 63, 3-23.

Fontaine, B., Khurana, T.S., Hoffman, E.P., Bruns, G.A., Haines, J.L., Trofatter, J.A., Hanson, M.P., Rich, J., McFarlane, H., Yasek, D.M., *et al.* (1990). Hyperkalemic periodic paralysis and the adult muscle sodium channel alpha-subunit gene. *Science* 250, 1000-1002.

Fontaine, B., Vale-Santos, J., Jurkat-Rott, K., Reboul, J., Plassart, E., Rime, C.S., Elbaz, A., Heine, R., Guimaraes, J., Weissenbach, J., *et al.* (1994). Mapping of the hypokalaemic periodic paralysis (HypoPP) locus to chromosome 1q31-32 in three European families. *Nat Genet* 6, 267-272.

Fozzard, H.A., and Hanck, D.A. (1996). Structure and function of voltage-dependent sodium channels: comparison of brain II and cardiac isoforms. *Physiol Rev* 76, 887-926.

Francis, D., Struyk, A., and Cannon, S. (2010). Arginine mutations in the S4 VSD of NaV1.4 associated with hypokalemic periodic paralysis, but not paramyotonia, create a gating pore conductance. *Biophys J* 98

Gamstorp, I. (1956). Adynamia episodica hereditaria. *Acta Paediatr Stockholm (Suppl)* 108, 1-126.

Gellens, M.E., George, A.L., Jr., Chen, L.Q., Chahine, M., Horn, R., Barchi, R.L., and Kallen, R.G. (1992). Primary structure and functional expression of the human cardiac tetrodotoxin-insensitive voltage-dependent sodium channel. *Proc Natl Acad Sci U S A* 89, 554-558.

George, A.L., Jr., Komisarof, J., Kallen, R.G., and Barchi, R.L. (1992). Primary structure of the adult human skeletal muscle voltage-dependent sodium channel. *Ann Neurol* 31, 131-137.

Glaaser, I.W., Bankston, J.R., Liu, H., Tateyama, M., and Kass, R.S. (2006). A carboxyl-terminal hydrophobic interface is critical to sodium channel function. Relevance to inherited disorders. *J Biol Chem* 281, 24015-24023.

- Goldin, A.L. (2001). Resurgence of sodium channel research. *Annu Rev Physiol* 63, 871-894.
- Goldin, A.L. (2002). Evolution of voltage-gated Na⁺ channels. *J Exp Biol* 205, 575-584.
- Goldin, A.L., Barchi, R.L., Caldwell, J.H., Hofmann, F., Howe, J.R., Hunter, J.C., Kallen, R.G., Mandel, G., Meisler, M.H., Netter, Y.B., *et al.* (2000). Nomenclature of Voltage-Gated Sodium Channels. *Neuron* 28, 365-368.
- Goldman, L. (1999). On Mutations that Uncouple Sodium Channel Activation from Inactivation. *Biophysical Journal* 76, 2553-2559.
- Groome, J.R., Fujimoto, E., George, A.L., and Ruben, P.C. (1999). Differential effects of homologous S4 mutations in human skeletal muscle sodium channels on deactivation gating from open and inactivated states. *The Journal of physiology* 516 (Pt 3), 687-698.
- Haufe, V., Camacho, J.A., Dumaine, R., Gunther, B., Bollensdorff, C., von Banchet, G.S., Benndorf, K., and Zimmer, T. (2005). Expression pattern of neuronal and skeletal muscle voltage-gated Na⁺ channels in the developing mouse heart. *The Journal of physiology* 564, 683-696.
- Hayward, L.J., Brown, R.H., Jr., and Cannon, S.C. (1996). Inactivation defects caused by myotonia-associated mutations in the sodium channel III-IV linker. *J Gen Physiol* 107, 559-576.
- Hayward, L.J., Brown, R.H., Jr., and Cannon, S.C. (1997). Slow inactivation differs among mutant Na channels associated with myotonia and periodic paralysis. *Biophys J* 72, 1204-1219.
- Hayward, L.J., Kim, J.S., Lee, M.Y., Zhou, H., Kim, J.W., Misra, K., Salajegheh, M., Wu, F.F., Matsuda, C., Reid, V., *et al.* (2008). Targeted mutation of mouse skeletal muscle sodium channel produces myotonia and potassium-sensitive weakness. *J Clin Invest* 118, 1437-1449.
- Hayward, L.J., Sandoval, G.M., and Cannon, S.C. (1999). Defective slow inactivation of sodium channels contributes to familial periodic paralysis. *Neurology* 52, 1447-1453.
- Heine, R., Plka, U., and Lehmann-Horn, F. (1993). A novel SCN4A mutation causing myotonia aggravated by cold and potassium. *Hum Mol Genet* 2, 1349-1353.
- Hille, B., and Campbell, D.T. (1976). An improved vaseline gap voltage clamp for skeletal muscle fibers. *J Gen Physiol* 67, 265-293.
- Hiyama, T.Y., Watanabe, E., Ono, K., Inenaga, K., Tamkun, M.M., Yoshida, S., and Noda, M. (2002). Na(x) channel involved in CNS sodium-level sensing. *Nat Neurosci* 5, 511-512.
- Hodgkin, A.L., and Huxley, A.F. (1952). A quantitative description of membrane current and its application to conduction and excitation in nerve. *The Journal of physiology* 117, 500-544.

- Isom, L.L., De Jongh, K.S., Patton, D.E., Reber, B.F., Offord, J., Charbonneau, H., Walsh, K., Goldin, A.L., and Catterall, W.A. (1992). Primary structure and functional expression of the beta 1 subunit of the rat brain sodium channel. *Science* 256, 839-842.
- Isom, L.L., Ragsdale, D.S., De Jongh, K.S., Westenbroek, R.E., Reber, B.F.X., Scheuer, T., and Catterall, W.A. (1995). Structure and function of the [beta]2 subunit of brain sodium channels, a transmembrane glycoprotein with a CAM motif. *Cell* 83, 433-442.
- Jarecki, B.W., Piekarz, A.D., Jackson, J.O., and Cummins, T.R. (2010). Human voltage-gated sodium channel mutations that cause inherited neuronal and muscle channelopathies increase resurgent sodium currents. *The Journal of Clinical Investigation* 120, 369-378.
- Ji, S., George, A.L., Jr., Horn, R., and Barchi, R.L. (1996). Paramyotonia congenita mutations reveal different roles for segments S3 and S4 of domain D4 in hSkM1 sodium channel gating. *J Gen Physiol* 107, 183-194.
- Jurkat-Rott, K., Holzherr, B., Fauler, M., and Lehmann-Horn, F. (2010). Sodium channelopathies of skeletal muscle result from gain or loss of function. *Pflügers Archiv* 460, 239-248.
- Jurkat-Rott, K., and Lehmann-Horn, F. (2005). Muscle channelopathies and critical points in functional and genetic studies. *The Journal of Clinical Investigation* 115, 2000-2009.
- Jurkat-Rott, K., Lehmann-Horn, F., Elbaz, A., Heine, R., Gregg, R.G., Hogan, K., Powers, P.A., Laple, P., Vale-Santos, J.E., Weissenbach, J., *et al.* (1994). A calcium channel mutation causing hypokalemic periodic paralysis. *Hum Mol Genet* 3, 1415-1419.
- Jurkat-Rott, K., Mitrovic, N., Hang, C., Kouzmekine, A., Iaizzo, P., Herzog, J., Lerche, H., Nicole, S., Vale-Santos, J., Chauveau, D., *et al.* (2000). Voltage-sensor sodium channel mutations cause hypokalemic periodic paralysis type 2 by enhanced inactivation and reduced current. *Proc Natl Acad Sci U S A* 97, 9549-9554.
- Jurman, M.E., Boland, L.M., Liu, Y., and Yellen, G. (1994). Visual identification of individual transfected cells for electrophysiology using antibody-coated beads. *Biotechniques* 17, 876-881.
- Kambouris, N.G., Hastings, L.A., Stepanovic, S., Marban, E., Tomaselli, G.F., and Balsler, J.R. (1998). Mechanistic link between lidocaine block and inactivation probed by outer pore mutations in the rat micro1 skeletal muscle sodium channel. *The Journal of physiology* 512 (Pt 3), 693-705.
- Kim, A.M., and Vergara, J.L. (1998). Supercharging accelerates T-tubule membrane potential changes in voltage clamped frog skeletal muscle fibers. *Biophys J* 75, 2098-2116.
- Kontis, K.J., Rounaghi, A., and Goldin, A.L. (1997). Sodium channel activation gating is affected by substitutions of voltage sensor positive charges in all four domains. *J Gen Physiol* 110, 391-401.

- Kubota, T., Kinoshita, M., Sasaki, R., Aoike, F., Takahashi, M.P., Sakoda, S., and Hirose, K. (2009). New mutation of the Na channel in the severe form of potassium-aggravated myotonia. *Muscle & nerve* 39, 666-673.
- Kuo, C.C., and Bean, B.P. (1994). Na⁺ channels must deactivate to recover from inactivation. *Neuron* 12, 819-829.
- Lehmann-Horn, F., and Jurkat-Rott, K. (1999). Voltage-gated ion channels and hereditary disease. *Physiol Rev* 79, 1317-1372.
- Lehmann-Horn, F., Kuther, G., Ricker, K., Grafe, P., Ballanyi, K., and Rudel, R. (1987). Adynamia episodica hereditaria with myotonia: a non-inactivating sodium current and the effect of extracellular pH. *Muscle & nerve* 10, 363-374.
- Lehmann-Horn, F., Rüdell, R., and Jurkat-Rott, K. (2004). nondystrophic myotonias and periodic paralyses. . In *Myology*, A.G. Engel, and C. Franzini-Armstrong, eds. (New York, McGraw-Hill), pp. 1257–1300
- Lehmann-Horn, F., Rudel, R., Ricker, K., Lorkovic, H., Dengler, R., and Hopf, H.C. (1983). Two cases of adynamia episodica hereditaria: in vitro investigation of muscle cell membrane and contraction parameters. *Muscle & nerve* 6, 113-121.
- Lerche, H., Heine, R., Pika, U., George, A.L., Jr., Mitrovic, N., Browatzki, M., Weiss, T., Rivet-Bastide, M., Franke, C., Lomonaco, M., *et al.* (1993). Human sodium channel myotonia: slowed channel inactivation due to substitutions for a glycine within the III-IV linker. *The Journal of physiology* 470, 13-22.
- Lerche, H., Mitrovic, N., Dubowitz, V., and Lehmann-Horn, F. (1996). Paramyotonia congenita: the R1448P Na⁺ channel mutation in adult human skeletal muscle. *Ann Neurol* 39, 599-608.
- Lueck, J.D., Mankodi, A., Swanson, M.S., Thornton, C.A., and Dirksen, R.T. (2007). Muscle chloride channel dysfunction in two mouse models of myotonic dystrophy. *J Gen Physiol* 129, 79-94.
- Mankodi, A., Takahashi, M.P., Jiang, H., Beck, C.L., Bowers, W.J., Moxley, R.T., Cannon, S.C., and Thornton, C.A. (2002). Expanded CUG repeats trigger aberrant splicing of ClC-1 chloride channel pre-mRNA and hyperexcitability of skeletal muscle in myotonic dystrophy. *Mol Cell* 10, 35-44.
- McClatchey, A.I., Cannon, S.C., Slaugenhaupt, S.A., and Gusella, J.F. (1993). The cloning and expression of a sodium channel beta 1-subunit cDNA from human brain. *Hum Mol Genet* 2, 745-749.
- McClatchey, A.I., McKenna-Yasek, D., Cros, D., Worthen, H.G., Kuncl, R.W., DeSilva, S.M., Comblath, D.R., Gusella, J.F., and Brown, R.H., Jr. (1992). Novel mutations in families with unusual and variable disorders of the skeletal muscle sodium channel. *Nat Genet* 2, 148-152.

- Mille, M., Koenig, X., Zebedin, E., Uhrin, P., Cervenka, R., Todt, H., and Hilber, K. (2009). Sodium current properties of primary skeletal myocytes and cardiomyocytes derived from different mouse strains. *Pflügers Archiv* 457, 1023-1033.
- Miller, T.M., Dias da Silva, M.R., Miller, H.A., Kwiecinski, H., Mendell, J.R., Tawil, R., McManis, P., Griggs, R.C., Angelini, C., Servidei, S., *et al.* (2004). Correlating phenotype and genotype in the periodic paralyses. *Neurology* 63, 1647-1655.
- Mitrovic, N., George, A.L., Jr., Heine, R., Wagner, S., Pika, U., Hartlaub, U., Zhou, M., Lerche, H., Fahlke, C., and Lehmann-Horn, F. (1994). K(+)-aggravated myotonia: destabilization of the inactivated state of the human muscle Na⁺ channel by the V1589M mutation. *The Journal of physiology* 478 Pt 3, 395-402.
- Mitrovic, N., George, A.L., Jr., Lerche, H., Wagner, S., Fahlke, C., and Lehmann-Horn, F. (1995). Different effects on gating of three myotonia-causing mutations in the inactivation gate of the human muscle sodium channel. *The Journal of physiology* 487 (Pt 1), 107-114.
- Moore, J.W., Ramon, F., and Joyner, R.W. (1975). Axon voltage-clamp simulations. II. Double sucrose-gap method. *Biophys J* 15, 25-35.
- Morel, J., Rannou, F., Talarmin, H., Giroux-Metges, M.A., Pennec, J.P., Dorange, G., and Gueret, G. (2010). Sodium Channel Na(V)1.5 Expression is Enhanced in Cultured Adult Rat Skeletal Muscle Fibers. *J Membr Biol*.
- O'Reilly, J.P., Wang, S.Y., Kallen, R.G., and Wang, G.K. (1999). Comparison of slow inactivation in human heart and rat skeletal muscle Na⁺ channel chimaeras. *J Physiol (Lond)* 515, 61-73.
- Ogata, N., and Ohishi, Y. (2002). Molecular diversity of structure and function of the voltage-gated Na⁺ channels. *Jpn J Pharmacol* 88, 365-377.
- Pappone, P.A. (1980). Voltage-clamp experiments in normal and denervated mammalian skeletal muscle fibres. *The Journal of physiology* 306, 377-410.
- Petitprez, S., Tiab, L., Chen, L., Kappeler, L., Rosler, K.M., Schorderet, D., Abriel, H., and Burgunder, J.-M. (2008). A novel dominant mutation of the Nav1.4 {alpha}-subunit domain I leading to sodium channel myotonia. *Neurology* 71, 1669-1675.
- Phillips, J.K., and Lipski, J. (2000). Single-cell RT-PCR as a tool to study gene expression in central and peripheral autonomic neurones. *Auton Neurosci* 86, 1-12.
- Plassart, E., Reboul, J., Rime, C.S., Recan, D., Millasseau, P., Eymard, B., Pelletier, J., Thomas, C., Chapon, F., Desnuelle, C., *et al.* (1994). Mutations in the muscle sodium channel gene (SCN4A) in 13 French families with hyperkalemic periodic paralysis and paramyotonia congenita: phenotype to genotype correlations and demonstration of the predominance of two mutations. *Eur J Hum Genet* 2, 110-124.
- Plummer, N.W., and Meisler, M.H. (1999). Evolution and Diversity of Mammalian Sodium Channel Genes. *Genomics* 57, 323-331.

- Popa, M.O., Alekov, A.K., Bail, S., Lehmann-Horn, F., and Lerche, H. (2004). Cooperative effect of S4-S5 loops in domains D3 and D4 on fast inactivation of the Na⁺ channel. *The Journal of physiology* 561, 39-51.
- Probstle, T., Rudel, R., and Ruppertsberg, J.P. (1988). Hodgkin-Huxley parameters of the sodium channels in human myoballs. *Pflügers Archiv* 412, 264-269.
- Ptacek, L.J., George, A.L., Jr., Griggs, R.C., Tawil, R., Kallen, R.G., Barchi, R.L., Robertson, M., and Leppert, M.F. (1991). Identification of a mutation in the gene causing hyperkalemic periodic paralysis. *Cell* 67, 1021-1027.
- Raman, I.M., and Bean, B.P. (2001). Inactivation and Recovery of Sodium Currents in Cerebellar Purkinje Neurons: Evidence for Two Mechanisms. *Biophysical Journal* 80, 729-737.
- Rannou, F., Droguet, M., Giroux-Metges, M.A., Penneç, Y., Gioux, M., and Penneç, J.P. (2009). Differences in sodium voltage-gated channel properties according to myosin heavy chain isoform expression in single muscle fibres. *The Journal of physiology* 587, 5249-5258.
- Ren, D., Navarro, B., Xu, H., Yue, L., Shi, Q., and Clapham, D.E. (2001). A prokaryotic voltage-gated sodium channel. *Science* 294, 2372-2375.
- Rich, M.M., and Pinter, M.J. (2003). Crucial role of sodium channel fast inactivation in muscle fibre inexcitability in a rat model of critical illness myopathy. *The Journal of physiology* 547, 555-566.
- Richmond, J.E., Featherstone, D.E., Hartmann, H.A., and Ruben, P.C. (1998). Slow inactivation in human cardiac sodium channels. *Biophys J* 74, 2945-2952.
- Roberts, W.M., and Almers, W. (1984). An improved loose patch voltage clamp method using concentric pipettes. *Pflügers Archiv* 402, 190-196.
- Rojas, C.V., Neely, A., Velasco-Loyden, G., Palma, V., and Kukuljan, M. (1999). Hyperkalemic periodic paralysis M1592V mutation modifies activation in human skeletal muscle Na⁺ channel. *Am J Physiol* 276, C259-266.
- Rojas, C.V., Wang, J.Z., Schwartz, L.S., Hoffman, E.P., Powell, B.R., and Brown, R.H., Jr. (1991). A Met-to-Val mutation in the skeletal muscle Na⁺ channel alpha-subunit in hyperkalaemic periodic paralysis. *Nature* 354, 387-389.
- Ruben, P.C., Fleig, A., Featherstone, D., Starkus, J.G., and Rayner, M.D. (1997). Effects of clamp rise-time on rat brain IIA sodium channels in *Xenopus* oocytes. *J Neurosci Methods* 73, 113-122.
- Rudel, R., Lehmann-Horn, F., Ricker, K., and Kuther, G. (1984). Hypokalemic periodic paralysis: in vitro investigation of muscle fiber membrane parameters. *Muscle & nerve* 7, 110-120.
- Rudy, B. (1978). Slow inactivation of the sodium conductance in squid giant axons. Pronase resistance. *The Journal of physiology* 283, 1-21.

- Ruff, R.L. (1992). Na current density at and away from end plates on rat fast- and slow-twitch skeletal muscle fibers. *Am J Physiol* 262, C229-234.
- Ruff, R.L. (1999). Effects of temperature on slow and fast inactivation of rat skeletal muscle Na(+) channels. *Am J Physiol* 277, C937-947.
- Ruff, R.L., Simoncini, L., and Stuhmer, W. (1988). Slow sodium channel inactivation in mammalian muscle: a possible role in regulating excitability. *Muscle & nerve* 11, 502-510.
- Ruff, R.L., and Whittlesey, D. (1992). Na⁺ current densities and voltage dependence in human intercostal muscle fibres. *The Journal of physiology* 458, 85-97.
- Satin, J., Kyle, J.W., Chen, M., Bell, P., Cribbs, L.L., Fozzard, H.A., and Rogart, R.B. (1992). A mutant of TTX-resistant cardiac sodium channels with TTX-sensitive properties. *Science* 256, 1202-1205.
- Sato, C., Sato, M., Iwasaki, A., Doi, T., and Engel, A. (1998). The sodium channel has four domains surrounding a central pore. *J Struct Biol* 121, 314-325.
- Sivilotti, L., Okuse, K., Akopian, A.N., Moss, S., and Wood, J.N. (1997). A single serine residue confers tetrodotoxin insensitivity on the rat sensory-neuron-specific sodium channel SNS. *FEBS Letters* 409, 49-52.
- Sokolov, S., Scheuer, T., and Catterall, W.A. (2007). Gating pore current in an inherited ion channelopathy. *Nature* 446, 76-78.
- Starace, D.M., and Bezanilla, F. (2001). Histidine scanning mutagenesis of basic residues of the S4 segment of the shaker k⁺ channel. *J Gen Physiol* 117, 469-490.
- Stein, P., and Palade, P. (1989). Patch clamp of sarcolemmal spheres from stretched skeletal muscle fibers. *Am J Physiol* 256, C434-440.
- Sternberg, D., Maisonobe, T., Jurkat-Rott, K., Nicole, S., Launay, E., Chauveau, D., Tabti, N., Lehmann-Horn, F., Hainque, B., and Fontaine, B. (2001). Hypokalaemic periodic paralysis type 2 caused by mutations at codon 672 in the muscle sodium channel gene SCN4A. *Brain* 124, 1091-1099.
- Struyk, A.F., and Cannon, S.C. (2007). A Na⁺ channel mutation linked to hypokalemic periodic paralysis exposes a proton-selective gating pore. *J Gen Physiol* 130, 11-20.
- Struyk, A.F., Markin, V.S., Francis, D., and Cannon, S.C. (2008). Gating pore currents in DIIS4 mutations of NaV1.4 associated with periodic paralysis: saturation of ion flux and implications for disease pathogenesis. *J Gen Physiol* 132, 447-464.
- Struyk, A.F., Scoggan, K.A., Bulman, D.E., and Cannon, S.C. (2000). The human skeletal muscle Na channel mutation R669H associated with hypokalemic periodic paralysis enhances slow inactivation. *J Neurosci* 20, 8610-8617.
- Stuhmer, W., and Almers, W. (1982). Photobleaching through glass micropipettes: sodium channels without lateral mobility in the sarcolemma of frog skeletal muscle. *Proc Natl Acad Sci U S A* 79, 946-950.

- Stühmer, W., Conti, F., Suzuki, H., Wang, X., Noda, M., Yahagi, N., Kubo, H., and Numa, S. (1989). Structural parts involved in activation and inactivation of the sodium channel. *Nature* *339*, 597-603.
- Stunnenberg, B.C., Ginjaar, H.B., Trip, J., Faber, C.G., van Engelen, B.G., and Drost, G. (2010). Isolated eyelid closure myotonia in two families with sodium channel myotonia. *Neurogenetics* *11*, 257-260.
- Takahashi, M.P., and Cannon, S.C. (1999). Enhanced slow inactivation by V445M: a sodium channel mutation associated with myotonia. *Biophys J* *76*, 861-868.
- Todt, H., Dudley, S.C., Jr., Kyle, J.W., French, R.J., and Fozzard, H.A. (1999). Ultra-slow inactivation in mul Na⁺ channels is produced by a structural rearrangement of the outer vestibule. *Biophys J* *76*, 1335-1345.
- Toib, A., Lyakhov, V., and Marom, S. (1998). Interaction between duration of activity and time course of recovery from slow inactivation in mammalian brain Na⁺ channels. *J Neurosci* *18*, 1893-1903.
- Tombola, F., Pathak, M.M., and Isacoff, E.Y. (2005). Voltage-Sensing Arginines in a Potassium Channel Permeate and Occlude Cation-Selective Pores. *Neuron* *45*, 379-388.
- Tombola, F., Pathak, M.M., and Isacoff, E.Y. (2006). How Does Voltage Open an Ion Channel? *Annual Review of Cell and Developmental Biology* *22*, 23-52.
- Townsend, C., and Horn, R. (1997). Effect of alkali metal cations on slow inactivation of cardiac Na⁺ channels. *J Gen Physiol* *110*, 23-33.
- Tsujino, A., Maertens, C., Ohno, K., Shen, X.M., Fukuda, T., Harper, C.M., Cannon, S.C., and Engel, A.G. (2003). Myasthenic syndrome caused by mutation of the SCN4A sodium channel. *Proc Natl Acad Sci U S A* *100*, 7377-7382.
- Van Der Meulen, J.P., Gilbert, G.J., and Kane, C.A. (1961). Familial hyperkalemic paralysis with myotonia. *N Engl J Med* *264*, 1-6.
- Vedantham, V., and Cannon, S.C. (1998). Slow inactivation does not affect movement of the fast inactivation gate in voltage-gated Na⁺ channels. *J Gen Physiol* *111*, 83-93.
- Veldkamp, M.W., Viswanathan, P.C., Bezzina, C., Baartscheer, A., Wilde, A.A., and Balsler, J.R. (2000). Two distinct congenital arrhythmias evoked by a multidysfunctional Na⁽⁺⁾ channel. *Circ Res* *86*, E91-97.
- Vicart, S., Sternberg, D., Fontaine, B., and Meola, G. (2005). Human skeletal muscle sodium channelopathies. *Neurol Sci* *26*, 194-202.
- Vilin, Y.Y., Fujimoto, E., and Ruben, P.C. (2001). A single residue differentiates between human cardiac and skeletal muscle Na⁺ channel slow inactivation. *Biophys J* *80*, 2221-2230.
- Vilin, Y.Y., Makita, N., George, A.L., Jr., and Ruben, P.C. (1999). Structural determinants of slow inactivation in human cardiac and skeletal muscle sodium channels. *Biophys J* *77*, 1384-1393.

- Vilin, Y.Y., and Ruben, P.C. (2001). Slow inactivation in voltage-gated sodium channels: molecular substrates and contributions to channelopathies. *Cell Biochem Biophys* 35, 171-190.
- Wagner, S., Lerche, H., Mitrovic, N., Heine, R., George, A.L., and Lehmann-Horn, F. (1997). A novel sodium channel mutation causing a hyperkalemic paralytic and paramyotonic syndrome with variable clinical expressivity. *Neurology* 49, 1018-1025.
- Wang, S., and Wang, G.K. (1997). A mutation in segment I-S6 alters slow inactivation of sodium channels. *Biophysical Journal* 72, 1633-1640.
- Wang, Z.M., Messi, M.L., and Delbono, O. (1999). Patch-clamp recording of charge movement, Ca(2+) current, and Ca(2+) transients in adult skeletal muscle fibers. *Biophys J* 77, 2709-2716.
- Wang, Z.M., Zheng, Z., Messi, M.L., and Delbono, O. (2005). Extension and magnitude of denervation in skeletal muscle from ageing mice. *The Journal of physiology* 565, 757-764.
- Webb, J., and Cannon, S.C. (2008). Cold-induced defects of sodium channel gating in atypical periodic paralysis plus myotonia. *Neurology* 70, 755-761.
- Webb, J., Wu, F.F., and Cannon, S.C. (2009). Slow inactivation of the NaV1.4 sodium channel in mammalian cells is impeded by co-expression of the beta1 subunit. *Pflügers Archiv* 457, 1253-1263.
- Woods, C.E., Novo, D., DiFranco, M., Capote, J., and Vergara, J.L. (2005). Propagation in the transverse tubular system and voltage dependence of calcium release in normal and mdx mouse muscle fibres. *The Journal of physiology* 568, 867-880.
- Wu, F.F., Gordon, E., Hoffman, E.P., and Cannon, S.C. (2005). A C-terminal skeletal muscle sodium channel mutation associated with myotonia disrupts fast inactivation. *The Journal of physiology* 565, 371-380.
- Yang, J.S., Bennett, P.B., Makita, N., George, A.L., and Barchi, R.L. (1993). Expression of the sodium channel beta 1 subunit in rat skeletal muscle is selectively associated with the tetrodotoxin-sensitive alpha subunit isoform. *Neuron* 11, 915-922.
- Yang, J.S., Sladky, J.T., Kallen, R.G., and Barchi, R.L. (1991). TTX-sensitive and TTX-insensitive sodium channel mRNA transcripts are independently regulated in adult skeletal muscle after denervation. *Neuron* 7, 421-427.
- Yang, N., Ji, S., Zhou, M., Ptacek, L.J., Barchi, R.L., Horn, R., and George, A.L., Jr. (1994). Sodium channel mutations in paramyotonia congenita exhibit similar biophysical phenotypes in vitro. *Proc Natl Acad Sci U S A* 91, 12785-12789.
- Yu, F.H., and Catterall, W.A. (2003). Overview of the voltage-gated sodium channel family. *Genome Biol* 4, 207.
- Yu, F.H., Westenbroek, R.E., Silos-Santiago, I., McCormick, K.A., Lawson, D., Ge, P., Ferriera, H., Lilly, J., DiStefano, P.S., Catterall, W.A., *et al.* (2003). Sodium channel

beta4, a new disulfide-linked auxiliary subunit with similarity to beta2. *J Neurosci* 23, 7577-7585.